

From the Klinik für Mund-, Kiefer- und Gesichtschirurgie
(Director: Prof. Dr. Med. Dr. Med. Dent. J. Wiltfang)
at the University Medical Center Schleswig-Holstein, Campus Kiel,
at Kiel University

**PROSPECT APPLICATION OF MAGNETO-ENZYMATIC SENSITIVE LIPOSOME
FOR IMAGING AND TARGETED RELEASE IN ORAL SQUAMOUS CELL
CARCINOMA**

Dissertation
to acquire the doctoral degree in dentistry (Dr. med. dent.)
at the Faculty of Medicine
at Kiel University

presented by
HANWEN CHU
from Ningbo, Zhejiang, P. R. China

Kiel 2019

From the Klinik für Mund-, Kiefer- und Gesichtschirurgie
(Director: Prof. Dr. Med. Dr. Med. Dent. J. Wiltfang)
at the University Medical Center Schleswig-Holstein, Campus Kiel,
at Kiel University

**PROSPECT APPLICATION OF MAGNETO-ENZYMATIC SENSITIVE LIPOSOME
FOR IMAGING AND TARGETED RELEASE IN ORAL SQUAMOUS CELL
CARCINOMA**

Dissertation
to acquire the doctoral degree in dentistry (Dr. med. dent.)
at the Faculty of Medicine
at Kiel University

presented by
HANWEN CHU
from Ningbo, Zhejiang, P. R. China

Kiel 2019

1st Reviewer: Prof. Dr. Yahya Açil

2nd Reviewer: Prof. Dr. Marcus Both

Date of oral examination: 17.07.2019

Approved for printing, Kiel,

Signed:

Contents

ABBREVIATIONS.....	III
1. INTRODUCTION.....	1
1.1 <i>Therapy of Head and Neck Squamous Cell Carcinoma.....</i>	1
1.2 <i>Nanoparticles Technologies for Cancer Medicine</i>	2
1.3 <i>Sphingomyelinase in biologicals systems</i>	5
1.4 <i>Indocyanine Green (ICG) Fluorescent Imaging for Clinical Use</i>	7
1.5 <i>The hypothesis of this study</i>	8
2. METHODS.....	11
2.1 <i>Optical properties of environment sensing ICG-MESL probe.....</i>	11
2.1.1 <i>Fluorescence of ICG-MESL and pure ICG in blood</i>	11
2.1.2 <i>Fluorescence change of ICG-MESL with SMase</i>	13
2.1.3 <i>Fluorescence change of ICG-MESL with SMase and AMF.....</i>	13
2.2 <i>In vitro characterization: ASMase activity as a cell stress indicator in HNSCC lines</i>	14
2.2.1 <i>Preparation of carcinoma cells.....</i>	14
2.2.1.1 <i>Culture of carcinoma cells</i>	14
2.2.1.2 <i>Passage of carcinoma cells.....</i>	14
2.2.1.3 <i>Cell frozen of carcinoma cells.....</i>	14
2.2.2 <i>Preparation of Keratinocyte.....</i>	15
2.2.2.1 <i>Culture of Keratinocyte.....</i>	15
2.2.2.2 <i>Passage of Keratinocyte</i>	15
2.2.3 <i>ASMase activity as a cell stress indicator after irradiation</i>	16
2.2.3.1 <i>Cells preparation for irradiation</i>	16
2.2.3.2 <i>ASMase activity measurement after irradiation</i>	16
2.2.3.3 <i>Evaluation of cell lines viability after irradiation.....</i>	17
2.2.3.4 <i>Cisplatin release from Cisplatin-MESL after irradiation.....</i>	17
2.2.3.5 <i>ASMase inhibition study in SCC9 after irradiation.....</i>	18
2.2.4 <i>ASMase activity as a cell stress indicator after cisplatin treatment</i>	19
2.2.4.1 <i>Cells preparation for cisplatin treatment</i>	19
2.2.4.2 <i>ASMase activity measurement after cisplatin treatment</i>	19
2.2.4.3 <i>Evaluation of cell lines viability after cisplatin treatment</i>	19
2.3 <i>In vivo characterization: aSMase activity of HNSCC and muscle in mouse</i>	19
2.3.1 <i>HNSCC mouse model</i>	19
2.3.1.1 <i>Cells preparation for HNSCC mouse</i>	19
2.3.1.2 <i>Mouse model construction</i>	20
2.3.2 <i>ASMase activity of HNSCC and muscle in mouse.....</i>	21
3. RESULTS	22
3.1 <i>Optical properties of environment sensing ICG-MESL probe.....</i>	22
3.1.1 <i>Fluorescence of ICG-MESL and pure ICG in blood</i>	22
3.1.2 <i>Fluorescence change of ICG-MESL with SMase</i>	22
3.1.3 <i>Fluorescence change of ICG-MESL with SMase and AMF.....</i>	23

3.2 <i>In vitro</i> characterization: ASMase activity as a cell stress indicator in HNSCC lines	24
3.2.1 ASMase activity of SCC9 and UDSCC2 after irradiation	24
3.2.2 ASMase activity of Keratinocyte after irradiation	25
3.2.3 Cisplatin release from Cisplatin-MESL after irradiation (SCC9)	26
3.2.4 ASMase inhibition study in SCC9 after irradiation	26
3.2.5 ASMase activity as a cell stress indicator after cisplatin treatment	27
3.3 ASMase activity of HNSCC and muscle in mouse	29
4. DISCUSSION OF RESULTS	32
4.1 Optical properties of environment sensing ICG-MESL probe	32
4.2 ASMase activity as a cell stress indicator after irradiation in HNSCC lines	33
4.3 ASMase activity as a cell stress indicator after cisplatin treatment in HNSCC lines	35
4.4 <i>In Vivo</i> characterization: aSMase activity of HNSCC and muscle in mouse	36
5. CONCLUSION	37
6. BIBLIOGRAPHY	39
7. APPENDICES	46
8. ACKNOWLEDGEMENT	68
9. PUBLICATION	69
10. ACADEMIC RESUME	72

Abbreviations

AMF	Alternating Magnetic Field
aSMase	Acid Sphingomyelinase
Defined K-SFM	Defined Keratinocyte - Serum Free Medium
DMEM	Dulbecco's Modified Eagle Medium
DMSO	Dimethyl Sulfoxide
EDTA	Ethylene Diamine Tetraacetic Acid
EGF	Epidermal Growth Factor
EGFR	Epidermal Growth Factor Receptor
EPR	Enhanced Permeability Retention
FCS	Fetal Calf Serum
FDA	Food and Drug Administration
FI	Fluorescence Imaging
FMT	Fluorescence Molecular Tomography
HCl	Hydrogen Chloride
HNSCC	Head and Neck Squamous Cell Carcinoma
ICG	Indocyanine Green
MESL	Magneto-Enzymatic Sensitive Liposome
MNPs	Magnetite Nanoparticles
MTT	Methyl Thiazolyl Tetrazolium
NIR	Near Infrared
PBS	Phosphate Buffered Saline
PCR	Polymerase Chain Reaction

pH	Potential of Hydrogen
ROIs	Regions Of Interests
SD	Standard Deviation
SDS	Sodium Dodecyl Sulfonate
SLN	Sentinel Lymph Node
SM	Sphingomyelin
SNR	Signal to Noise Ratio
UVB	Ultraviolet B
3D	Three-dimensional
M	Mole
U	Unit

1. Introduction

1.1 Therapy of Head and Neck Squamous Cell Carcinoma

Head and Neck Squamous Cell Carcinoma (HNSCC) is the sixth most common cancer. The worldwide incidence increases with age, especially after 50 years old, exceeding half a million cases annually. It carries a mortality rate of over 50%, with stagnant 5-year survival rates (Siegel et al., 2011; Méry et al., 2016). HNSCC often develop with preneoplastic fields of genetically altered cells on the surface of the oral cavity, oropharynx, nasal cavity, sinuses or larynx. It is thought to be caused by the molecular effects of environmental carcinogens. Although many epidemiological studies have conclusively identified carcinogen exposures of tobacco and alcohol that are associated with an increased risk of HNSCC, human papillomavirus (HPV) infection, especially HPV-16 and HPV-18, has been increasingly associated with this group of cancers (Leemans et al., 2010; Michaud et al., 2014). HPV associated HNSCC comprise a distinct molecular, clinical and pathologic entity that has a markedly better prognosis than HPV negative cancers. Whether the intense therapy is too aggressive in HPV positive patients remains a controversial issue (Ramshankar et al., 2013). Future therapeutic concepts for HNSCC may be personalized in relation to HPV-status to avoid unnecessary toxicity, which makes understanding of the relationship between HPV and HNSCC more important than ever.

HNSCC therapies include surgical intervention, chemotherapy (e.g. cisplatin, axitinib) and radiation. Surgery and radiotherapy remain the primary modalities for management of early and loco regionally advanced HNSCC. The existing chemotherapy is non-selective and associated with significant adverse effects. These aggressive therapies for HNSCC have done little to improve overall 5 years survival. For patients with recurrent and metastatic disease, the therapeutic options are further limited (Méry et al., 2016; Leemans et al., 2010; Bonner et al., 2006). The gene therapy, immunotherapy and molecularly targeted therapy (e.g. cetuximab, EGFR inhibitor) provide a promising approach and are having been a major focus of research over the decades. Therefore, integration of molecular imaging and dose adaptation during treatment is the future directions which are promising strategies to improve the

efficacy and minimizing associated toxicity accuracy (Leemans et al., 2010; Sacco and Worden, 2016).

1.2 Nanoparticles Technologies for Cancer Medicine

Nanotechnology commonly refers to materials and devices up to several hundred nanometers or less. The application of nanotechnology to medicine, designated as nanomedicine has greatly accelerated advances in detection, diagnosis, imaging and therapy of many diseases. Use of nanoparticles as drug delivery systems in cancer therapy is a growing research field over the past two decades (Alexis et al., 2010; Wang et al., 2012; Matsumura and Maeda, 1986).

Classical potent chemotherapeutic agents have the disadvantage of affecting both tumor cells and normal cells, with the concomitant secondary effects including cytotoxicity. Some of these chemotherapeutic associated problems have been solved by the use of nanoparticles as drug delivery systems. By encapsulating a variety of chemotherapeutic agents inside nanoparticles, the bioavailability of the drugs can be improved including stability, solubility, biodistribution and blood circulation half-life (Wang et al., 2012; Ocheke et al., 2009). One important advantage of these nanoparticles is that they accumulate in specific tissue, as well as solid tumors. This effect is called enhanced permeability retention effect (EPR) and is based on the higher leakage of capillaries in solid tumors compared to healthy tissue (Fig. 1.1). Selective accumulation in tumor sites due to EPR effect increases local therapeutic drugs concentration, consequently, the required dose of drug is lower and the reduced drug concentration in healthy tissue minimizes undesirable toxic effects (Matsumura and Maeda, 1986; Ocheke et al., 2009; Minko et al., 2000; Maeda, 2001).

A large number of nanoparticles as drug delivery system have been developed for cancer therapy, including organic and inorganic materials (Bangham et al., 1965; Torchilin, 2005; Danhier et al., 2009; Ocheke et al., 2009). The surface of nanoparticles is further modified with small functional groups that increase their specificity targeting potential (Fig. 1.2).

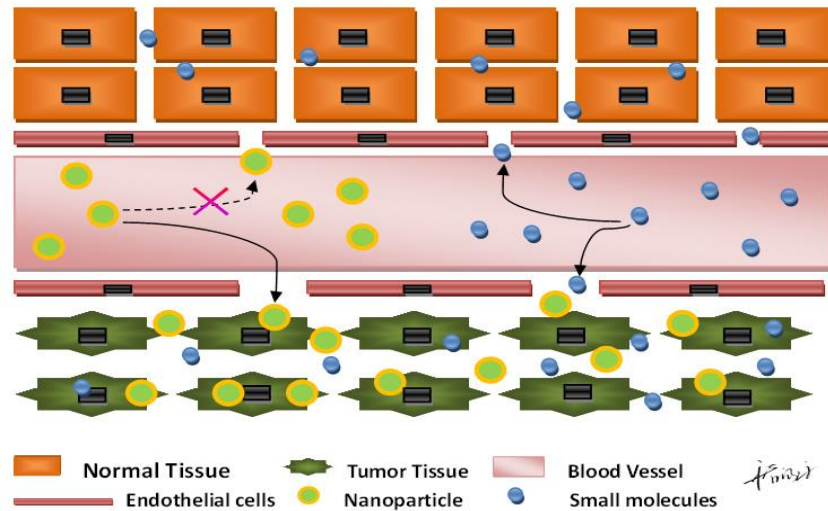


Fig. 1.1 Schematic representation of the enhanced permeability and retention effect (EPR effect): Nanoparticle size plays a significant role in their ability to extravasate from the bloodstream and reach the tumor tissues which are leaky and disorganized. This however does not occur in normal tissue as the blood vessels are well formed and non-porous. Small molecules are capable of entering both tumor and normal tissue (Draw by Hanwen Chu).

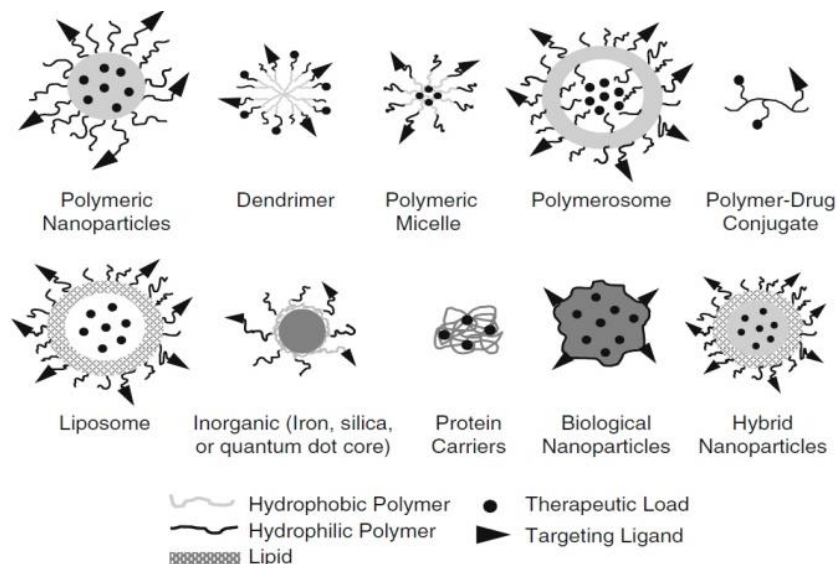


Fig. 1.2 Nanoparticle as drug delivery system is characterized by their physicochemical structures. (Picture excerpted from article: Nanoparticle Technologies for Cancer Therapy; Alexis et al., 2010).

Magnetic nanoparticles (MNPs) as drug targeting carriers have attracted significant attention because of the promising site-directed application in the field of nanomedicine which is directed at the target tissue by means of an external magnetic field. Materials most commonly used for magnetic drug delivery contain metal or metal oxide nanoparticles which are well-tolerated. Conjugation of magnetic materials with drugs, in combination with an external magnetic field to target the nanoparticles has additionally emerged as a promising strategy of drug delivery. MNPs based drug delivery is a sophisticated overall concept and a multitude of magnetic delivery carriers have been developed. Targeting mechanism-exploiting, tumor-specific attributes are becoming more and more sophisticated. The same is true for controlled-release strategies for the diseased site (Gómez-Sotomayor et al., 2015; Tietze et al., 2015).

Lipid vesicles are the first and most used nanoparticle drug delivery system which were later known as liposomes or nanoliposomes. It is formed by expontaneous self-assembly of amphiphilic phospholipids such as phosphatidylcholine, phosphatidylglycerol or phosphatidylserine, which can also be found in the human body (Abreu et al., 2011; Khosravi-Darani et al., 2010; Ochekepe et al., 2009). Hydrophilic drugs can be encapsulated into the central aqueous phase, while hydrophobic molecules can be embedded into the hydrophobic parts of the lipid bilayer (Fig. 1.3). Physicochemical properties of liposome can be precisely changed to control surface charge, size and functionality (Abreu et al., 2011). Currently, there are around ten liposomal-drug formulations for different conditions in clinical use and hundreds of ongoing clinical trials are registered by US Food and Drug Administration (FDA) (Ochekepe et al., 2009; Wang et al., 2012; Matsuzaki et al., 2012), The most common ones are DaunoXome (liposomal daunorubicin) for blood tumors, Doxil and Lipod-dox (PEGylated liposomal doxorubicin) for ovarian and breast cancers, and for Kaposi's sarcoma patients (Wang et al., 2012). There are currently few liposomal formulations with triggered drug release approved for clinical use or in early phases of clinical trials.

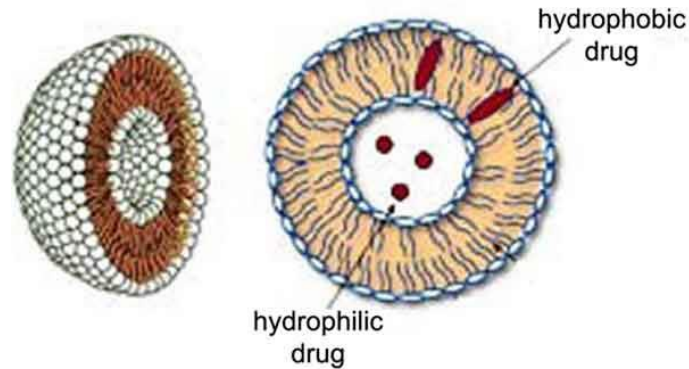


Fig. 1.3 General Structure of a liposome (Picture excerpted from article: Recent Progress in Liposome Production, Relevance to Drug Delivery and Nanomedicine; Koynova and Tenchov, 2015).

1.3 Sphingomyelinase in biological systems

Like phosphatidylcholine, sphingomyelin (SM) are considered as an important structural component and tends to be of the greatest concentration of the plasma membrane, especially in the outer leaflet of cells (Testi, 1996). SM and the enzyme sphingomyelinase (SMase), which converts SM to ceramide, are increasingly recognized as bioactive markers involved in numerous biological functions. Increase of SMase and/or ceramide have been confirmed to be associated with various cellular physiologic and pathophysiologic processes that include cell cycle, apoptosis and inflammatory responses. The most studied form of sphingomyelinases is acid form. Different stimuli including ionizing radiation, heat or chemotherapeutic drugs trigger a translocation of the acid sphingomyelinase (ASMase) localized in intracellular vesicles (Lysosome ASMase) to fuse with the cell membrane and expose the ASMase on the outer leaflet of the cell membrane (Secretory ASMase) (Grassme et al., 2001) (Fig. 1.4).

The release of ceramide from sphingomyelin by secretory ASMase in the cell membrane results in the formation of ceramide-enriched microdomains which serve the transmission of the stress signal into the cell. This sphingolipid ASMase / ceramide signaling pathway occupies a prominent position in principal physical and molecular early events induced at the plasma membrane after radiation (Corre et al., 2010; Vit and Rosselli, 2003).

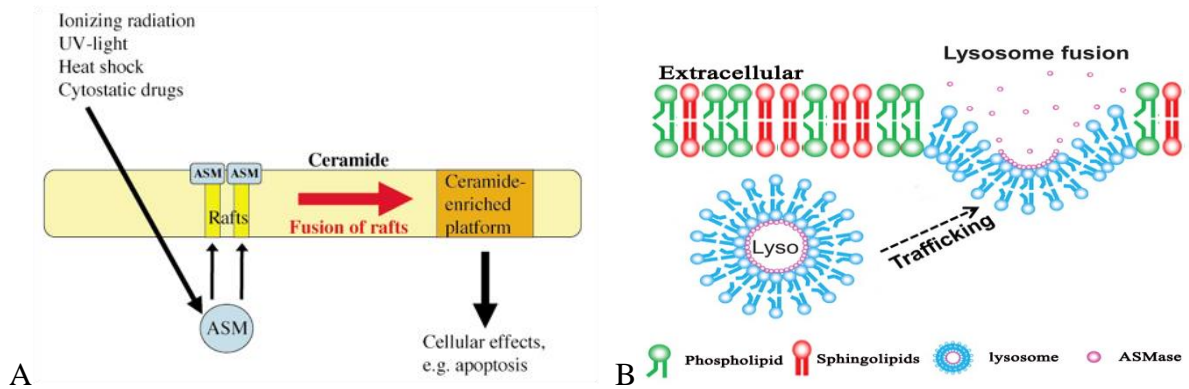


Fig. 1.4 (A) Different stimuli trigger a translocation of the ASMase onto the extracellular leaflet of the cell membrane. The formation of ceramide from sphingomyelin by ASMase in the cell membrane results in the formation of ceramide-enriched microdomains which serve the transmission of the stress signal into the cell (Picture excerpted from article: Ceramide in malignant tumors; Gunawardena et al., 2004). (B) ASMase transport to the extracellular part of PM from lysosome (Picture adapted from article: Membrane raft-lysosome redox signalling platforms in coronary endothelial dysfunction induced by adipokine visfatin; Xia et al., 2011).

The reaction product of SM, ceramide, has been regarded being part in apoptosis signaling by forming ceramide-enriched microdomains in cell membranes. It was shown in biophysical model membrane studies the ceramide domain formation in both fluid and gel state phosphatidylcholine membranes when ceramide has been added (Holopainen, et al., 1997; Huang et al., 1996). Ceramide-enriched microdomains have been shown to exclude cholesterol from cell membranes, alter membrane fluidity, change membrane curvature and induce transbilayer flip-flop (Megha and London, 2004; Rebillard, et al., 2007; Ira and Johnston, 2008; López-Montero, et al., 2005). The membrane invagination and vesiculation of the bilayer result from augmented bending rigidity of the ceramide-containing domains have been observed (Fig. 1.5) (Holopainen, et al., 2000; Nurminen, et al., 2002).

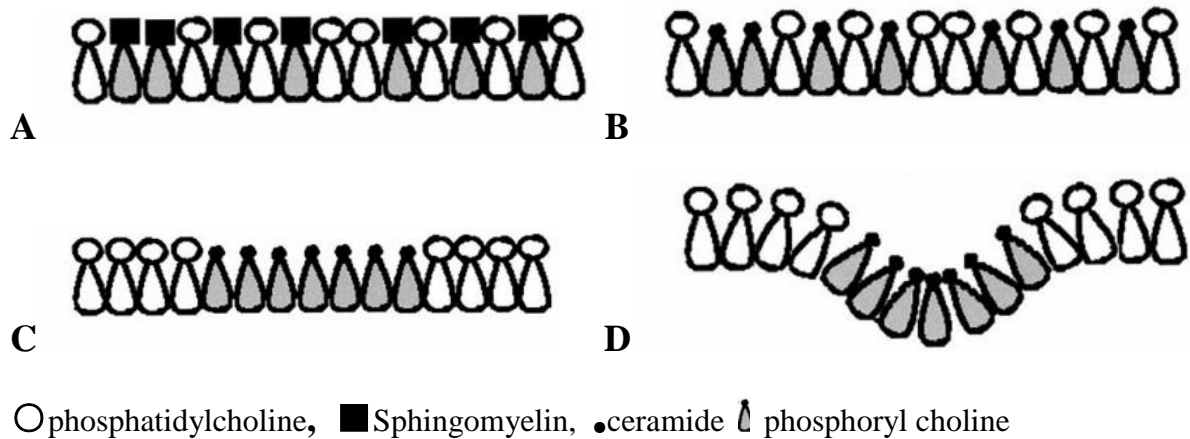


Fig. 1.5 (A) The lipids in the phosphatidylcholine /Sphingomyelin monolayer are randomly distributed; (B) Hydrolytic cleavage of the phosphocholine head group from SM by sphingomyelinase generates ceramide; (C) Leaflet containing ceramide condenses and the formed ceramide segregates into a domain (D) Tendency of ceramide to form inverted on-lamellar phases, an invagination is formed by the ceramide-enriched domain. (Picture excerpted from article: Vectorial budding of vesicles by asymmetrical enzymatic formation of ceramide in giant liposomes; Holopainen, et al., 2000).

1.4 Indocyanine Green (ICG) Fluorescent Imaging for Clinical Use

Fluorescence Imaging (FI) is one of the most popular imaging methods in biomedical sciences for visualization of cells and tissues. ICG is considered as an ideal contrast agent (820 nm wavelength NIR, near infrared) with minimal interference from tissue and blood auto-fluorescence (500-600 nm). It is a clinically approved NIR fluorescence dye and has been used in some medical applications routinely already for decades including retinal angiography, liver clearance tests and cardiac output monitoring (Nguyen and Tsien, et al., 2013). ICG has several excellent clinical properties: (i) patient safety: nontoxic and nonionizing, (ii) ideal for angiography: confinement to the vascular compartment through efficiently binding to blood lipoproteins, that is, it does not leak from circulation, (iii) short life time in blood circulation allowing repeated applications, (iv) good signal to noise ratio (SNR): there is not much NIR auto-fluorescence in tissue giving low noise background, (v) deep imaging: operates in tissue optical window (NIR) and (vi) simple and cheap imaging

devices. There have been very recently used ICG in sentinel lymph node navigation (SLN) detection in lung and prostate cancer patients (Jarmo et al., 2012; Zhang et al., 2008; Frangioni, 2008).

However, ICG is limited by its aqueous instability, concentration-dependent aggregation and rapid degradation for medical diagnosis (Jarmo et al., 2012; Kraft and Ho, 2014; Desmettre et al., 2000). To overcome these limitations, ICG encapsulated to liposomes was developed that can enhance ICG stability for light exposure and storage. It can also maximize ICG fluorescence intensity and stability (Fig. 1.6). Finally, liposome can be engineered to be multi-functional with the ability to target diseased tissue, carry imaging agents for detection and deliver multiple therapeutic agents for combined delivery.

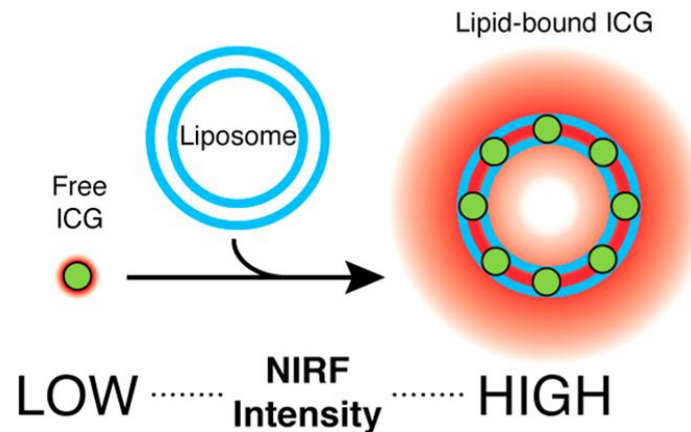


Fig. 1.6 ICG is incorporated into the hydrophobic domains of the lipid bilayer. (Picture excerpted from article: Interactions of Indocyanine Green and Lipid in Enhancing Near-Infrared Fluorescence Properties: The Basis for Near-Infrared Imaging in Vivo; Kraft and Ho, 2014).

1.5 The hypothesis of this study

Multimodal capabilities of nanoparticle delivery system offer the opportunity to develop novel approaches to deliver drugs that may result in alternative or complementary therapeutic options for the treatment of disease. Our research group has designed a magneto-enzymatic sensitive liposome (MESL), which contains ICG for fluorescent labeling and cisplatin as a

chemotherapeutic agent for targeted optical imaging and local drug release. The MESL contains sphingomyelin distinguish from previous liposomes other scientists researched. SM can be hydrolyzed by acid ASMase, which is excreted in site of cancer and thus subsequently causes a local enzymatic drug release from SM-liposomes. Iron particles added into the lipid bilayer of the liposome will amplify the activation process through Brownian motion on lipids, when alternating magnetic field (AMF) is used. When these two activation mechanisms are combined locally controlled drug release is possible. (Fig. 1.7).

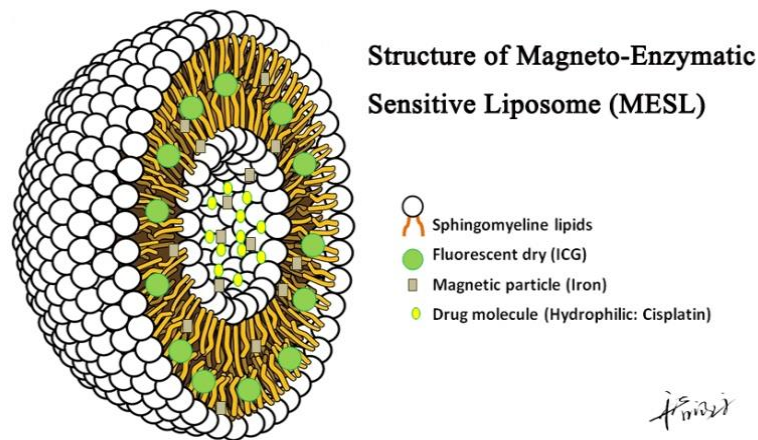


Fig. 1.7 Schematic representation of Magneto-Enzymatic Sensitive Liposome (MESL).

This environment sensing ICG-MESL probe has become optical/fluorescence changes after reacting with SMase and additional AMF, which can be detected and thus follow the fate of the liposomes in vivo. First objective was to study and find the optimal concentration of ICG in MESL for imaging purposes. We also wanted to quantify endogenous ASMase available in the squamous tumor cells. While our disease model as squamous cell carcinoma SCC9 and UDSCC2 cells were chosen to evaluate the ASMase activity. First, we studied ASMase activity in a situation where stress was induced through irradiation or cisplatin. HNSCC mice model is already established previously in our clinic for vivo studies. We wanted to study ASMase activity also in this mice model in which SCC9 cells were injected to grown in mice and further analyze the SMase activity in those tumors. Therefore, the aim of this study was to

evaluate the optical properties of environment sensing ICG-MESL probe; Vitro characterization of ASMase activity as a cell stress indicator in HNSCC; Vivo characterization of ASMase activity of mice tumor and muscle.

2. Methods

2.1 Optical properties of environment sensing ICG-MESL probe

2.1.1 Fluorescence of ICG-MESL and pure ICG in blood

Fluorescent dye of ICG (Sigma, Germany) was diluted into 0.033 mg/ml, 0.066 mg/ml, 0.165 mg/ml, and 0.330 mg/ml with PBS (Biochrom, Germany). 10 μ l of different concentration of ICG was added into 4-strip PCR tubes (Thomas Scientific, Germany) together with 90 μ l blood and mixed carefully. Four-strip PCR tubes were placed on a phantom and measured in the fluorescence molecular tomography (FMT2500) image system (Perkin Elmer, USA) which is commonly applied for quantitative three-dimensional (3D) vivo imaging (Fig. 2.1). Images were created and analyzed with TrueQuant (GenxPro, USA). Each experiment was performed in triplicate.

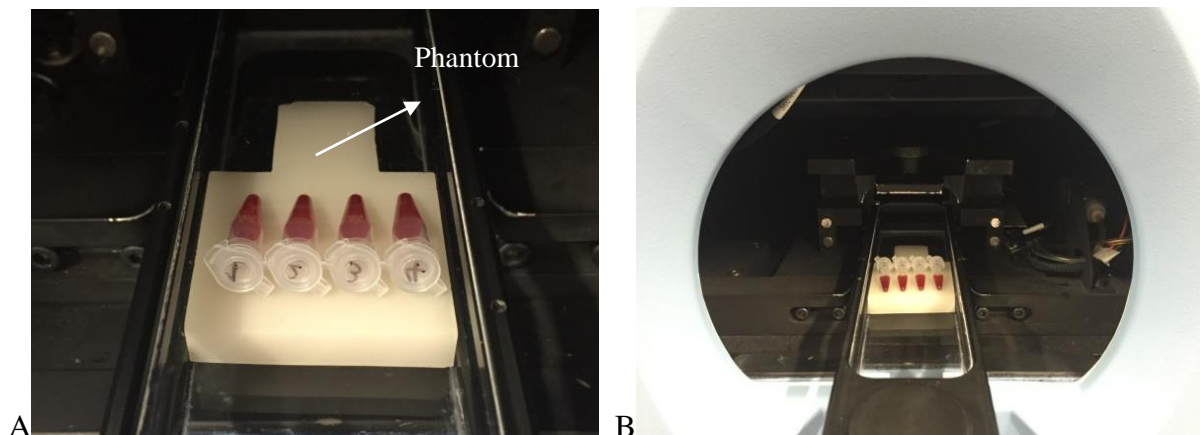


Fig. 2.1 Fluorescence of ICG was measured by fluorescence molecular tomography (FMT).

Setting the parameters of FMT program as below: Laser Channel: 790 nm; Agent: 800 conjugates; Cassette Depth: 19 mm. Reflectance image areas were captured and modified manually as we needed (72 points). Regions of interest (ROIs) were drawn with the same size of ellipsoid around the tubes and the mean value of the fluorescent signal outputs automatically (Fig. 2.2).

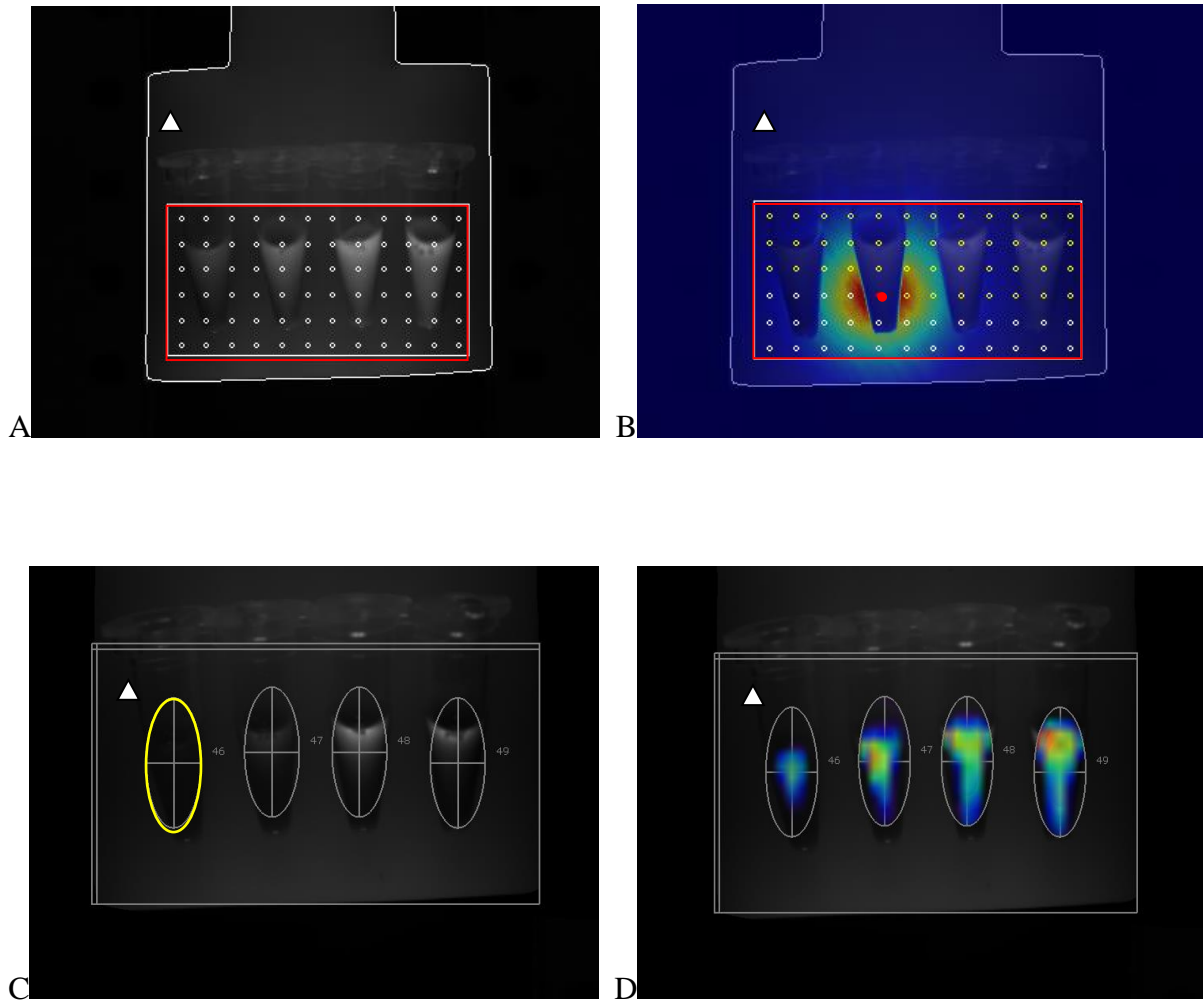


Fig. 2.2 (A) Capture the reflectance image area (Red rectangle). (B) Measuring the fluorescence point by point (\triangle phantom \bullet measuring point). (C) Regions of interest (ROIs) was drawn with the same size of ellipsoid around the tubes (Yellow ellipsoid). (D) Fluorescent signal of pure ICG.

MESL was from Prof. Oula Penate Medina's research group, Molecular Imaging North Competence Center (MOIN CC), University Hospital Schleswig-Holstein Campus Kiel (UKSH). MESL containing varying concentration of ICG (0.05 mg/ml, 0.10 mg/ml, 0.25 mg/ml, and 0.50 mg/ml) was diluted into the final ICG concentration of 0.033 mg/ml, 0.066 mg/ml, 0.165 mg/ml and 0.330 mg/ml in PBS. Fluorescence was measured as described previously. Each experiment was performed in triplicate.

2.1.2 Fluorescence change of ICG-MESL with SMase

MESL containing varying concentration of ICG (0.05 mg/ml, 0.10 mg/ml, 0.25 mg/ml, and 0.50 mg/ml) were diluted into the final concentration of 0.033 mg/ml, 0.066 mg/ml, 0.165 mg/ml and 0.330 mg/ml in PBS. 10 μ l of different concentration of ICG-MESL was added into 4-strip PCR tubes together with 90 μ l blood and 10 μ l of 1.0 U/ml SMase (from *B. cereus*; Sigma, Germany). Samples were mixed carefully and incubated in the room temperature for 10 minutes. 10 μ l PBS instead of SMase was added into the control group. Measurement and analysis were done as previously described. Each experiment was performed in triplicate.

2.1.3 Fluorescence change of ICG-MESL with SMase and AMF

ICG loaded MESL was prepared containing 0.330 mg/ml ICG in PBS. 10 μ l of this ICG-MESL was added into 4-strip PCR tubes together with 90 μ l blood. The samples were measured for the first time. Then 10 μ l different concentration of SMase was added, resulting final activities of 0.364 U/ml, 0.727 U/ml, 1.091 U/ml and 1.454 U/ml. The samples were measured after 20 minutes incubation in the room temperature. The AMF group of 4-strip PCR tubes was treated with AMF for additional 20 minutes incubations in room temperature before measurement (Fig. 2.3). The fluorescence percentage increases of each sample were compared. Each experiment was performed in triplicate.

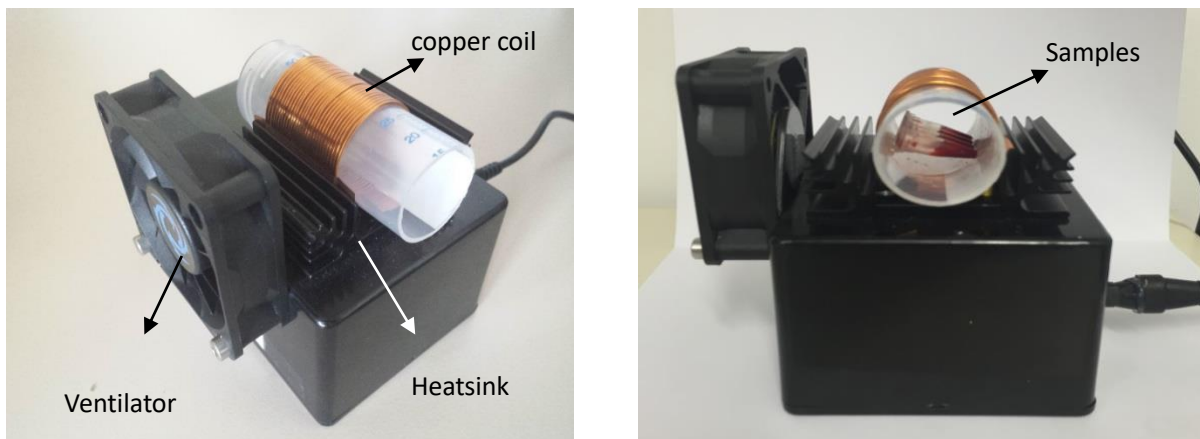


Fig. 2.3 AMF device where the coil size allows samples to be treated.

2.2 In vitro characterization: ASMAse activity as a cell stress indicator in HNSCC lines

2.2.1 Preparation of carcinoma cells

2.2.1.1 Culture of carcinoma cells

SCC9 cell lines were kindly provided by Prof. Yahya Açı, Scientific laboratories, department of Oral and Maxillofacial, Plastic Surgery, UKSH. Cells were maintained in a complete medium containing DMEM (Biochrom, Germany) supplemented with 10% FCS (HyClone, UK), 100 IU/ml of penicillin (Biochrom, Germany), 100 µg/ml of streptomycin (Biochrom, Germany) and 400 ng / ml hydrocortisone (Biochrom, Germany). Cells were cultivated in 5% CO₂ humidified atmosphere at 37 °C. Medium was changed every three days.

UDSCC2 cell lines were kindly provided by Dr. Tibor Görögh, Clinic of Ear, Nose, Throat, Head and Neck Surgery, UKSH. Cells were maintained in a complete medium containing DMEM supplemented with 10% FCS, 100 IU/ml of penicillin, and 100 µg/ml of streptomycin. Cells were cultivated in 5% CO₂ humidified atmosphere at 37 °C. Culture medium was refreshed every three days.

2.2.1.2 Passage of carcinoma cells

Until the cells reached 60–80% confluences, cells were harvested by tryptic digestion. Medium was aspirated, cells were washed with warmed PBS and detached by 5 minutes incubation in 0.01% trypsin-EDTA (Biochrom, Germany) at 37 °C. The suspension was transferred to a sterile 50 ml falcon tube with cell culture medium to neutralize the trypsin reaction and centrifuged at 1200 rpm for 5 minutes. After aspirating the supernatant, the cells were resuspended in a small volume of cell culture medium and counted with hemocytometer. Finally, 1×10^5 cells were subculture in 75 cm² cell culture flasks.

2.2.1.3 Cell frozen of carcinoma cells

After centrifugation prior to harvesting and counting of cells, the pellet of cells was resuspended in warm cryopreservation medium containing 90% FCS, 10% DMSO (Sigma, USA) in a final concentration of 1×10^6 per vial. The vials were maintained in an alcohol freezing container and transferred to a -80 °C refrigerator in which the vials were cooled

slowly, at approximately 1 °C every minute, until they reach -80 °C. The cells were stored at -80 °C overnight prior to transfer to a liquid nitrogen container for long term storage.

2.2.2 Preparation of Keratinocyte

2.2.2.1 Culture of Keratinocyte

Keratinocyte cell lines were kindly provided by Prof. Dr. Yahya Açı, Head of the scientific laboratories, department of Oral and Maxillofacial, Plastic Surgery, UKSH. Keratinocyte were maintained in Defined Keratinocyte- serum free medium (Defined K-SFM; Gibco, USA) supplemented with 0.005 µg/ml EGF human recombinant (Gibco, USA) and 0.05 mg/ml bovine pituitary extract (Gibco, USA), 100 IU/ml of penicillin, 100 µg/ml of streptomycin. Cells were cultivated in 5% CO₂ humidified atmosphere at 37 °C. Medium change took place every two days until the cells reached 60–80% confluences.

2.2.2.2 Passage of Keratinocyte

The medium was aspirated and the cells were harvested by washing with warmed PBS when the cells reached 60–80% confluence. All the cells were detached by brief incubation in 1.5 ml accutase (PAA, Austria) at 37 °C. The suspension was transferred a sterile 50 ml falcon tube with Defined K-SFM medium to neutralize the enzyme reaction and centrifuged at 1200 rpm for 5 minutes. After aspirating the supernatant, the cells were resuspended in a small volume of cell culture medium and counted using a hemocytometer. Finally, 1×10^5 cells subculture in 75 cm² cell culture flask. Keratinocyte at passage 2-3 were used in the experiment (Fig. 2.4).

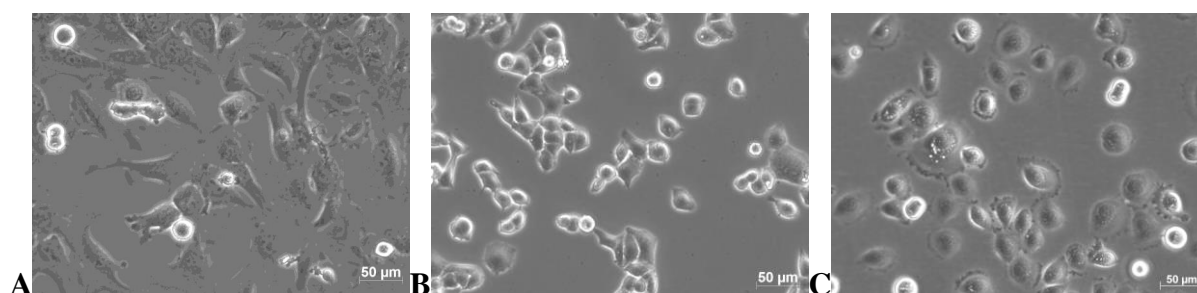


Fig. 2.4 SCC9 (A), UDSCC2 (B), Keratinocyte (C) under the electron microscope (phase contrast microscope $\times 20$).

2.2.3 ASMase activity as a cell stress indicator after irradiation

2.2.3.1 Cells preparation for irradiation

Half million of SCC9 or UDSCC2 cells were subculture in 75 cm² cell culture flask day before. The complete medium was aspirated carefully and changed the medium to 3 ml of PBS to each flask just before irradiation.

Three different doses of irradiation (12 Gy, 24 Gy and 36 Gy) were given to the cells. Control group was treated otherwise similarly but without irradiation. Supernatant was preserved immediately after irradiation for the measurement of ASMase activity. Each experiment of SCC9 and UDSCC2 was performed in triplicate.

Three flasks of Keratinocytes were treated with irradiation (24 Gy) and another three kept as controls. Supernatant from the cell flasks was collected immediately after irradiation for the measurement of ASMase activity. Experiment was performed three times.

2.2.3.2 ASMase activity measurement after irradiation

ASMase activity was measured using an Amplex Red Sphingomyelinase Assay Kit (Thermo Fisher, Germany). The kit utilizes a multi-enzyme reaction that generates a fluorescent product, equal to produced ceramide, to quantify ASMase activity. A two-step assay of SMase activity was performed according to the manufacturer's instructions. The SMase reaction was carried out in an acidic buffer. 50 µl of acidic reaction buffer (50 mM sodium citrate, pH 5.0), 10 µl of 5 mM sphingomyelin in 2% Triton-X were added to each well of a 96-well plate prior to the addition of 50 µl supernatant of cells treated with irradiation. The reactions were incubated at 37 °C for 60 minutes. Phosphocholine (end product of lysis) detection reaction was carried out in a neutral pH environment. 100 µl of base-buffered Amplex Red detection solution (100 µM Amplex Red, 2 U/ml horseradish peroxidase, 0.2 U/ml choline oxidase, 8U/ml alkaline phosphatase, 100 mM Tris-HCl, pH 8.0) was added to each well. The reaction was incubated at 37 °C for 30 min. Fluorescence values were determined by SPECTRAFLUOR Plus (Tecan, Germany) using an excitation filter of 550 nm and an emission filter of 595 nm. Wells containing hydrogen peroxide solution were incorporated as positive reaction controls. Fluorescence values were corrected by subtracting the background

fluorescence represented by blank wells containing only acidic reaction buffer, sphingomyelin, and base-buffered Amplex Red detection solution. Each experiment was performed in triplicate.

2.2.3.3 Evaluation of cell lines viability after irradiation

MTT assay (Roche, Germany) was applied to evaluate the viability of the treated cells. MTT salt is cleaved by mitochondrial dehydrogenase in the metabolic active cells and is reduced to an insoluble formazan crystal which displays a purple color. The color was detected by a scanning multi-well spectrophotometer (Molecular Devices, USA).

Carcinoma cells were seeded at a density of 5×10^4 cells/well in 96-well plate. Three different doses of irradiation (12 Gy, 24 Gy and 36 Gy) were given. Another two plates were prepared, one for control and the other one as standard curve without irradiation. Serial dilutions (1:2) were made using complete medium as the diluents. Cell densities ranged from approximately 50,000 to 780 cells/well in 100 μ l medium with 3 replicates per density. Cells were allowed to grow overnight at 37 °C in a humidified 5% CO₂ environment.

Keratinocyte were seeded at a density of 5×10^4 cells/well in 96-well plate and treated with irradiation 24 Gy. Another two plates were prepared, one for control and the other one as standard curve without irradiation. Serial dilutions (1:2) were made using complete medium as the diluents. Cell densities ranged from approximately 50,000 to 780 cells/well in 100 μ l medium with 3 replicates per density. Cells were allowed to grow overnight at 37 °C in a humidified 5% CO₂ environment.

Supernatant of each well was aspirated 6 hours after irradiation, and 10 μ l of MTT (5 mg/ml) with 90 μ l complete medium were added to wells and the plates which were incubated for 4 h at 37 °C. 100 μ l of solubilization buffer (10% SDS in 0.01M HCl) was added to the wells and the plates were incubated at 37 °C overnight. After the incubation, the absorbance was measured at 550 nm in a scanning multi well spectrophotometer (Molecular Devices, USA).

2.2.3.4 Cisplatin release from Cisplatin-MESL after irradiation

The SCC9 cells (5×10^5) were subcultured in 75 cm² cell culture flask day before the treatment.

Nine flasks were prepared for three different doses of irradiation and three flasks were prepared without irradiation as control group. Just before irradiation, culture medium was replaced with 3 ml PBS as described previously. After irradiation 500 μ l of cisplatin loaded MESL (Cisplatin-MESL) were added to each flask and incubated for an hour at room temperature in shaking. The media from flask was collected and dialyzed against 45 ml PBS for 24 hours in Snake Skindialysis bag (Thermo Scientific, Germany) (Fig. 2.9). Released cisplatin from outside of the Snake Skin dialysis bag and cisplatin loaded in MESL inside were analyzed by measuring the absorbance at 301 nm in spectrometer (Agilent, Germany). The percentage release of cisplatin was calculated and background corrected by the control group. Experiment was performed in triplicate.

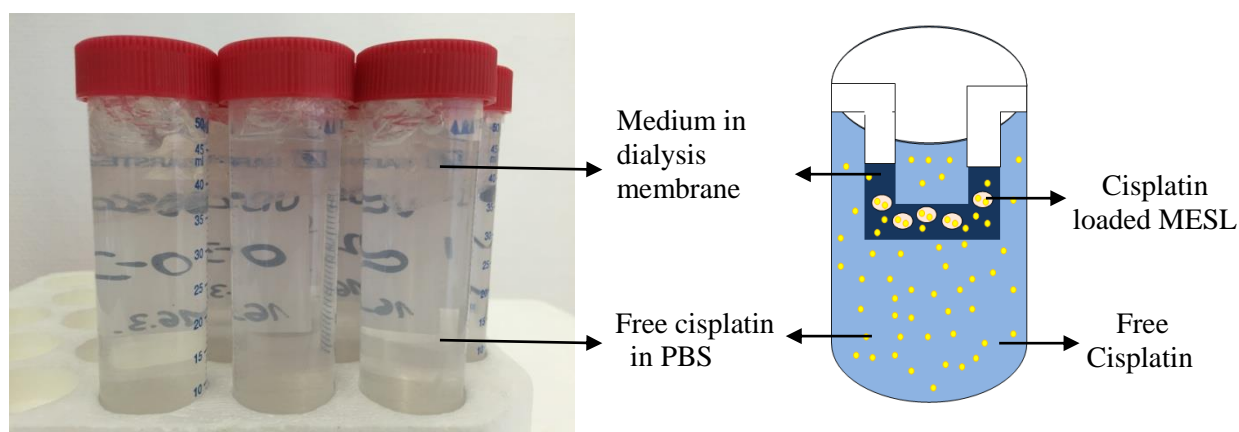


Fig. 2.9 The media was collected and dialyzed against PBS for twenty-four hours in shaking.

2.2.3.5 ASMase inhibition study in SCC9 after irradiation

Half million SCC9 cells were subculture in 75 cm² cell culture flask day before. Media were aspirated and cells were cultured with 10 ml fresh medium containing 100 μ l/ml desipramine (dissolved in 304 μ l ethanol), ASMase inhibitor (Elojeimy, et al., 2006). For control cells 304 μ l of plain ethanol was added. The inhibitor was incubated for 2 hours at 37 °C in a humidified 5% CO₂ environment and then the medium was changed to 3ml PBS before the cells were subjected to irradiation (24 Gy). Cells treated without ASMase inhibitor or without irradiation were used as control groups. After irradiation, ASMase activity was measured and ability to release the cisplatin was studied as previously described (2.3.3.4 and 2.3.4). The experiments were performed three times.

2.2.4 ASMase activity as a cell stress indicator after cisplatin treatment

2.2.4.1 Cells preparation for cisplatin treatment

Cells (SCC9 or UDSCC2) were prepared day before the experiment. Serial dilutions (1:2) were made using complete medium as the diluents. Cell densities ranged from approximately 15,000 to 234 cells/well in 100 μ l medium with 3 replicates per density as a standard curve. The treatment group were seeded at a density of 1.5×10^4 cells/well in 96-well plate. Cells were allowed to grow overnight at 37 °C in a humidified 5% CO₂ environment.

2.2.4.2 ASMase activity measurement after cisplatin treatment

Medium was removed and replaced with 100 μ l of different concentration (0 μ M as control, 0.1 μ M/ml, 1 μ M/ml, 10 μ M/ml and 100 μ M/ml) of cisplatin (Sigma, Germany) diluted in serum-free medium. Cells were treated with the drug for 12 hours, 24 hours and 48 hours and the incubation was terminated at the same time in all groups. Fifty μ l supernatant were transferred to a new 96-well plate and ASMase activity from the supernatant was measured using an Amplex Red Sphingomyelinase Assay Kit as described previously. Experiment was carried out in triplicate.

2.2.4.3 Evaluation of cell lines viability after cisplatin treatment

After ASMase activity measurement, the medium was removed, 10 μ l of MTT (5 mg/ml) with 90 μ l complete medium were added to each well and the plate was incubated for 4 h at 37 °C. Then 100 μ l of solubilization buffer (10% SDS in 0.01 M HCl) was added to the wells and the plates were incubated at 37 °C overnight. After the incubation, the absorbance was measured at 550 nm in a scanning multi well spectrophotometer (Spectra max plus, Molecular Devices). Standard curve derived from automatically.

2.3 In vivo characterization: aSMase activity of HNSCC and muscle in mouse

2.3.1 HNSCC mouse model

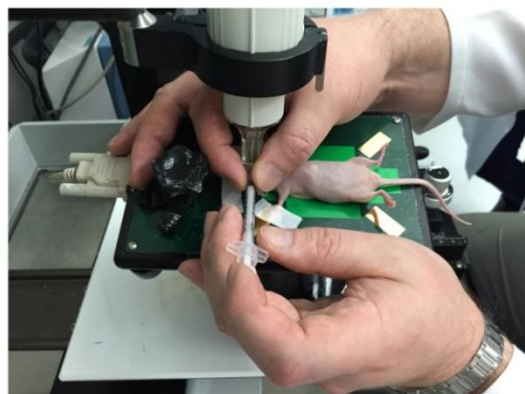
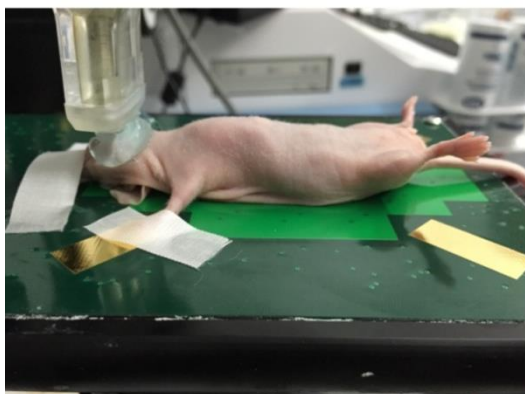
2.3.1.1 Cells preparation for HNSCC mouse

Five million SCC9 cells in 1 ml complete medium were transferred to the Eppendorf tube,

and centrifuged at 1200 rpm for 5 minutes. After aspirating the supernatant, the cells were resuspended with 100 μ l PBS carefully and cooled for 10 minutes on ice. 100 μ l Matrigel (Corning, Germany) kept at low temperature was combined with precooled cell suspension, resulting in a final cell concentration of 2.5×10^7 cells / ml. All equipment and reagents, including syringes (Becton, USA), pipettes, and sterile Eppendorf tubes are chilled on the ice prior to injection. 20 μ l cell suspension with matrigel was filled into the precooled syringes, resulting in a final cell number 5×10^5 cells / syringe.

2.3.1.2 Mouse model construction

Ten NMRI-Foxn1nu/foxn1nu female Mice were obtained from Roger JANVIER (Roger JANVIER, Germany) at the age of 5 weeks and quarantined for one week before use. The animal experiments were performed in accordance with the German ethical approval of animal experiments and had received approval by institute authorities. Mice were anesthetized with 1-2% isoflurane and injected at the middle of the mouth floor for SCC9 xenografts under the guidance of small animal ultrasound (Fig. 2.12). All mice were kept in a temperature and humidity-controlled environment with a 12-hour light-dark-cycle and access to food and water ad libitum. The mice were observed for tumor's growth every week with small animal ultrasound until the 50th day after implantation.



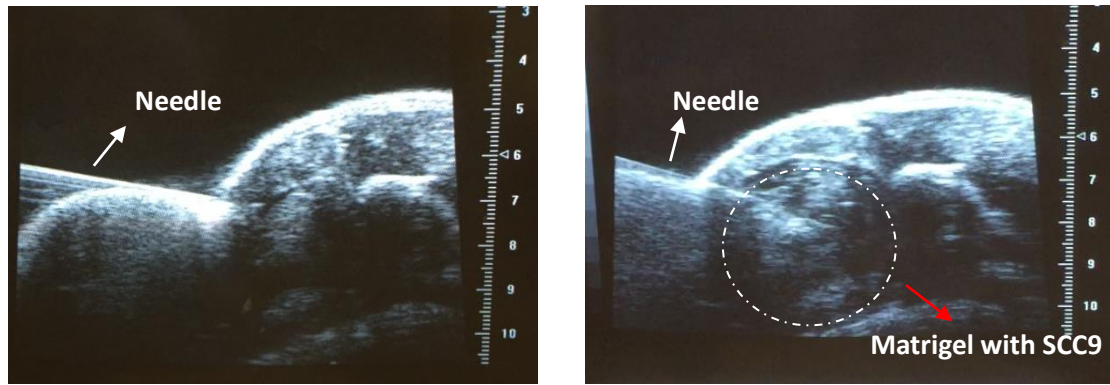


Fig. 2.12 Implantation of SCC9 xenografts in the middle of mouth floor under the guidance of small animal ultrasound.

2.3.2 ASMase activity of HNSCC and muscle in mouse

Ten mice were sacrificed, and two samples of each mouth floor carcinoma and hind leg muscle were excised from each mouse. The weight of the tissue samples was scaled and 100 μ l of acidic reaction buffer (50 mM sodium citrate, pH 5.0), 10 μ l of 5 mM sphingomyelin in 2% Triton-X were added. The samples were shaken at 350 rpm at 37 °C for 60 min (Thermomixer comfort). ASMase activity was measured as follows: 100 μ l supernatant was transferred to 96-well plates, and 100 μ l of base-buffered Amplex Red detection solution (100 μ M Amplex Red, 2 U/ml horseradish peroxidase, 0.2 U/ml choline oxidase, 8U/ml alkaline phosphatase, 100 mM Tris-HCl, pH 8.0) was added to each well. The detection reactions were incubated at 37 °C for 30 min. Fluorescence values were detected as described previously and ASMase activity was standardized by weight of the samples.

3. Results

3.1 Optical properties of environment sensing ICG-MESL probe

3.1.1 Fluorescence of ICG-MESL and pure ICG in blood

The fluorescence signal between ICG-MESL and pure ICG was compared to identify the optical properties of ICG in different environment. The signal of ICG-MESL is significantly higher than pure ICG in the concentrated dilution ($p < 0.01$). The fluorescence signal of ICG-MESL climbed dramatically with linear concentration effects. Nevertheless, the fluorescence of pure ICG increases until it reaches a plateau at the concentration of 0.0165 mg/ml (Fig. 3.1). It appears that ICG-MESL has apparent advantage when measuring fluorescence intensity.

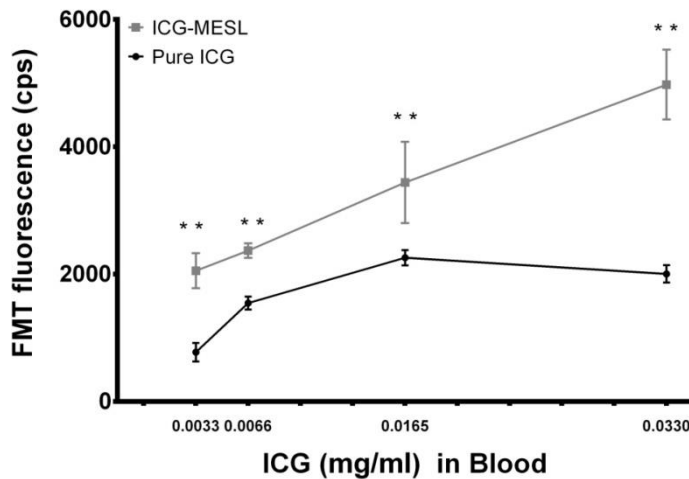


Fig. 3.1 FMT fluorescence of ICG-MESL and pure ICG in blood. Lines denote the mean \pm standard error of the mean (SD). **, $p < 0.01$, Independent-Sample T-Test

3.1.2 Fluorescence change of ICG-MESL with SMase

Effects in fluorescence after enzymatic manipulation of MESL was studied. The significant increase of signal was observed in the ICG-MESL at the concentration of 0.030 mg/ml ($p < 0.01$) (Fig. 3.2). This concentration we chose to use in the future in vitro and cell studies and in the animal experiment. The enzymatic treatment did not have any effect in pure ICG

fluorescence as expected.

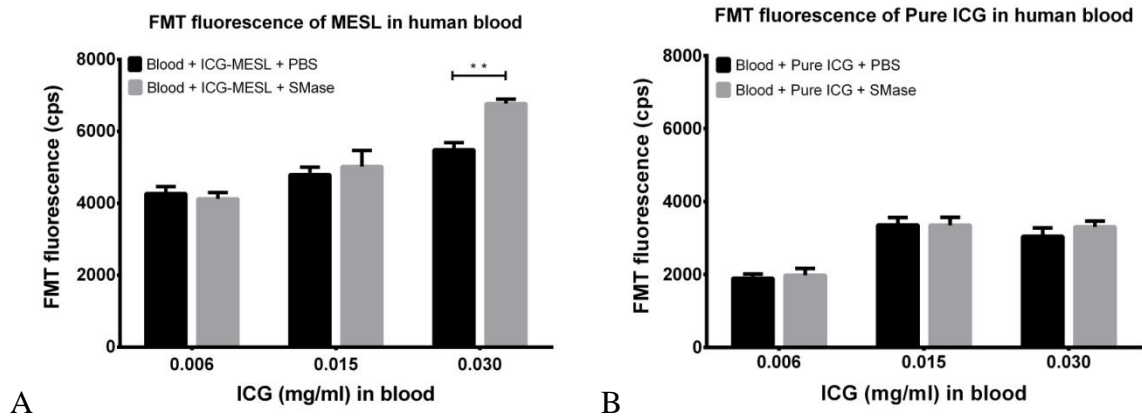


Fig. 3.2 (A) FMT Fluorescence change of ICG-MESL after adding 10 μ l 1.0 U/ml SMase. (B) FMT Fluorescence change of pure ICG after adding 10 μ l 1.0 U/ml SMase. Columns denote the mean \pm SD, **, $p < 0.01$, Independent-Sample T-Test.

3.1.3 Fluorescence change of ICG-MESL with SMase and AMF

Synergistic effects of SMase and AMF treatment in ICG-MESL (0.030 mg/ml) were studied. The fluorescence signal increases both after adding enzyme and additional AMF. AMF could significantly increase the FMT fluorescence compared with only adding SMase in some groups (Fig. 3.3). Some synergistic effect could be seen when higher SMase activities were used

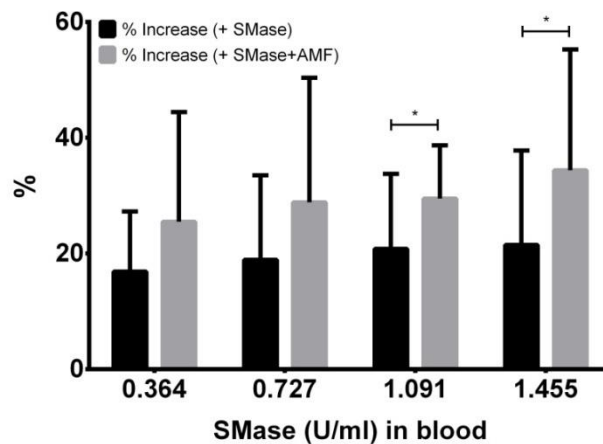


Fig. 3.3 Percentage increase of FMT fluorescence after adding SMase without /with AMF. Columns denote the mean \pm SD, *, $P < 0.05$, Paired-Samples T-Test.

3.2 In vitro characterization: ASMase activity as a cell stress indicator in HNSCC lines

3.2.1 ASMase activity of SCC9 and UDSCC2 after irradiation

ASMase activity after irradiation caused stress was measured using Amplex Red Sphingomyelinase Assay Kit. Quantitative calculation of the SMase release was done according to the standard curve. The SMase release was corrected with control group (without irradiation). High doses (24 Gy, 36 Gy) of irradiation could trigger significantly more ASMase in supernatant than low doses (12 Gy) in SCC9 (Fig. 3.4A). Dose response of SMase release was observed after different intensity of irradiation in UDSCC2 (Fig. 3.4B). UDSCC2 are significantly more sensitive than SCC9 in triggering the ASMase activity in the high doses of irradiation (Fig. 3.4C). Cells viability was measured by MTT assay 6 hours after irradiation. No significant differences were observed among different doses of irradiation or different cell lines. ($p \geq 0.05$, Independent-Sample T-Test) (Fig. 3.4D).

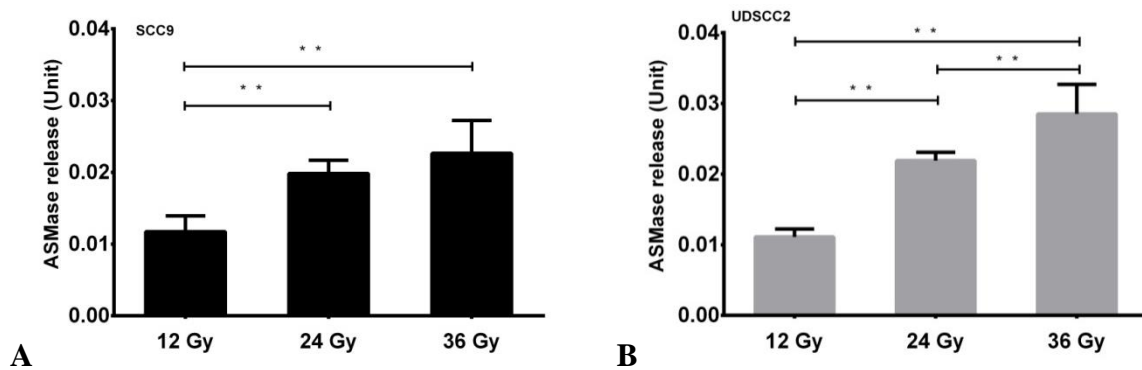


Fig. 3.4 (A) SMase increase of SCC9 after different doses of irradiation. (B) SMase increase of UDSCC2 after different doses of irradiation. Columns denote the mean \pm SD, **, $p < 0.01$, Independent-Sample T-Test.

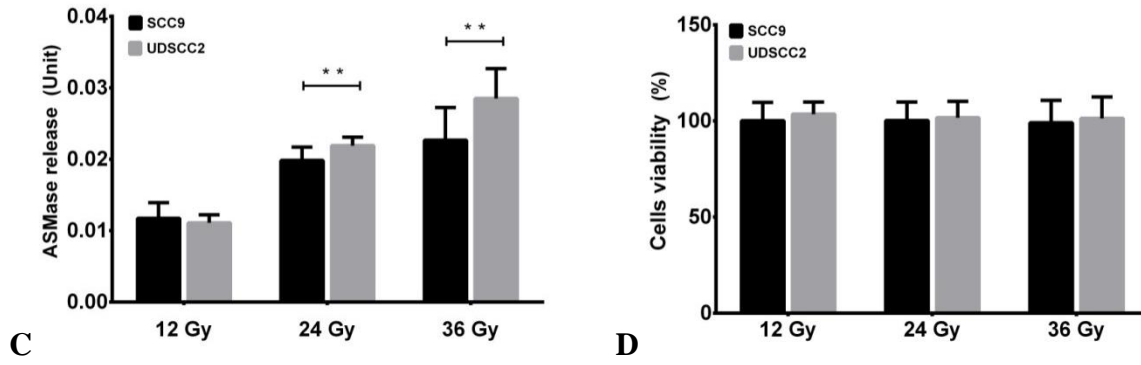


Fig. 3.4 (C) Comparison of SMase increase in SCC9 and UDSCC2 after different doses of irradiation. Columns denote the mean \pm SD, * $p < 0.05$, Independent-Sample T-Test. (D) Cells viability of SCC9 and UDSCC2 after different doses of irradiation (measure in 6 hours later). Columns denote the mean \pm SD, $p \geq 0.05$, Independent-Sample T-Test.

3.2.2 ASMase activity of Keratinocyte after irradiation

We wanted to study irradiation response of normal keratinocyte grown from patient samples. The ASMase activity in Keratinocyte was studied to compare the regular tissue cells with carcinoma cells. ASMase activity of Keratinocyte is significantly lower than in both SCC9 and UDSCC2 cells after 24 Gy irradiation (Fig. 3.5A). Cells viability was measured with MTT assay 6 hours after irradiation. No significant differences were observed with different cell lines after 24 Gy irradiation. ($p \geq 0.05$, Independent-Sample T-Test; Fig. 3.5B).

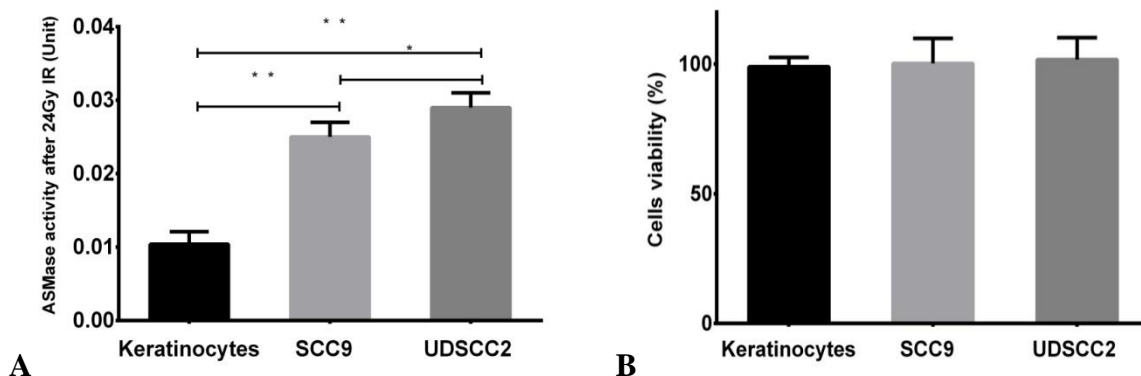


Fig. 3.5 ASMase activity (A) and cells viability (B) of Keratinocyte, SCC9 and UDSCC2 after 24 Gy irradiation. Columns denote the mean \pm SD, *, $p < 0.05$, **, $p < 0.01$, Independent-Sample T-Test.

3.2.3 Cisplatin release from Cisplatin-MESL after irradiation (SCC9)

While we have shown that the radiation increases ASMase activity in SCC9 and UDSCC2 cell media, we wanted to study if this enzymatic activity enough to cause drug release from Cisplatin-MESL like we have previously shown in our vitro studies. The experiment shows that Cisplatin could be released from Cisplatin-MESL and that the release is dose-dependent (Fig. 3.6A).

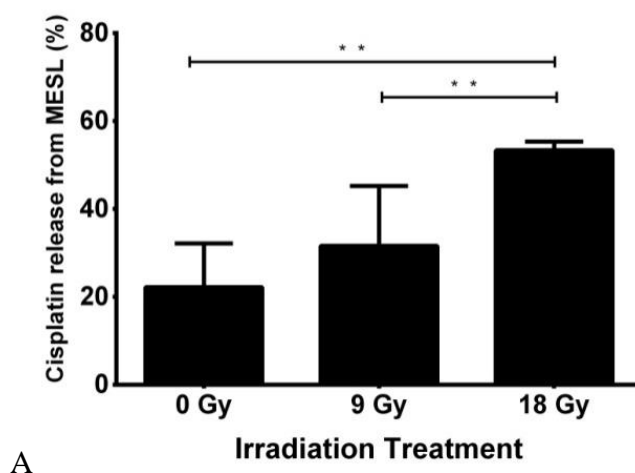


Fig. 3.6 (A) Cisplatin release from Cisplatin-MESL after different doses radiotherapy. (SCC9).

** , $p < 0.01$, Independent -Sample T-Test.

3.2.4 ASMase inhibition study in SCC9 after irradiation

While we have shown that the ASMase activities enough to cause drug release from Cisplatin-MESL after irradiation, we wanted to extra proof if enzymatic activities are necessary to cause drug release. Desipramine, SMase inhibitor, inhibits ASMase activity of SCC9 after 24 Gy irradiation. UDSCC2 was not tested yet. ASMase activity in desipramine group is significant lower than in normal treated group (Fig. 3.7A). Desipramine, SMase inhibitor, not only inhibits the ASMase activity after irradiation, also inhibits the release of cisplatin from Cisplatin-MESL after 24 Gy irradiation (Fig. 3.7B).

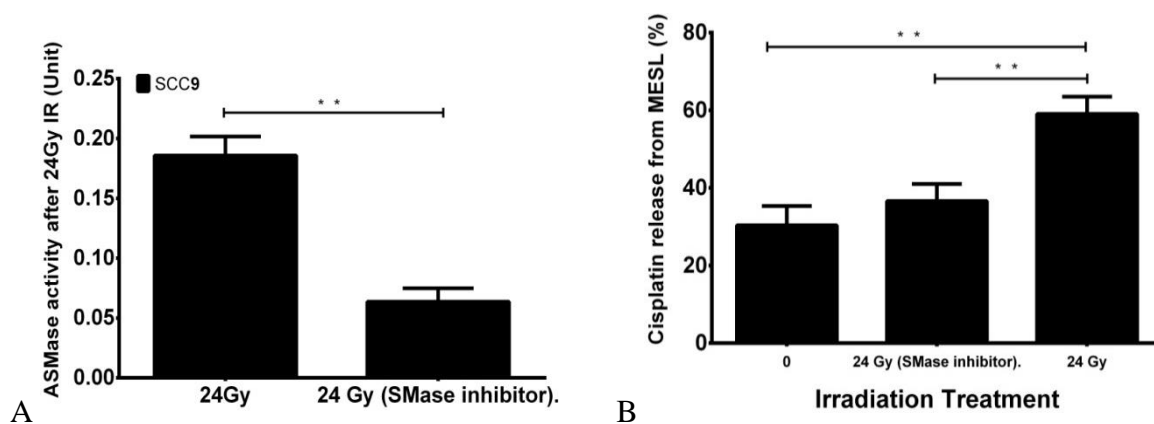


Fig. 3.7 (A) Desipramine, SMase inhibitor, inhibits ASMase activity in SCC9 after 24 Gy irradiation. Columns denote the mean \pm SD, $p \geq 0.05$, Independent-Sample T-Test. (B) Cisplatin release from Cisplatin-MESL of desipramine treated SCC9 compare with control groups after 24 Gy radiotherapy. Columns denote the mean \pm SD, **, $p < 0.01$, Independent-Sample T-Test.

3.2.5 ASMase activity as a cell stress indicator after cisplatin treatment

While it has shown previously that irradiation treatment increases ASMase activities, we wanted to study how other stress inducer, cisplatin treatment, effects SCC9 and UDSCC2 cells. ASMase activity was measured by Amplex Red Sphingomyelinase Assay Kit. Quantitative calculation of the ASMase activity was calculated from standard curve which was done analyzing fluorescence of the known SMase activities. The SMase activity is background corrected with control group. SMase activity of UDSCC2 showed marked significance as well a dose response of cisplatin in 48 hours treatment. Significant increases of SMase activity and decrease of cell viability were observed with treatment time of higher dose cisplatin. Similar phenomenon was not seen in the SCC9 (Fig. 3.7).

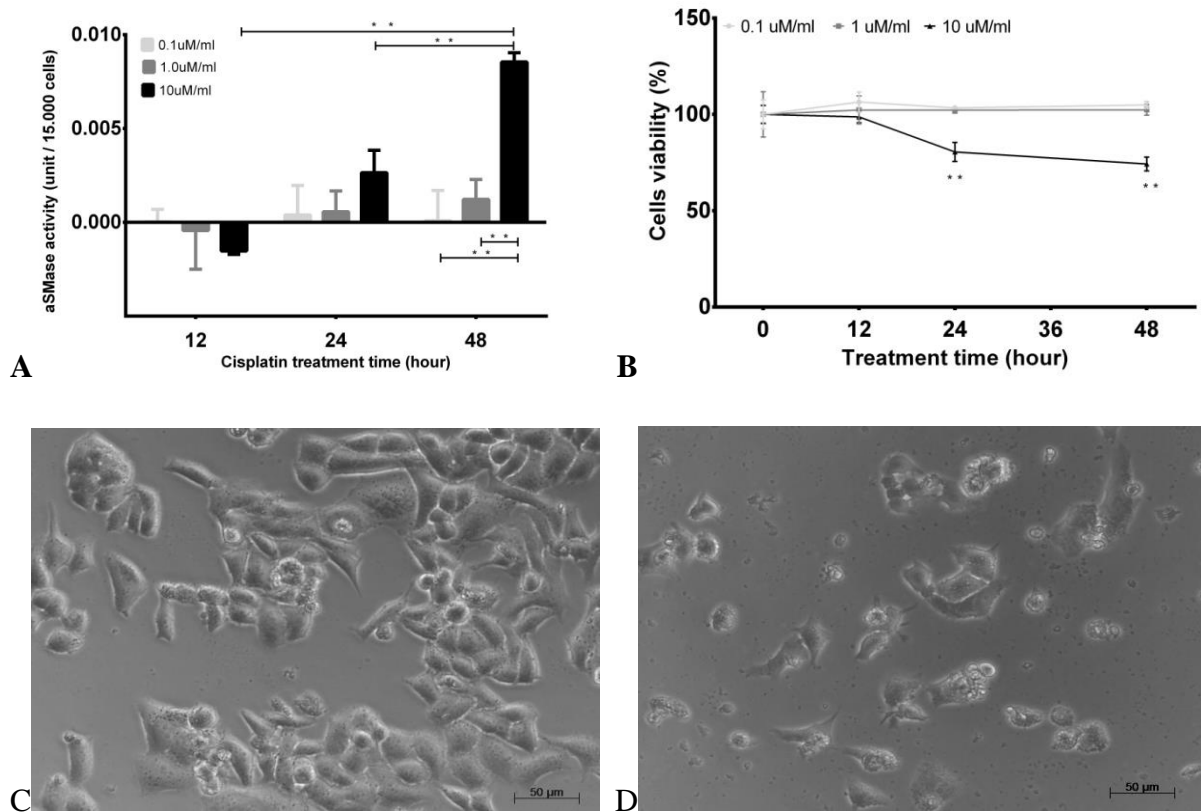
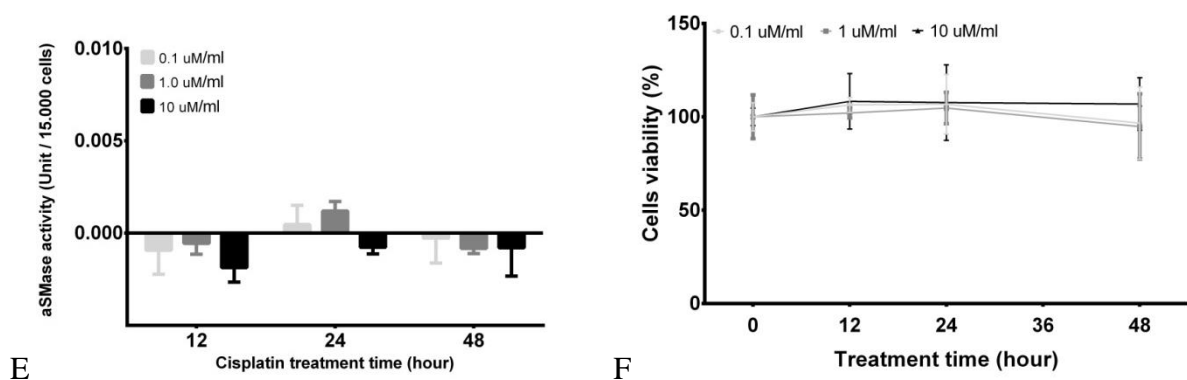


Fig. 3.7 (A) ASMase activation after different concentration of cisplatin treatment (0.1 $\mu\text{M}/\text{ml}$, 1.0 $\mu\text{M}/\text{ml}$ and 10 $\mu\text{M}/\text{ml}$) for different times (12 hours, 24 hours and 48 hours) in UDSCC2. (B) Cells viability after cisplatin treatment for different times. Columns and lines denote the mean \pm SD**, $p < 0.01$, Independent-Sample T-Test. (C) UDSCC2 Cells before cisplatin treatment. (D) Cells after 10 $\mu\text{M}/\text{ml}$ cisplatin treatment for 48 hours (Phase contrast microscope $\times 20$).



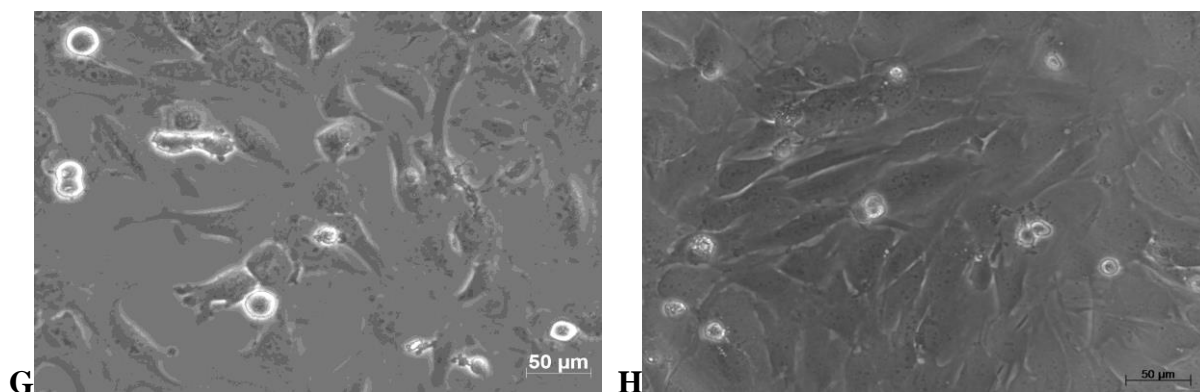


Fig. 3.7 (E) ASMase activation after different concentration of cisplatin treatment (0.1 $\mu\text{M}/\text{ml}$, 1.0 $\mu\text{M}/\text{ml}$ and 10 $\mu\text{M}/\text{ml}$) for different times (12 hours, 24 hours and 48 hours) in SCC9. (F) Cells viability after cisplatin treatment for different times. (G) SCC9 Cells before cisplatin treatment. (H) Cells after 10 $\mu\text{M}/\text{ml}$ cisplatin treatment for 48 hours (Phase contrast microscope $\times 20$).

3.3 ASMase activity of HNSCC and muscle in mouse

We wanted to study whether SCC9 tumor grown in mice has higher SMase activity compared to muscle and if MESL system can be used *in vivo* in imaging of tumor / tumor targeting. The tumor tissues from ten mice were studied. Tumor size was measured by the ultrasound (Fig. 3.8A). MESL/ICG could be seen accumulated in the tumor area after intravenous injection of ICG-MESL from caudal (Fig. 3.8C). ASMase activity was measured using Amplex Red Sphingomyelinase Assay Kit. Quantitative calculation of the SMase activity was analyzed against the standard curve. Tumors have significantly higher ASMase activity compared to the control tissue back leg muscle (Fig. 3.8D).

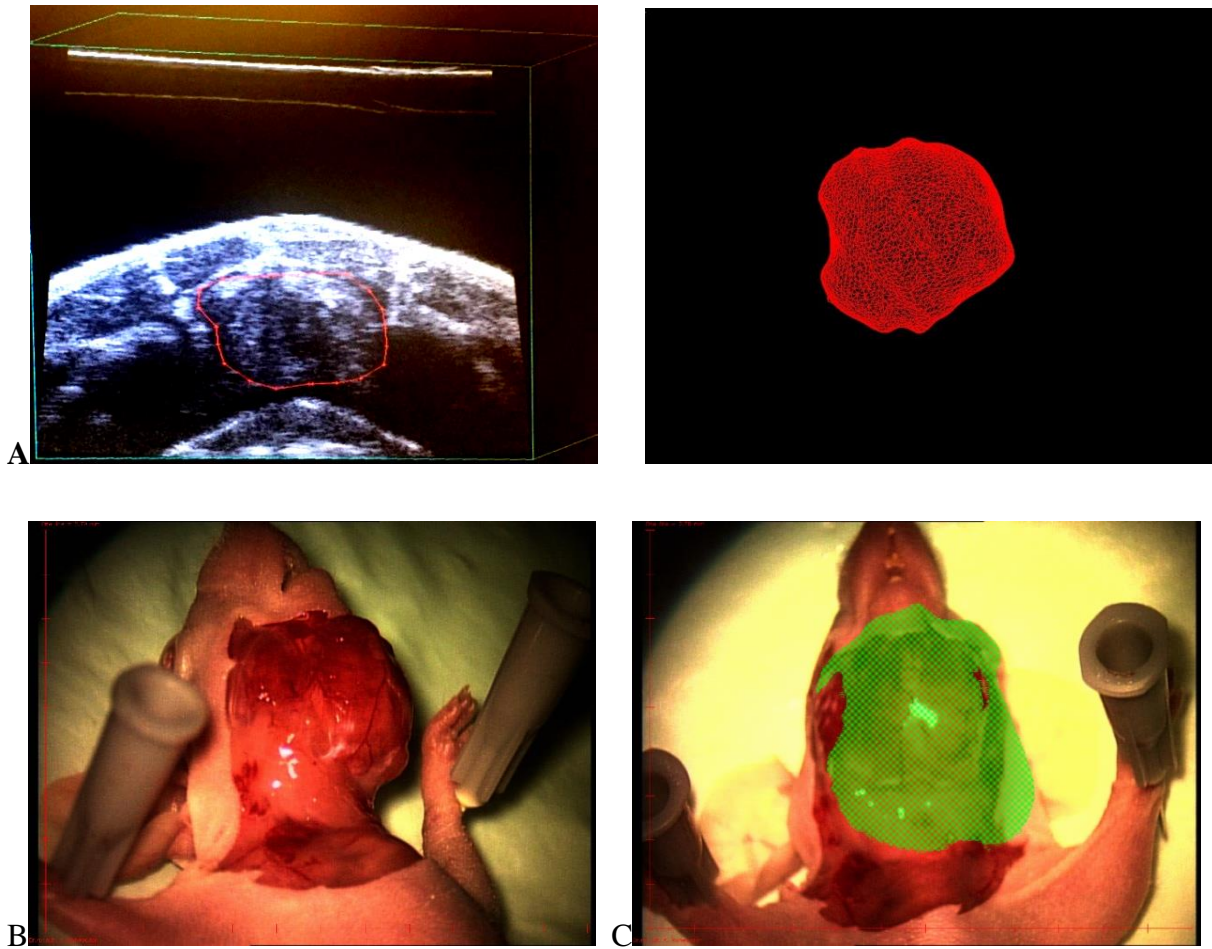


Fig. 3.8 (A) 3-Dimensional image reconstruction of mouse carcinoma was simulated by the ultrasound. (B) Carcinoma of the mouse by visual inspection. (B) Operation-microscope image of a nude mouse with mouth floor tumors. The skin was removed in the neck area for a better representation of the tumor. (C) A visual marker of the tumor is possible using a fluorescence filter after intravenous injection of ICG-MESL from caudal.

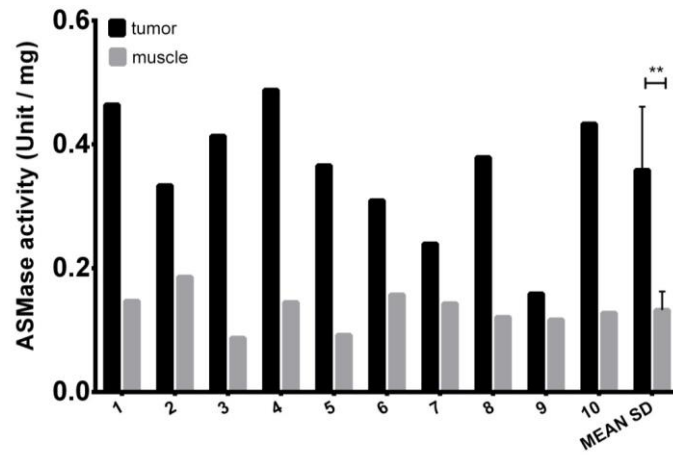


Fig. 3.8 (D) ASMase activity of tumor and muscle in 10 mice (Individual and mean value of ten mice). Tumor has significantly higher ASMase activation than muscle. **, $p < 0.01$, Paired-Samples T-Test.

4. Discussion of results

4.1 Optical properties of environment sensing ICG-MESL probe

ICG is one of the only clinically approved contrast agents that have been used for several decades. ICG is widely used contrast agent but there are limitations like its low stability, rapid degradation in aqueous environments and its strong binding to serum albumin that leads to a degradation or fluctuation of the optical signal (Mordon, et al., 2013; Saxena, et al., 2003). Previously have been reports of developed liposomes with ICG, encapsulated or adsorbed to lipid membrane with various compositions and physiochemical properties to overcome these limitations (Steven, et al., 2010; Jeong, et al., 2013). However, most of these liposomes with varying compositions containing ICG were prepared without a full understanding of the interactions between ICG and lipids. ICG can physically interact with phospholipids in the liposome membrane and modify the stability of and quantum yield of ICG as well as the structure and stability of the lipid membrane. ICG may also be encapsulated in the aqueous compartment of liposome. These properties and variations could profoundly impact optical NIR imaging quality. (Kraft and Ho, 2014; Beziere, et al., 2014). In our liposomal in vitro experiments, we wanted to study if free ICG and liposomal ICG can be differentiate by fluorescence. ICG-MESL demonstrates significant fluorescence enhancement compared to free ICG. This fluorescence enhancement may be related to insertion of ICG within the hydrophobic compartment of the lipid bilayer. The ICG is known to be photos table in hydrophobic organic microenvironments. The fluorescence of pure ICG decreases in high concentration which is probably because of fluorescence quenching (self-quenching) (Kraft and Ho, 2014; Beziere, et al., 2014).

The purpose of our in vitro study was to find ICG concentration loaded in MESL that exhibits both maximal fluorescence intensity and minimal self-quenching. From our concentration studies we decided to use 0,030 mg/ml ICG in our future studies.

One of the main components of MESL liposomes, sphingomyelin, is converted to ceramide by SMase. The formed ceramide destabilizes the bilayer structure of the liposomes (Megha and London, 2004; Rebillard, et al., 2007; Ira and Johnston, 2008; López-Montero, et al.,

2005). This may contribute to ICG redistribution and leakage of ICG from liposome. ICG fluorescence may also be increased after SMase treatment because the enzyme makes liposomes leakier and ICG is released and redistribution, which change the environment for ICG (self-quenching decreased when ICG free). MESL containing 0.50 mg/ml of ICG reveals optimal fluorescence increase after enzymatic reaction in our research. Nevertheless, the precise mechanism of fluorescence enhancement after reaction with enzyme is not clear.

ICG-MESL prepared by adding Fe₃O₄ nanoparticles could produce an additive response if an external magnetic field would also add. This would probably be due to Brownian motion. Addition AMF adds effects on the ICG fluorescence signal when used together with ASMase in MESL. We could see synergistic increase in our vitro studies when both AMF and enzyme was used. Similar effect has also seen previously with different methods in other research group. The interaction between a magnetic field and the ferromagnetic moments induces magneto mechanical forces, which may be employed to change the structure of the liposome and increase encapsulated substance release (Behrens and Appel, 2016). Here we propose that this phenomenon can be utilized in cisplatin delivery and release in MESL.

4.2 ASMase activity as a cell stress indicator after irradiation in HNSCC lines

DNA double helix damaging has been considered as the main deleterious effects of irradiation for decades. Signals alterations on cellular membranes are also identified having role in radiation-induced apoptosis. SM degradation pathway causes SM hydrolysis on the cell membrane and subsequent ceramide generation which can participate the cellular signaling of programmed cell death. (Hannun and Obeid, 2008; Grassme et al., 2001; Adada, et al., 2016). Here we have shown first time the difference in the radiation response of ASMase secretion of SCC cells and papilloma infected UDSCC cells.

Transitory increase of ceramide has been observed within minutes after irradiation exposure as a consequence of DNA damage independent ASMase activation (Vit and Rosselli, 2003; Wang, et al., 2015). How they form ASMase after irradiation and what are the different levels of ASMase in SCC9 and UDSCC2 were evaluated in our study. Medium supernatant without cells was collected immediately after irradiation to measure the secreted ASMase activity.

MTT investigation suggested that all the cells (6 hours after irradiation) were alive. This means that the ASMase activity we measured in medium was mainly secretory ASMase rather than lysosome ASMase released from death cells.

Dose response for the ASMase activity by increased irradiation doses was observed both in SCC9 and UDSCC2 cell lines. ASMase activity induced by irradiation in UDSCC2 was significantly higher than that in SCC9, which is in accordance with the clinical observation that HPV positive carcinoma better respond to irradiation than HPV negative carcinoma (Ang and Sturgis, 2012; Marcu, 2016). The molecular mechanisms are at present still incompletely understood. One hypothesis for enhanced responsiveness of HPV positive HNSCC to radiotherapy might be caused by cell cycle dysregulation and impaired DNA repair (Arenz, et al., 2014). Our data supposes that sphingolipid ASMase / ceramide signaling pathway probably play an important role in HPV-associated HNSCC after radiotherapy as well. The differences of ASMase activation possibly lead tumors individualized treatment of HPV-associated HNSCC with MESL Nanoparticle carrier system in future.

Keratinocyte was chosen to compare the effect of radiation on normal tissue and cancer tissues. It has previously shown that ASMase activation and ceramide generation associated apoptosis can be induced by Ultraviolet B (UVB) radiation in human Keratinocyte (Magnoni, et al., 2002). No studies have yet focused activation of ASMase in Keratinocyte induced by irradiation, as well as compared the differences of ASMase levels to HNSCC lines. Our research data showed that exposure to irradiation also result in rapid generation of ASMase activity in Keratinocyte, although the ASMase activity was significantly lower than HNSCC lines. This data still needs to be repeated before any assumptions can be made.

In model liposomal membranes it has previously been shown that bacterial SMase can make SM containing liposomes leakier (Begoña Ruiz-Argüello, et al., 1998 and 1999). This makes MESL an interesting potential candidate for triggered drug release. ASMase secreted from SCC9 and UDSCC2 in quantities that are sufficient to release the payload of cisplatin. The dose responsive release of cisplatin from MESL was observed after increased heavy irradiation in SCC9 cells. SMase inhibitor, desipramine, which inhibits the ASMase maturation process and thus decrease its formation (Elojeimy, et al., 2006), cause drop in

ASMase activity after irradiation in our studies thus proving ASMase indeed is part of the process. In addition, desipramine pretreatment inhibits the cisplatin release from MESL after radiation. These results reveal that ASMase is needed in the payload cisplatin release process in MESL.

4.3 ASMase activity as a cell stress indicator after cisplatin treatment in HNSCC lines

The chemotherapeutic agent cisplatin has been cornerstones in the treatment of solid tumor. Once classically considered as a nuclear DNA damaging agent, cisplatin has been regarded to induce apoptosis through plasma membrane disruption in recent studies (Maurmann et al., 2015). ASMase emerges as key enzyme which induces a critical step for ceramide generation. Pro-apoptotic receptors, including FAS death receptor pathways, could be induced through activation of ceramide (Noda et al., 2001; Rebillard, et al., 2006 and 2007).

MTT test was performed simultaneously after cisplatin treatment. We could also show a clear dose-response relationship between the cisplatin concentration and the activation of ASMase after 48 hours' treatment in UDSCC2 cells. Negative correlation has been observed between the cells viability and ASMase activity. It is hard to distinguish the increase of ASMase activity from extra nuclear (secretory ASMase) or released from dead cells (lysosome ASMase). We suppose that overwhelming majority of ASMase activity was from the lysosome ASMase of dead cells for their positive correlation. Further experimental proof for this hypothesis needs to be characterized. Regardless ASMase activity in supernatant from extra nuclear or lysosome, we suppose that ASMase activity induced by cisplatin treatment should be performed to amplify the release of payload cisplatin from MESL.

Our data shows that UDSCC2 better respond to cisplatin than SCC9, which is in accordance to the other vitro studies that higher sensitivity of the group of HPV positive cells to Cisplatin (Ziemann et al., 2015). Whether the invasive growth level or treatment sensitivity differences of these two HNSCC lines would affect the ASMase activity after cisplatin treatment remains further research.

In order to evaluate the secretory ASMase of extranuclear induced by cisplatin, temporary increase of ASMase activity in the supernatant was measured after short time of cisplatin

treatment ranging from 1 minutes to 60 minutes. Nevertheless, activation trend hardly could be observed in the result. We suppose that such amount of ASMase activation induced by short time treatment of cisplatin was too small to be measured or might be disordered by other cellular stress induced ASMase. The experimental design was imperfect to measure the short time of cisplatin treatment and need to be improved in the future study. Other methods like flow cytometry or immunoblotting might serve better for these studies.

4.4 In Vivo characterization: aSMase activity of HNSCC and muscle in mouse

Of the several studies generically reporting ASMase induced ceramide accumulation commonly observed to induce apoptosis in some specific cell lines, rare research has addressed the exactly ASMase activity in any cell lines. To the best of our knowledge, our study is the first report to evaluate the secretory ASMase activity of SCC9 tumor grown in mice into the comparison with muscle. Our study has revealed an almost two-fold higher of ASMase activity among tumor than muscles in mice. Similar results we have also observed in samples from HNSCC cancer patients (data are not shown here). Whether the extremely high ASMase activity of tumor could enzymatic release more payload cisplatin from MESL in target tissue remain to be further corroborated in vivo.

The imaging of ICG has been applied to intraoperative identification of several solid tumors and sentinel lymph node detection. Nevertheless, it also shows several drawbacks, which limit its clinical application (Jarmo et al., 2012; Kraft and Ho, 2014; Desmettre et al., 2000). The fluorescence image of SCC9 tumor in mice has been observed using a fluorescence filter after intravenous injection of ICG-MESL from caudal. Whether ICG-MESL could overcome the limitation of ICG and perform the promising advantages as our vitro study in mice remain to be well characterized.

5. Conclusion

Magneto-enzymatic sensitive liposome (MESL) carrier system combines the stress related enzyme, acid sphingomyelinase (ASMase), and alternating magnetic field (AMF) treatment together. Local enzymatically activated release will be triggered by ASMase, which is produced in cancer tissue or induced by cellular stress through radiation, hypoxia or chemical drugs. Iron particles in the lipid bilayer membrane of the liposome will amplify activation through alternating magnetic field by harmless magnetic fields. These two activation mechanisms enable locally controlled release. Investigation of the combined opening power of SMase and AMF, the efficiency of Indocyanine Green (ICG) for fluorescent labeling and cisplatin as a chemotherapeutic agent for treatment of MESL nanoparticle carrier was studied in vitro assay.

The fluorescent signal of ICG-MESL in blood shows significantly higher than pure ICG. ASMase has effects on the fluorescent signal of ICG-MESL that increases with AMF. However, results obtained from vitro experimental model cannot represent the fluorescent signal in vivo. Blood circulation, macrophage phagocytosis and metabolism of the MESL in vivo should be considered in the further research.

Endogenous ASMase activation on extracellular can be induced by cellular stress through irradiation. The dose response for the ASMase activities by increased radiation dose has been observed in both SCC9 and UDSCC2 cells. ASMase activity in UDSCC2 was significantly higher than that in SCC9, which is in accordance with the clinical observation that HPV positive carcinoma better respond to irradiation than HPV negative carcinoma. Endogenous ASMase activation is needed and sufficient to release the payload of cisplatin from MESL. The dose response for the liposomal cisplatin release by increased radiation doses and increased ASMase activities was observed.

Temporary increase of ASMase activity on extracellular induced by cisplatin is hard to be measured. Nevertheless, dose-response has been observed between long treatment time and ASMase activity in high dose concentration of cisplatin (10 μ M/ml). Negative correlation has been observed between the cells viability and ASMase activity in long

time cisplatin treatment. We suppose that majority of ASMase activity is from the lysosome of dead cells for their positive correlation. Regardless ASMase activity from extracellular or lysosome, we suppose that ASMase activity induced by cisplatin treatment could be performed to amplify the release of payload cisplatin from MESL. Further experimental proof for this hypothesis needs to be characterized.

Mouse model of HNSCC has been generated by our research group. Results revealed an almost two-fold higher of ASMase activity among tumor than muscles in mice. Whether the extremely high ASMase activity of tumor could enzymatic release more payload cisplatin from MESL in target tissue remain to be further corroborated in vivo.

6. Bibliography

Abreu AS, Castanheira EM, Queiroz MJR, Ferreira PM, Vale-Silva LA, Pinto E. (2011): Nanoliposomes for encapsulation and delivery of the potential antitumoral methyl 6-methoxy-3-(4-methoxyphenyl)-1H-indole-2-carboxylate. *Nanoscale Res. Lett*, 6, 482.

Adada M, Luberto C, Canals D. (2016): Inhibitors of the sphingomyelin cycle: Sphingomyelin synthases and sphingomyelinases. *Chem Phys Lipids*, 197, 45-59.

Alexis F, Pridgen EM, Langer R, Farokhzad OC. (2010): Nanoparticle technologies for cancer therapy. *Handb Exp Pharmacol*, 197, 55-86.

Ang. KK, Sturgis EM. (2012): Human papillomavirus as a marker of the natural history and response to therapy of head and neck squamous cell carcinoma. *Semin. Radiat. Oncol*, 22, 128–142.

Arenz A, Ziemann F, Mayer C, Wittig A, Dreffke K, Preising S, Wagner S, Klussmann JP, Engenhart-Cabillic R, Wittekindt C. (2014): Increased radiosensitivity of HPV-positive head and neck cancer cell lines due to cell cycle dysregulation and induction of apoptosis. *Strahlenther Onkol*, 190, 839-846.

Bangham AD, Standish MM, Watkins JC. (1965): Diffusion of univalent ions across the lamellae of swollen phospholipids. *J. Mol. Biol*, 13, 238–252.

Begoña Ruiz-Argüello. M, Félix M. Goñi, Alicia Alonso. (1998): Vesicle Membrane Fusion Induced by the Concerted Activities of Sphingomyelinase and Phospholipase C. *J. Biol. Chem*, 273, 22977–22982.

Begoña Ruiz-Argüello. M, Gorka Basáñez, Félix M. Goñi, Alicia Alonso. (1999): Different Effects of Enzyme-generated Ceramides and Diacylglycerols in Phospholipid Membrane Fusion and Leakage. *J. Biol. Chem*, 271, 26616–26621.

Behrens S, Appel I. (2016): Magnetic nanocomposites. *Curr Opin Biotechnol*, 39, 89-96.

Beziere N, Lozano N, Nunes A, Salichs J, Queiros D, Kostarelos K, Ntziachristos V. (2014): Dynamic imaging of PEGylated indocyanine green (ICG) liposomes within the tumor microenvironment using multi-spectral optoacoustic tomography (MSOT). *Biomaterials*. 37, 415-424.

Bonner JA, Harari PM, Giralt J, Azarnia N, Shin DM, Cohen RB, Jones CU, Sur R, Raben D, Jassem J, Ove R, Kies MS, Baselga J, Youssoufian H, Amellal N, Rowinsky EK, Ang KK. (2006): Radiotherapy plus cetuximab for squamous-cell carcinoma of the head and neck. *N Engl J Med*, 354, 567-578.

Corre I, Niaudet C, Paris F. (2010): Plasma membrane signaling induced by ionizing radiation. *Mutat Res*, 704, 61-67.

Danhier F, Vroman B, Lecouturier N, Crockart N, Pourcelle V, Freichels H, Jérôme C, Marchand-Brynaert J, Feron O, Prétat V. (2009): Targeting of tumor endothelium by RGD-grafted PLGA-nanoparticles loaded with paclitaxel. *J. Control. Release*, 140, 166–173.

Desmettre T, Devoisselle JM, Mordon S. (2000): Fluorescence properties and metabolic features of indocyanine green (ICG) as related to angiography. *Surv Ophthalmol*, 45, 15-27.

Elojeimy S, Holman DH, Liu X, El-Zawahry A, Villani M, Cheng JC, Mahdy A, Zeidan Y, Bielwaska A, Hannun YA, Norris JS. (2006): New insights on the use of desipramine as an inhibitor for acid ceramidase. *FEBS Lett*, 580, 4751-4756.

Frangioni JV. (2008): New technologies for human cancer imaging. *J Clin Oncol*, 26, 4012-4021.

Gómez-Sotomayor R, Ahualli S, Viota JL, Rudzka K, Delgado AV. (2015): Iron/Magnetite Nanoparticles as Magnetic Delivery Systems for Antitumor Drugs. *J Nanosci Nanotechnol*, 15, 3507-3514.

Grassme H, Jekle A, Riehle A, Schwarz H, Berger J, Sandhoff K, Kolesnick R, Gulbins E.

(2001): CD95 signaling via ceramide-rich membrane rafts. *J Biol Chem*, 276, 20589-20596.

Gunawardena B, Teichgräber V, Hessler G, Gulbins E. (2004): Ceramide in malignant tumors. *Cancer Therapy*, 2, 13-20.

Hannun YA, Obeid LM. (2008): Principles of bioactive lipid signalling: lessons from sphingolipids. *Nat Rev Mol Cell Biol*, 9, 139-150.

Hashimoto S. (2012): Antitumor activity of IHL-305, a novel pegylated liposome containing irinotecan, in human xenograft models. *Oncol. Rep*, 27, 189–197.

Holopainen J.M., Lehtonen J.Y.A., Kinnunen P.K.J. (1997): Lipid microdomains in dimyristoylphosphatidylcholine-ceramide liposomes. *Chem. Phys. Lipids*, 88, 1–13.

Holopainen JM, Angelova MI, Kinnunen PK. (2000): Vectorial budding of vesicles by asymmetrical enzymatic formation of ceramide in giant liposomes. *Biophys J*, 78, 830-838.

Huang, H. W., E. M. Goldberg, and R. Zidovetzki. (1996): Ceramide induces structural defects into phosphatidylcholine bilayers and activates phospholipase A2. *Biochem. Biophys. Res. Commun*, 220, 834–838.

Ira, Johnston LJ. (2008): Sphingomyelinase generation of ceramide promotes clustering of nanoscale domains in supported bilayer membranes. *Biochim Biophys Acta*, 1778, 185-197.

Jarmo T, Alander, Ilkka Kaartinen, Aki Laakso, Tommi Pätilä, Thomas Spillmann, Valery V, Tuchin, Maarit Venermo, Petri Välisuo. (2012): A Review of Indocyanine Green Fluorescent Imaging in Surgery. *Int J Biomed Imaging*, 940585

Jeong HS, Lee CM, Cheong SJ, Kim EM, Hwang H, Na KS, Lim ST, Sohn MH, Jeong HJ. (2013): The effect of mannosylation of liposome-encapsulated indocyanine green on imaging of sentinel lymph node. *J Liposome Res*. 23, 291-297

Khosravi-Darani K, Mozafari MR. (2010): Nanoliposome Potentials in Nanotherapy: A

Concise Overview. *Int. J. Nanosci. Nanotechnol*, 6, 3–13.

Koynova R, Tenchov B. (2015): Recent Progress in Liposome Production, Relevance to Drug Delivery and Nanomedicine. *Recent Pat Nanotechnol*, 9, 86-93.

Kraft JC, Ho RJ. (2014): Interactions of indocyanine green and lipid in enhancing near-infrared fluorescence properties: the basis for near-infrared imaging in vivo. *Biochemistry*, 53, 1275-1283.

Leemans CR, Braakhuis BJ, Brakenhoff RH. (2010): The molecular biology of head and neck cancer. *Nat Rev Cancer*, 11, 9-22.

López-Montero I, Rodriguez N, Cribier S, Pohl A, Vélez M, Devaux PF. (2005): Rapid transbilayer movement of ceramides in phospholipid vesicles and in human erythrocytes. *J Biol Chem*, 280, 25811-25819.

Maeda H. (2001): The enhanced permeability and retention (EPR) effect in tumor vasculature: the key role of tumor-selective macromolecular drug targeting. *Adv Enzyme Regul*, 41,189–207.

Magnoni C, Euclidi E, Benassi L, Bertazzoni G, Cossarizza A, Seidenari S, Giannetti A. (2002): Ultraviolet B radiation induces activation of neutral and acidic sphingomyelinases and ceramide generation in cultured normal human keratinocytes. *Toxicol In Vitro*, 16, 349-355.

Marcu LG. (2016): Future treatment directions for HPV-associated head and neck cancer based on radiobiological rationale and current clinical evidence. *Crit Rev Oncol Hematol*, 103, 27-36.

Matsumura Y, Maeda H. (1986): A new concept for macromolecular therapeutics in cancer chemotherapy: mechanism of tumor tropic accumulation of proteins and the antitumor agent smancs. *Cancer Res*, 46, 6387-6392.

Matsuzaki T, Takagi A, Furuta T, Ueno S, Kurita A, Nohara G, Kodaira H, Sawada S, Hashimoto S. (2012): Antitumor activity of IHL-305, a novel pegylated liposome containing

irinotecan, in human xenograft models. *Oncol Rep*, 27, 189-197.

Maurmann L, Belkacemi L, Adams N. R, Majmudar P. M, Moghaddas S, Bose R. N. (2015): A novel cisplatin mediated apoptosis pathway is associated with acid sphingomyelinase and FAS pro-apoptotic protein activation in ovarian cancer. *Apoptosis*, 20:960–974

Megha, London E. (2004): Ceramide selectively displaces cholesterol from ordered lipid domains (rafts): implications for lipid raft structure and function. *J Biol Chem*, 279, 9997–10004.

Méry B, Guy JB, Espenel S, Wozny AS, Simonet S, Vallard A, Alphonse G, Ardail D, Rodriguez-Lafrasse C, Magné N. (2016): Targeting head and neck tumoral stem cells: From biological aspects to therapeutic perspectives. *World J Stem Cells*, 26, 13-21.

Michaud DS, Langevin SM, Eliot M, Nelson HH, Pawlita M, McClean MD, Kelsey KT. (2014): High-risk HPV types and head and neck cancer. *Int J Cancer*, 135, 1653-1661.

Minko T, Kopeckova P, Pozharov V, Jensen KD, Kopecek J. (2000): The influence of cytotoxicity of macromolecules and of VEGF gene modulated vascular permeability on the enhanced permeability and retention effect in resistant solid tumors. *Pharm Res*, 17, 505–514.

Mordon S, Devoisselle JM, Soulie-Begu S, Desmettre T. (1998): Indocyanine green: physicochemical factors affecting its fluorescence in vivo. *Microvasc Res*, 55, 146-152.

Nguyen QT, Tsien RY. (2013): Fluorescence-guided surgery with live molecular navigation--a new cutting edge. *Nat Rev Cancer*, 13, 653-662.

Noda S, Yoshimura S, Sawada M, Naganawa T, Iwama T, Nakashima S, Sakai N. (2001): Role of ceramide during cisplatin-induced apoptosis in C6 glioma cells. *J Neurooncol*, 52,11-21.

Nurminen TA, Holopainen JM, Zhao H, Kinnunen PK. (2002): Observation of topical catalysis by sphingomyelinase coupled to microspheres. *J Am Chem Soc*, 124, 12129-12134.

Ochekpe NA, Olorunfemi PO, Ngwuluka N. (2009): Nanotechnology and Drug Delivery Part 1: Background and Applications. *Trop. J. Pharm. Res*, 8, 265–274.

Ochekpe N A, Olorunfemi PO, Ngwuluka N. (2009): Nanotechnology and Drug Delivery Part 2: Nanostructures for Drug Delivery. *Trop. J. Pharm. Res*, 8, 275–287.

Ramshankar V, Krishnamurthy A. (2013): Human papilloma virus in head and neck cancers-role and relevance in clinical management. *Indian J Surg Oncol*, 4, 59-66.

Rebillard A, Tekpli X, Meurette O, Sergent O, LeMoigne-Muller G, Vernhet L, Gorria M, Chevanne M, Christmann M, Kaina B, Counillon L, Gulbins E, Lagadic-Gossmann D, Dimanche-Boitrel MT. (2007): Cisplatin-induced apoptosis involves membrane fluidification via inhibition of NHE1 in human colon cancer cells. *Cancer Res*. 15, 7865-7874.

Rebillard A, Lagadic-Gossmann D, Dimanche-Boitrel MT. (2008): Cisplatin cytotoxicity: DNA and plasma membrane targets. *Curr Med Chem*, 15, 2656-2663.

Sacco AG1, Worden FP. (2016): Molecularly targeted therapy for the treatment of head and neck cancer: a review of the ErbB family inhibitors. *Onco Targets Ther*, 9, 1927-1943.

Saxena V, Sadoqi M, Shao J. (2003): Degradation kinetics of indocyanine green in aqueous solution. *J Pharm Sci*, 92, 2090-2097.

Siegel R, Ward E, Brawley O, Jemal A. (2011): Cancer statistics, 2011: the impact of eliminating socioeconomic and racial disparities on premature cancer deaths. *CA Cancer J Clin*, 61, 212-236.

Steven T. Proulx, Paola Luciani, Stefanie Derzsi, Matthias Rinderknecht, Viviane Mumprecht, Jean-Christophe Leroux, Michael Detmar. (2010): Quantitative Imaging of Lymphatic Function with Liposomal Indocyanine Green. *Cancer Res*, 15, 7053–7062.

Testi R. (1996): Sphingomyelin breakdown and cell fate. *Trends Biochem Sci*, 21, 468-471.

Tietze R, Zaloga J, Unterweger H, Lyer S, Friedrich RP, Janko C, Pöttler M, Dürr S, Alexiou

C. (2015): Magnetic nanoparticle-based drug delivery for cancer therapy. *Biochem Biophys Res Commun*, 18, 463-470.

Torchilin VP. (2005): Recent advances with liposomes as pharmaceutical carriers. *Nat. Rev. Drug Discov*, 4, 145–160.

Vit JP, Rosselli F. (2003): Role of the ceramide-signaling pathways in ionizing radiation-induced apoptosis. *Oncogene*, 22, 8645-8652.

Wang AZ, Langer R, Farokhzad OC. (2012): Nanoparticle delivery of cancer drugs. *Annu Rev Med*, 63, 185-198.

Wang SW, Hojabrpour P, Zhang P, Kolesnick RN, Steinbrecher UP, Gómez-Muñoz A, Duronio V. (2015): Regulation of ceramide generation during macrophage apoptosis by ASMase and de novo synthesis. *Biochim Biophys Acta*, 1851, 1482-1489.

Xia M, Zhang C, Boini KM, Thacker AM, Li PL. (2011): Membrane raft-lysosome redox signalling platforms in coronary endothelial dysfunction induced by adipokine visfatin. *Cardiovasc Res*, 89, 401-409.

Zhang Z, Berezin MY, Kao JL, d'Avignon A, Bai M, Achilefu S. (2008): Near-infrared dichromic fluorescent carbocyanine molecules. *Angew Chem Int Ed Engl*, 47, 3584-3587

Ziemann F, Arenz A, Preising S, Wittekindt C, Klussmann JP, Engenhardt-Cabillic R, Wittig A. (2015): Increased sensitivity of HPV-positive head and neck cancer cell lines to x-irradiation ± Cisplatin due to decreased expression of E6 and E7 oncoproteins and enhanced apoptosis. *Am J Cancer Res*, 5, 1017-1031.

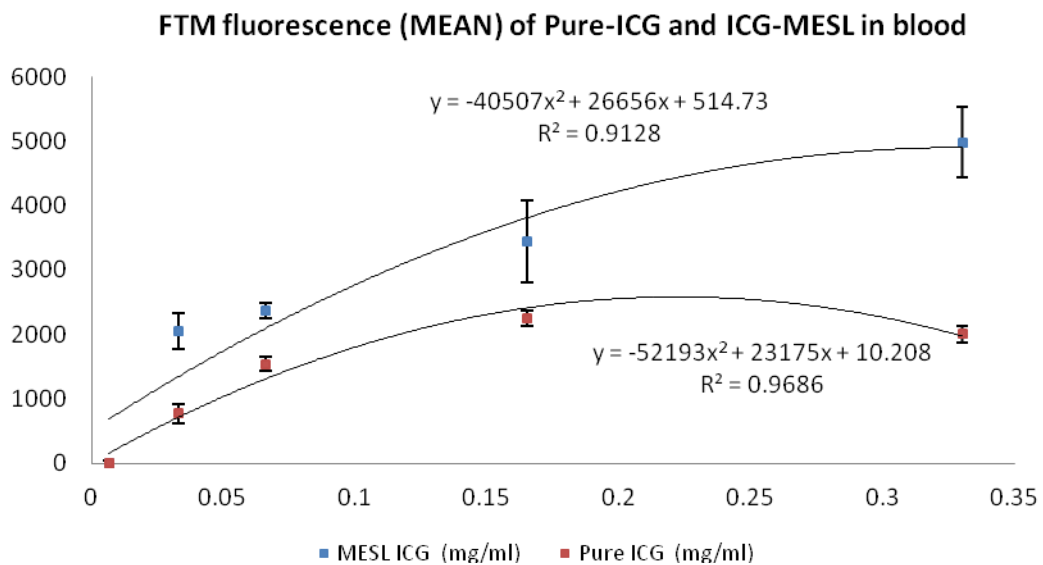
7. Appendices

7.1 Fluorescence of ICG-MESL and pure ICG in blood

FMT fluorescence of different concentration of Pure - ICG									
mg/ml	Series 1			Series 2			Series 3		
0.330	2071.08	2080.38	2137.49	1866.93	1821.68	1850.78	2239.95	1990.69	1971.78
0.165	2380.39	2418.14	2353.52	2050.16	2203.25	2179.65	2349.68	2185.41	2194.67
0.066	1596.75	1559.02	1525.28	1388.61	1406.75	1515.20	1722.70	1547.94	1639.51
0.033	618.29	603.83	599.71	796.55	829.38	879.61	998.08	798.62	838.07

FMT fluorescence of different concentration of ICG - MESL									
mg/ml	Series 1			Series 2			Series 3		
0.330	4172.55	4450.59	4635.03	5072.46	4955.40	4954.15	5584.09	5437.35	5519.97
0.165	2727.81	2535.27	2977.06	3536.45	3609.60	3533.35	4094.87	3877.10	4045.00
0.066	2368.54	2102.36	2344.87	2365.44	2328.82	2317.71	2489.97	2469.98	2523.97
0.033	1796.65	1672.20	1752.08	2279.75	2268.79	2227.96	2162.77	2153.63	2157.35

FMT fluorescence of different concentration of Pure - ICG & ICG - MESL					
mg/ml	Pure - ICG		ICG - MESL		p. value
	MEAN	SD	MEAN	SD	
0.330	2003.4182	136.6902	4975.7316	547.4359	7.70×10^{-12}
0.165	2257.2075	120.4380	3437.3894	638.3367	1.52×10^{-05}
0.066	1544.6391	100.8538	2367.9632	114.4774	6.67×10^{-11}
0.033	773.5712	145.6172	2052.3528	274.9084	2.58×10^{-10}



7.2 Fluorescence change of ICG-MESL and pure ICG with SMase

FMT fluorescence (MEAN) of Pure - ICG after adding SMase						
mg/ml	Without SMase			With SMase		
0.006	1772.78	2044.02	1841.57	1759.46	2073.81	2093.22
0.015	3471.82	3198.57	3490.71	3100.15	3466.50	3484.45
0.030	3056.04	3273.60	3307.40	3186.10	3486.80	3242.27

mg/ml	Without SMase		With SMase		p. value
	MEAN	SD	MEAN	SD	
0.006	1886.125	141.0018	1975.498	187.3455	0.5452
0.015	3387.033	163.4892	3350.366	216.8771	0.8266
0.030	3212.345	136.4115	3305.058	159.8808	0.4874

FMT fluorescence (MEAN) of ICG - MESL after adding SMase						
mg/ml	Without SMase			With SMase		
0.006	4498.40	4279.78	4303.23	4045.29	4004.15	4323.58
0.015	4626.92	5089.97	4892.41	4511.15	5209.17	5346.25
0.030	5452.24	5631.25	5742.27	6815.54	6868.09	6639.36

mg/ml	Without SMase		With SMase		p. value
	MEAN	SD	MEAN	SD	
0.006	4360.468	120.0226	4124.337	173.7693	0.1249
0.015	4869.769	232.3524	5022.192	447.848	0.6284
0.030	5608.585	146.3391	6774.332	119.8047	0.0004

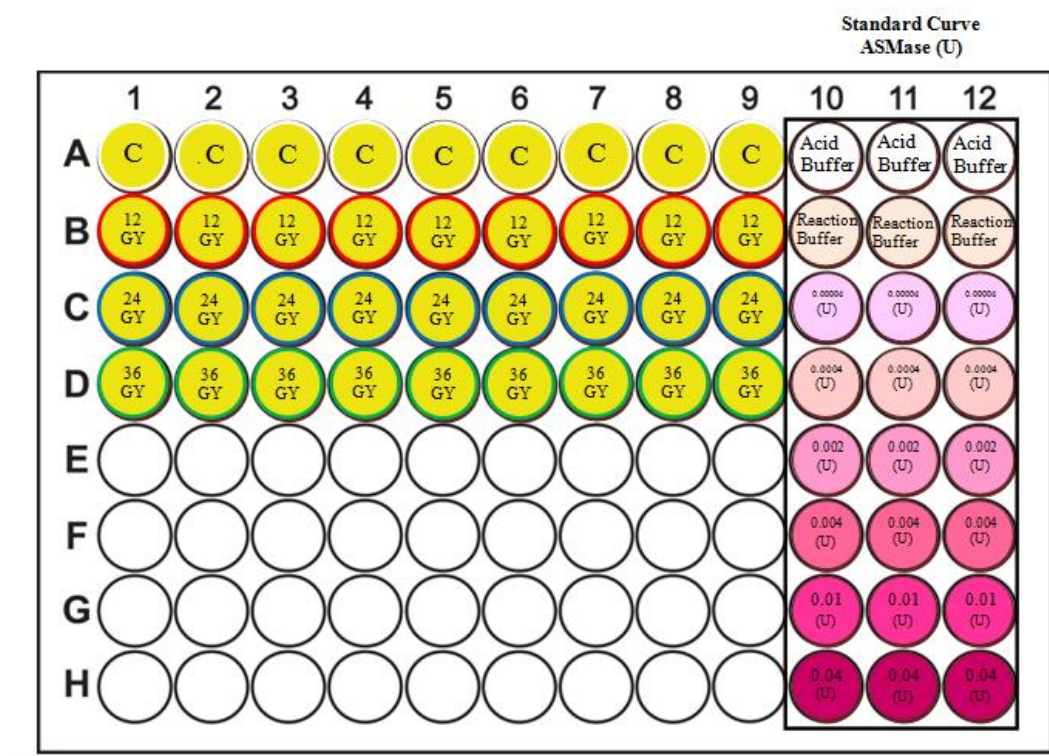
7.3 Fluorescence % increase of ICG-MESL with SMase and AMF

SMase U/ml		Serie1	Serie2	Serie3	MEAN	SD
+SMase +20min	0.364	0.322	0.263	0.140	0.169	0.104
	0.727	0.276	0.136	0.025	0.189	0.216
	1.091	0.098	0.172	0.103	0.208	0.130
	1.455	0.319	0.123	0.044	0.215	0.163
+SMase +20min AFM	0.364	0.469	0.249	0.285	0.255	0.190
	0.727	0.181	0.240	0.111	0.288	0.305
	1.091	0.222	0.251	0.200	0.295	0.092
	1.455	0.612	0.346	0.565	0.344	0.209

SMase U/ml	+SMase		+SMase & AFM		p. value
	MEAN	SD	MEAN	SD	
0.364	0.169	0.104	0.255	0.190	0.346
0.727	0.189	0.216	0.288	0.305	0.718
1.091	0.208	0.130	0.295	0.092	0.024
1.455	0.215	0.163	0.344	0.209	0.040

7.4 ASMasE activity after irradiation

Schematic of 96-wells plate



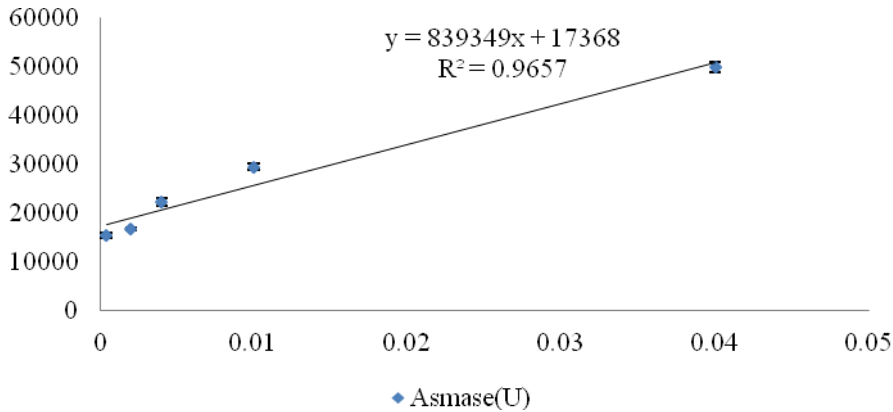
<>	1	2	3	4	5	6	7	8	9	10	11	12
A	0 Gy - 1			0 Gy - 2			0 Gy - 3					
B	12 Gy - 1			12 Gy - 2			12 Gy - 3			Reaction buffer		
C	24 Gy - 1			24 Gy - 2			24 Gy - 3			0.0004 U		
D	36 Gy - 1			36 Gy - 2			36 Gy - 3			0.002 U		
E										0.004 U		
F										0.01 U		
G										0.04 U		
H												

Original data of absorbance value (SCC9)

<>	1	2	3	4	5	6	7	8	9	10	11	12
A	24534	23197	24301	24728	22774	23478	24731	24396	26200	441	439	452
B	34517	32461	35596	36509	33877	35752	38053	37911	39274	23451	23119	448
C	43893	42704	44704	48607	45816	47249	43952	43849	45033	15175	15936	479
D	47250	35483	47743	46894	46002	49128	50478	48451	50801	16679	16947	449
E	441	394	496	435	454	464	483	428	426	22906	21756	450
F	471	439	428	471	514	389	453	467	439	29037	29963	426
G	496	478	424	464	468	449	414	521	407	50793	49167	445
H	447	413	439	440	521	442	445	462	403	441	418	498

Standard Curve (SCC9)

aSMase (U)	Absorbance Value		Average	Std
0.04	50793	49167	49980	1149.75563
0.01	29037	29963	29500	654.780879
0.004	22906	21756	22331	813.172798
0.002	16679	16947	16813	189.504617
0.0004	15175	15936	15555.5	538.10826

**ASMase release (calculate by standard curve) (SCC9)**

0 Gy	0.009	0.007	0.008	0.009	0.006	0.007	0.009	0.008	0.011
12 Gy	0.020	0.018	0.022	0.023	0.020	0.022	0.025	0.024	0.026
24 Gy	0.032	0.030	0.033	0.037	0.034	0.036	0.032	0.032	0.033
36 Gy	0.036	0.022	0.036	0.035	0.034	0.038	0.039	0.037	0.040

ASMase release (compare to the control group) (SCC9)

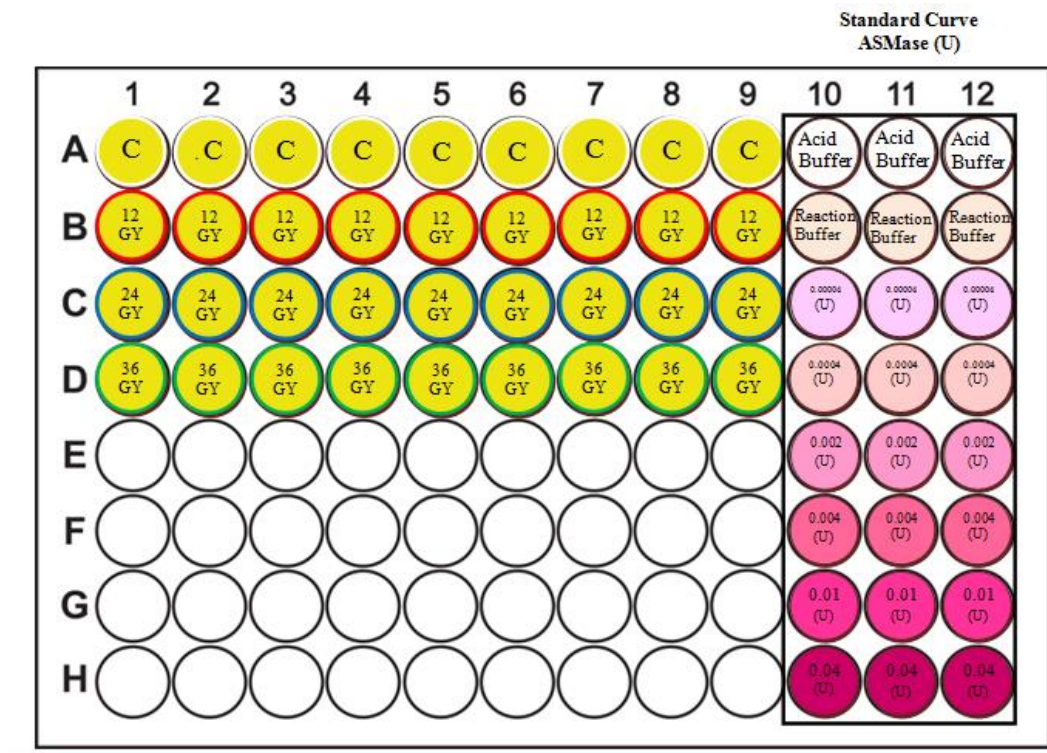
12 Gy	0.012	0.010	0.014	0.015	0.011	0.014	0.016	0.016	0.018
24 Gy	0.023	0.022	0.024	0.029	0.026	0.027	0.023	0.023	0.025
36 Gy	0.027	0.013	0.028	0.027	0.026	0.030	0.031	0.029	0.032

Average and std value (SCC9)

Radiation	MEAN	SEM
12 Gy	0.0140	0.0026
24 Gy	0.0248	0.0022
36 Gy	0.0270	0.0054

P. value	
12 Gy Vs. 24 Gy	5.57×10^{-8}
12 Gy Vs. 36 Gy	7.86×10^{-6}
24 Gy Vs. 36 Gy	0.284

Schematic of 96-wells plate



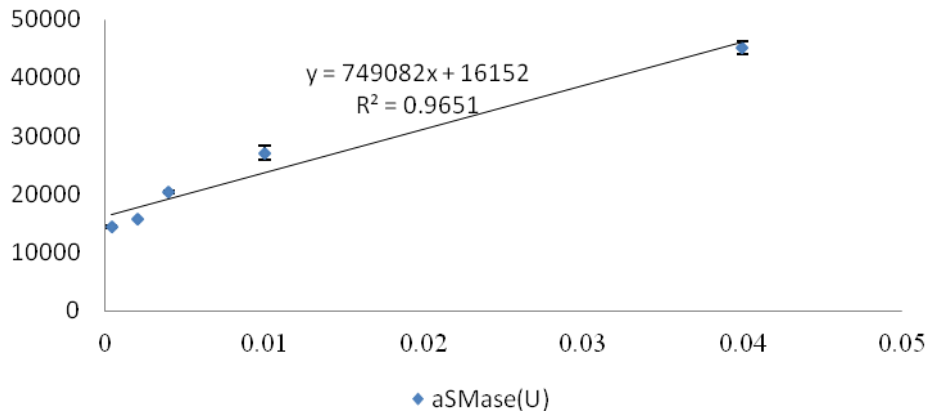
<>	1	2	3	4	5	6	7	8	9	10	11	12
A	0 Gy - 1			0 Gy - 2			0 Gy - 3					
B	12 Gy - 1			12 Gy - 2			12 Gy - 3			Reaction buffer		
C	24 Gy - 1			24 Gy - 2			24 Gy - 3			0.0004 U		
D	36 Gy - 1			36 Gy - 2			36 Gy - 3			0.002 U		
E										0.004 U		
F										0.01 U		
G										0.04 U		
H												

Original data of absorbance value (UDSCC2)

<>	1	2	3	4	5	6	7	8	9	10	11	12
A	22039	22877	23227	24072	23837	24688	24383	24008	23939	323	319	337
B	32907	33342	34996	36293	34509	35346	35178	34310	36044	20832	21499	308
C	45410	45744	46772	45582	43110	44681	46408	45448	47031	14292	14597	334
D	46113	47095	48815	54767	53994	54185	57110	55379	Overflow	15787	15737	314
E	303	360	322	370	343	316	330	354	317	20647	20310	304
F	306	334	322	329	314	346	343	328	341	27923	26252	339
G	354	334	343	288	351	324	323	354	295	44429	46042	288
H	309	311	347	342	332	327	330	338	305	317	307	334

Standard Curve (UDSCC2)

aSMase (U)	Absorbance Value		Average	Std
0.04	44429	45235.5	45235.5	1140.6
0.01	27923	27087.5	27087.5	1181.6
0.004	20647	20478.5	20478.5	238.3
0.002	15787	15762.0	15672.0	35.4
0.0004	14292	14444.5	14444.5	215.7

**ASMase release (calculate by standard curve) (UDSCC2)**

0 Gy	0.008	0.009	0.009	0.011	0.010	0.011	0.011	0.010	0.010
12 Gy	0.022	0.023	0.025	0.027	0.025	0.026	0.025	0.024	0.027
24 Gy	0.039	0.040	0.041	0.039	0.036	0.038	0.040	0.039	0.041
36 Gy	0.040	0.041	0.044	0.052	0.051	0.051	0.055	0.052	

ASMase release (compare to the control group) (UDSCC2)

12 Gy	0.012	0.013	0.015	0.017	0.014	0.016	0.015	0.014	0.017
24 Gy	0.029	0.029	0.031	0.029	0.026	0.028	0.030	0.029	0.031
36 Gy	0.030	0.031	0.034	0.042	0.040	0.041	0.045	0.042	

MEAN, SEM and P. value (UDSCC2)

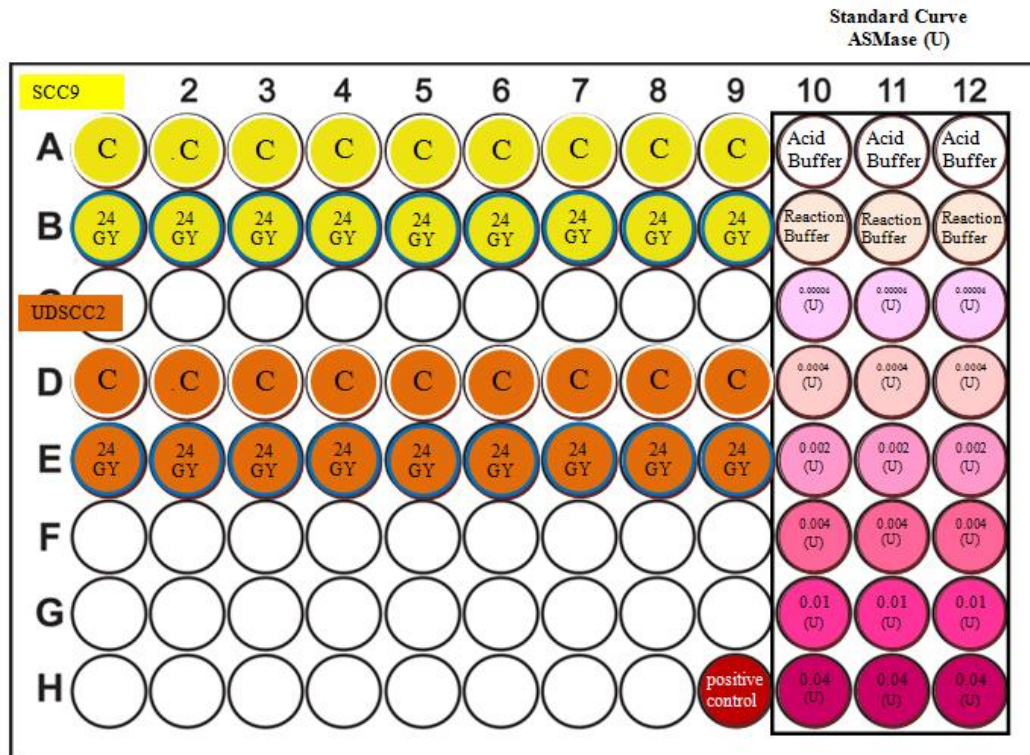
Radiation	MEAN	SEM
12 Gy	0.0148	0.0015
24 Gy	0.0292	0.0016
36 Gy	0.0381	0.0056

P. value	
12Gy Vs. 24 Gy	1.12×10^{-12}
12Gy Vs. 36 Gy	4.11×10^{-9}
24Gy Vs. 36 Gy	3.80×10^{-4}

Compare of aSMase activity of SCC9 and UDSCC2 after irradiation

Radiation	SCC9		UDSCC2		P. value
	MEAN	SEM	MEAN	SEM	
12 Gy	0.0140	0.0026	0.0148	0.0015	0.420413
24 Gy	0.0248	0.0022	0.0292	0.0016	0.000168
36 Gy	0.0270	0.0054	0.0381	0.0056	0.000889

7.5 ASMase activity of Keratinocyte and SCC9 after 24 Gy irradiation



Schematic of 96-wells plate (Keratinocyte & SCC9)

<>	1	2	3	4	5	6	7	8	9
A	SCC9 0 Gy -1			SCC9 0 Gy -2			SCC9 0 Gy -3		
B	SCC9 24 Gy -1			SCC9 24 Gy -2			SCC9 24 Gy -3		
C	keratinocyte 0 Gy -1			keratinocyte 0 Gy -2			keratinocyte 0 Gy -3		
D	Keratinocyte 24 Gy -1			Keratinocyte 24 Gy -2			Keratinocyte 24 Gy -3		

Original data of absorbance value (Keratinocyte & SCC9)

<>	1	2	3	4	5	6	7	8	9
A	16773	17533	17095	20392	20192	19863	20088	21078	20093
B	45827	45444	46378	46753	42392	41568	42923	41419	47728
C	23121	21828	21090	25505	23447	26121	21823	22223	23413
D	34931	36103	35488	34818	34699	31566	30720	32700	32495

ASMase release (calculate by standard curve) (Keratinocyte & SCC9)

<>	1	2	3	4	5	6	7	8	9
A	0.0082	0.0089	0.0085	0.0118	0.0116	0.0112	0.0115	0.0124	0.0115
B	0.0369	0.0366	0.0375	0.0379	0.0335	0.0327	0.0341	0.0326	0.0388
C	0.0145	0.0132	0.0125	0.0168	0.0148	0.0174	0.0132	0.0136	0.0148
D	0.0262	0.0273	0.0267	0.0260	0.0259	0.0228	0.0220	0.0239	0.0237

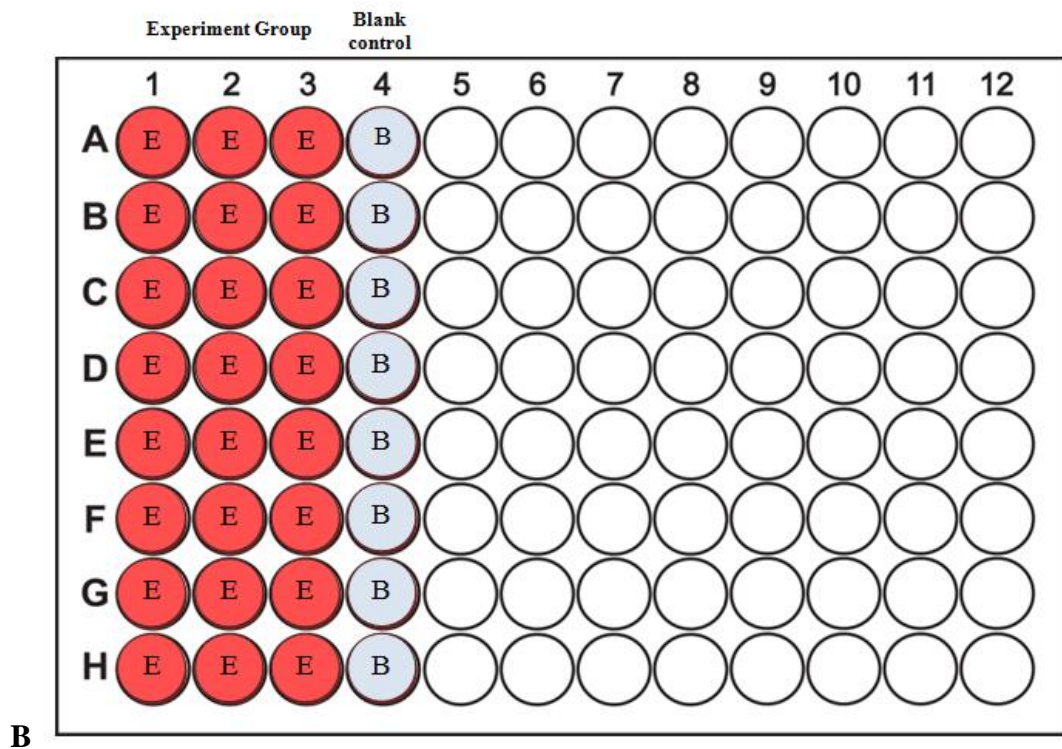
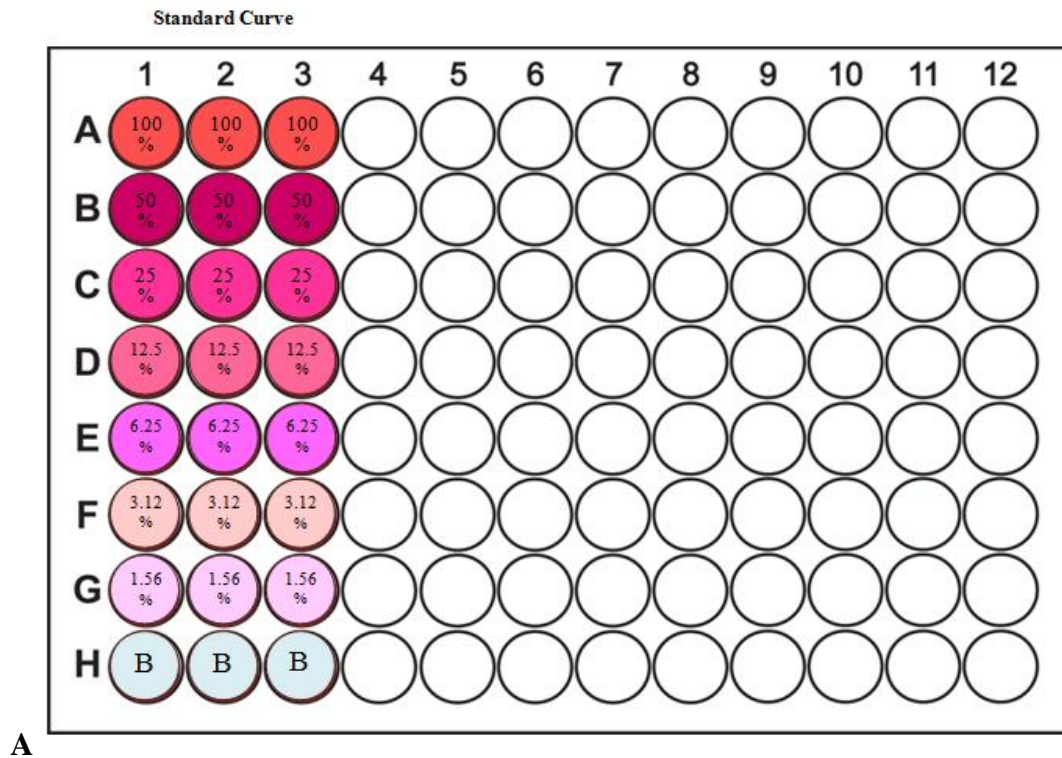
Compare with each control group

$\langle \rangle$	Average	Std
SCC9 24 GY	0.0250	0.0024
Keratinocyte 24 GY	0.0104	0.0017

Date of UDSCC2 from another plate

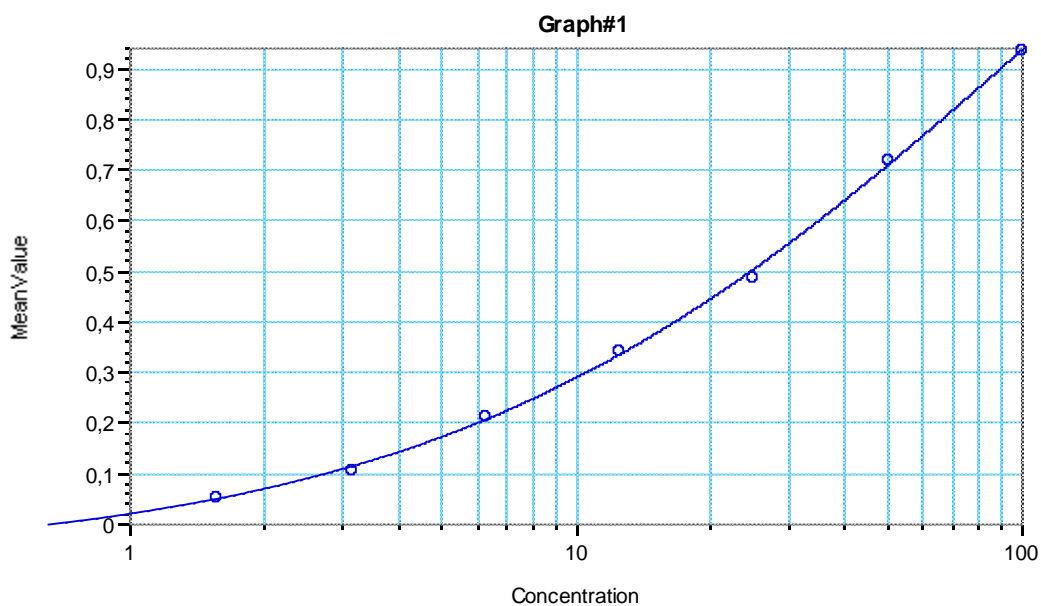
$\langle \rangle$	Average	Std
UDSCC2 24 GY	0.0290	0.0020

7.6 MTT test: 6 hours after different irradiation



Schematic of 96-wells plate for the MTT test after irradiation. (A) Standard curve group; (B) Experiment group (1-3 lines) and blank control group (4th line) for one dose of irradiation.

Standard Curve



$y = (A - D) / (1 + (x/C)^B) + D$: A B C D R²
 (SCC9) Std (Standards: Concentration vs MeanValue) -0,068 0,667 99,063 1,937 0,999

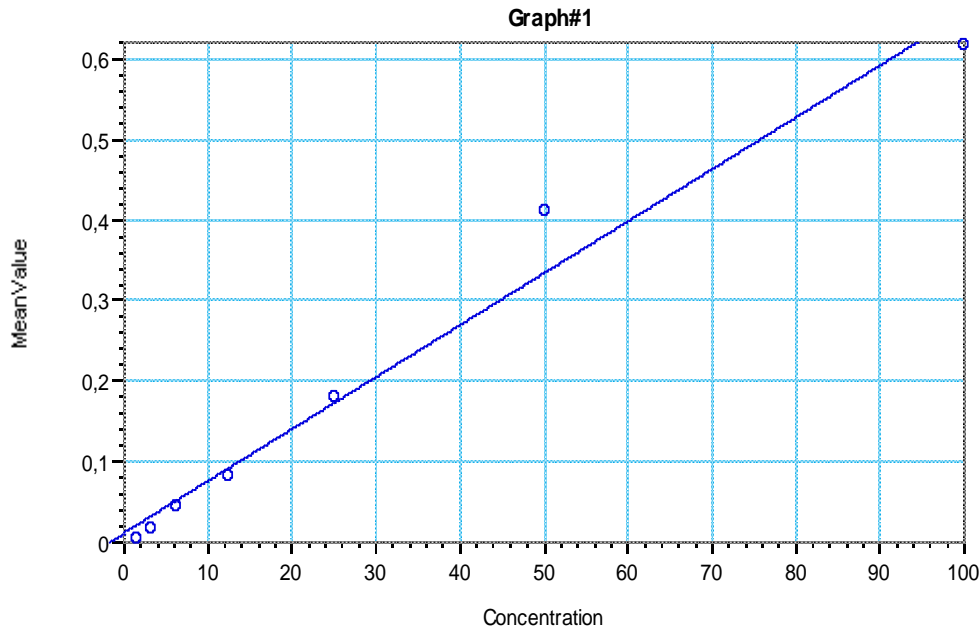
Absorbance Value (SCC9)

12 Gy			24 Gy			36 Gy		
0.956	0.971	0.948	0.980	0.947	1.018	1.001	0.989	1.014
0.976	0.793	0.928	0.858	0.747	0.962	1.021	0.850	0.905
0.969	0.893	0.931	0.974	0.873	0.916	1.004	0.850	0.877
0.977	0.897	0.937	0.934	0.884	0.912	1.013	0.779	0.855
0.978	0.902	0.895	0.937	0.932	0.987	0.958	0.829	0.975
0.938	0.992	0.744	0.986	0.888	0.963	1.025	0.831	0.926
1.017	0.871	0.906	1.013	0.807	0.965	1.098	0.852	0.955
1.037	0.992	1.007	1.059	0.982	0.924	1.026	1.012	1.044

Cells viability (% of Control) (SCC9)

12 Gy			24 Gy			36 Gy		
97.09%	95.15%	98.11%	94.02%	98.26%	89.37%	91.47%	92.86%	89.86%
94.50%	120.79%	100.80%	110.65%	128.69%	96.38%	89.02%	111.90%	103.95%
95.42%	105.58%	100.34%	94.75%	108.46%	102.37%	91.11%	111.79%	107.80%
94.46%	105.03%	99.55%	99.97%	106.90%	102.93%	89.94%	123.06%	111.12%
94.34%	104.28%	105.24%	99.57%	100.25%	93.18%	96.81%	115.01%	94.71%
99.41%	92.49%	129.11%	93.26%	106.23%	96.24%	88.60%	114.74%	101.05%
89.55%	108.67%	103.82%	90.04%	118.55%	95.98%	80.20%	111.55%	97.18%
87.14%	92.49%	90.76%	84.58%	93.77%	101.36%	88.46%	90.12%	86.31%

Standard Curve (UDSCC2)



$y = A + Bx$: A B R²

○ Std (Standards: Concentration vs MeanValue) 0,012 0,006 0,975

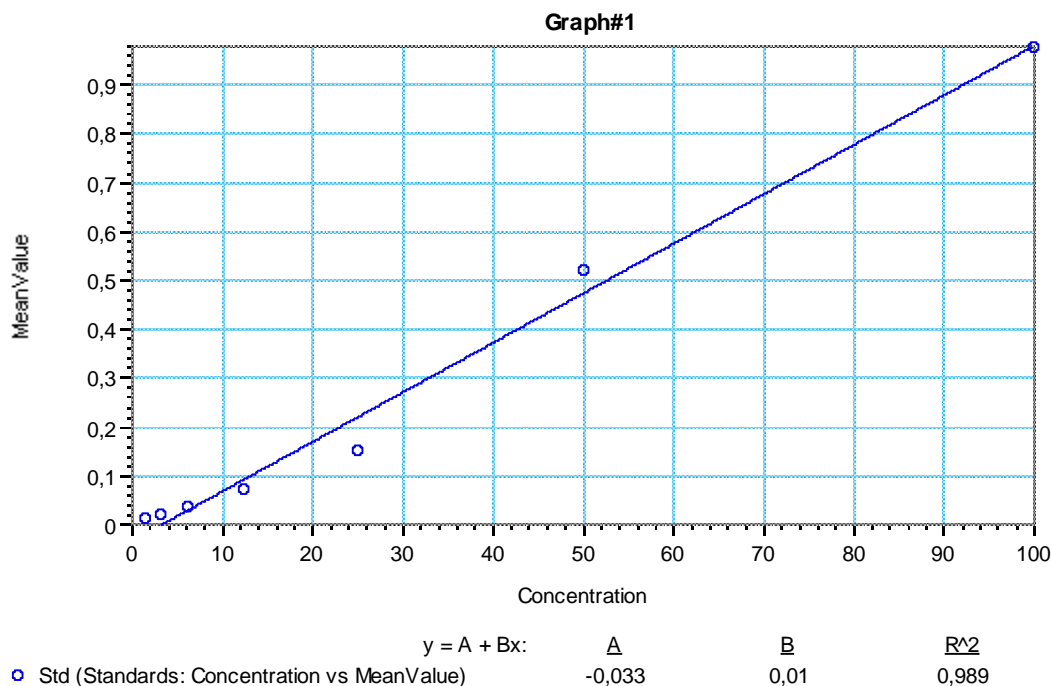
Absorbance Value (UDSCC2)

12 Gy			24 Gy			36 Gy		
0.713	0.718	0.693	0.656	0.636	0.605	0.641	0.630	0.626
0.713	0.668	0.738	0.688	0.615	0.580	0.708	0.603	0.585
0.656	0.603	0.678	0.680	0.615	0.559	0.659	0.542	0.553
0.730	0.619	0.654	0.637	0.592	0.579	0.669	0.545	0.512
0.688	0.652	0.656	0.657	0.548	0.546	0.680	0.661	0.502
0.699	0.723	0.676	0.674	0.624	0.636	0.688	0.641	0.583
0.667	0.688	0.598	0.674	0.677	0.625	0.703	0.693	0.637
0.677	0.637	0.668	0.744	0.672	0.702	0.749	0.713	0.652

Cells viability (% of Control) (UDSCC2)

12 Gy			24 Gy			36 Gy		
115.81%	116.75%	112.50%	106.31%	102.98%	97.88%	103.77%	102.05%	101.32%
115.76%	108.35%	119.98%	111.71%	99.55%	93.68%	115.05%	97.57%	94.54%
106.38%	97.43%	110.00%	110.31%	99.43%	90.25%	106.85%	87.27%	89.15%
118.68%	100.18%	105.93%	103.20%	95.71%	93.48%	108.52%	87.82%	82.29%
111.66%	105.73%	106.31%	106.53%	88.28%	88.00%	110.30%	107.12%	80.62%
113.46%	117.50%	109.63%	109.33%	101.03%	103.03%	111.59%	103.79%	94.14%
108.15%	111.66%	96.61%	109.31%	109.80%	101.10%	114.12%	112.44%	103.12%
109.81%	103.18%	108.35%	121.06%	109.06%	114.01%	121.82%	115.82%	105.62%

Standard Curve (Keratinocyte)



Absorbance Value (Keratinocyte)

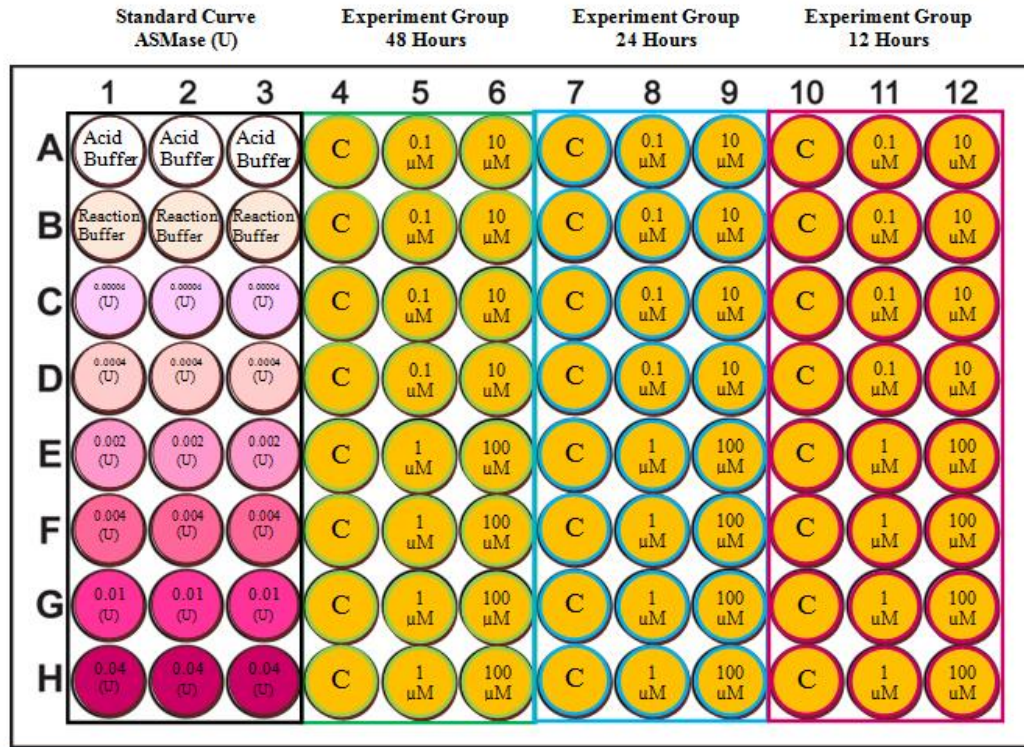
Standard curve			24 Gy		
0.928	0.999	1.001	0.938	0.913	0.937
0.563	0.535	0.467	0.959	0.951	0.928
0.156	0.125	0.169	0.862	0.896	0.951
0.076	0.070	0.068	0.964	0.844	0.944
0.042	0.029	0.030	0.873	0.967	0.924
0.020	0.017	0.019	0.900	0.868	0.915
0.011	0.007	0.012	0.960	0.949	0.941
-0.001	-0.001	0.002	0.962	0.934	0.955

Cells viability (% of Control) (Keratinocyte)

Standard curve			24 Gy		
96.08%	103.20%	103.35%	100.10%	97.57%	100.05%
59.62%	56.77%	50.02%	102.20%	101.45%	99.12%
18.92%	15.77%	20.19%	92.51%	95.87%	101.43%
10.86%	10.30%	10.11%	102.75%	90.66%	100.66%
7.54%	6.22%	6.30%	93.62%	103.00%	98.74%
5.26%	5.00%	5.22%	96.31%	93.13%	97.85%
4.35%	4.02%	4.54%	102.28%	101.17%	100.43%
3.16%	3.21%	3.52%	102.50%	99.71%	101.80%

7.7 ASMase activity after cisplatin treatment

ASMase activity after cisplatin treatment (12, 24 and 48 hours) (UDSCC2)



Original data of absorbance value (UDSCC2)

Hour	Average				Std			
	Control	0.1 μ M	1 μ M	10 μ M	Control	0.1 μ M	1 μ M	10 μ M
12	39628	39644	39264	38346	888	560	1737	153
24	37050	37378	37525	39270	451	1322	930	1001
48	33453	33518	34478	40626	451	1359	893	412

Background correct of absorbance value (UDSCC2)

Hour	Average			Std		
	0.1 μ M	1 μ M	10 μ M	0.1 μ M	1 μ M	10 μ M
12	16	-364	-1282	560	1737	153
24	328	475	2220	1322	930	1001
48	65	1025	7173	1359	893	412

ASMase release (calculate by standard curve) (UDSCC2)

Hour	0.1 μ M cisplatin		1 μ M 0.1 μ M cisplatin		10 μ M 0.1 μ M cisplatin	
	MEAN	SD	MEAN	SD	MEAN	SD
12	0.0000199	0.0006676	-0.0004333	0.0020694	-0.0015270	0.0001828
24	0.0003904	0.0015751	0.0005659	0.0011082	0.0026441	0.0011925
48	0.0000774	0.0016186	0.0012208	0.0010638	0.0085459	0.0004908

Original data of absorbance value (SCC9)

Hour	Average				Std			
	Control	0.1 μM	1 μM	10 μM	Control	0.1 μM	1 μM	10 μM
12	43921	42990	43359	42054	1922	1305	587	791
24	41471	41931	42663	40703	309	1046	522	355
48	39226	38957	38392	38433	775	1354	278	1541

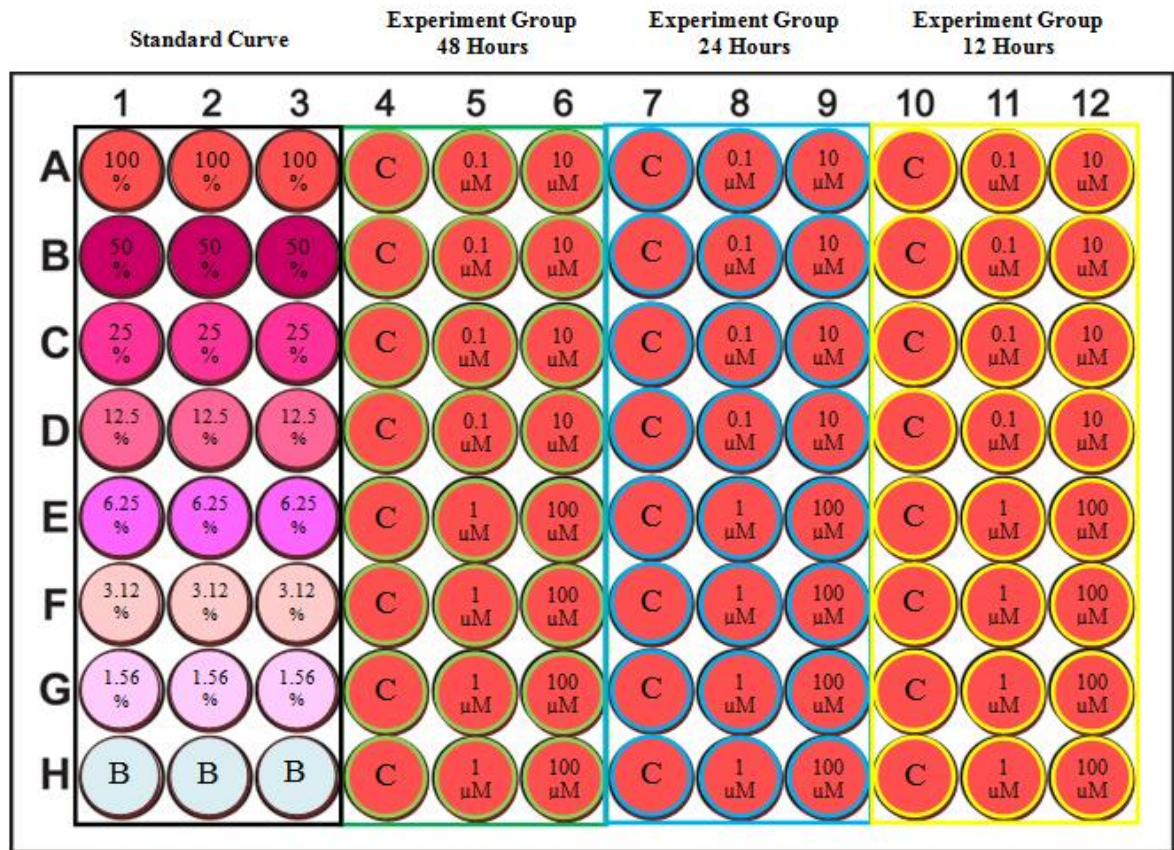
Background correct of absorbance value (SCC9)

Hour	Average			Std		
	0.1 μM	1 μM	10 μM	0.1 μM	1 μM	10 μM
12	-931	-562	-1867	1305	587	791
24	460	1192	-768	1046	522	355
48	-269	-834	-793	1354	278	1541

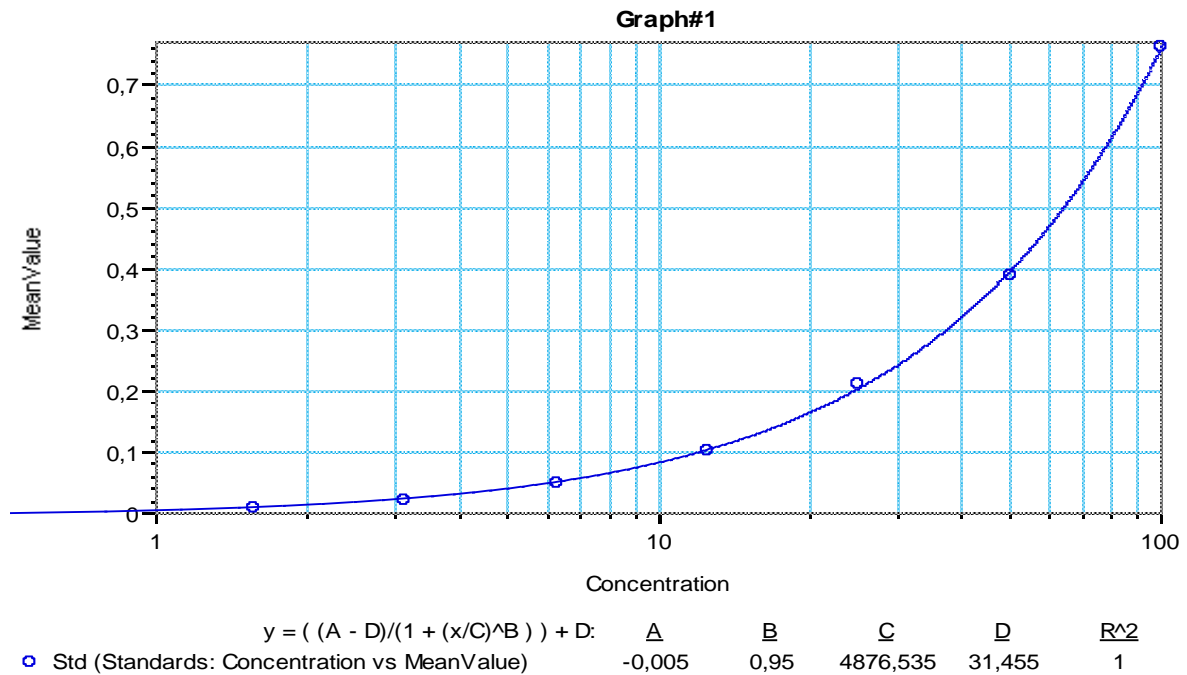
ASMase release (calculate by standard curve) (SCC9)

Hour	0.1 μM cisplatin		1 μM 0.1 μM cisplatin		10 μM 0.1 μM cisplatin	
	MEAN	SD	MEAN	SD	MEAN	SD
12	-0.00093	0.001305	-0.00056	0.000587	-0.00187	0.000791
24	0.00046	0.001046	0.001192	0.000522	-0.00077	0.000355
48	-0.00027	0.001354	-0.00083	0.000278	-0.00079	0.001541

7.8 MTT test: 12, 24 and 48 hours after cisplatin treatment



Standard Curve: UDSCC2



Schematic of 96-wells plate (UDSCC2)

◇	1	2	3	4	5	6	7	8	9	10	11	12
	Standard (%)			48 hours			24 hours			12 hours		
A	100	100	100	control	0.1	10	control	0.1	10	control	0.1	10
B	50	50	50	control	0.1	10	control	0.1	10	control	0.1	10
C	25	25	25	control	0.1	10	control	0.1	10	control	0.1	10
D	12.5	12.5	12.5	control	0.1	10	control	0.1	10	control	0.1	10
E	6.25	6.25	6.25	control	1	100	control	1	100	control	1	100
F	3.12	3.12	3.12	control	1	100	control	1	100	control	1	100
G	1.56	1.56	1.56	control	1	100	control	1	100	control	1	100
H	0	0	0	control	1	100	control	1	100	control	1	100

Original data of absorbance value (UDSCC2)

◇	1	2	3	4	5	6	7	8	9	10	11	12
	Standard			48 hours			24 hours			12 hours		
A	0.774	0.744	0.770	0.651	0.795	0.576	0.759	0.729	0.508	0.683	0.713	0.687
B	0.400	0.384	0.383	0.754	0.765	0.578	0.719	0.736	0.489	0.696	0.754	0.673
C	0.204	0.205	0.228	0.779	0.784	0.578	0.719	0.735	0.563	0.688	0.709	0.651
D	0.113	0.103	0.097	0.759	0.778	0.526	0.721	0.737	0.546	0.682	0.675	0.645
E	0.055	0.053	0.045	0.742	0.788	0.000	0.718	0.732	0.093	0.688	0.680	0.226
F	0.026	0.025	0.015	0.762	0.767	0.003	0.704	0.724	0.096	0.647	0.724	0.249
G	0.010	0.011	0.010	0.751	0.752	0.001	0.706	0.737	0.078	0.672	0.719	0.224
H	0.000	0.002	-0.002	0.773	0.744	-0.001	0.646	0.713	0.072	0.623	0.625	0.198

Cells viability after cisplatin treatment (calculate by standard curve) (UDSCC2)

◇	1	2	3	4	5	6	7	8	9	10	11	12
	Standard (%)			48 hours (%)			24 hours (%)			12 hours (%)		
A	102.046	97.855	101.551	84.773	105.005	74.450	99.870	95.772	65.103	89.286	93.442	89.845
B	50.620	48.464	48.384	99.250	100.788	74.752	94.354	96.715	62.606	91.131	99.278	87.919
C	25.079	25.129	28.062	102.696	103.432	74.656	94.284	96.532	72.679	90.027	92.938	84.870
D	13.645	12.472	11.693	99.927	102.640	67.566	94.649	96.841	70.392	89.077	88.086	83.953
E	6.699	6.510	5.585	97.573	103.999	0.465	94.200	96.068	11.256	89.999	88.812	27.896
F	3.360	3.281	2.069	100.294	101.014	0.841	92.209	95.056	11.669	84.245	94.958	30.758
G	1.606	1.672	1.541	98.784	98.996	0.568	92.433	96.897	9.495	87.696	94.312	27.551
H	0.527	0.683	0.262	101.876	97.841	0.353	84.162	93.442	8.776	80.918	81.153	24.266

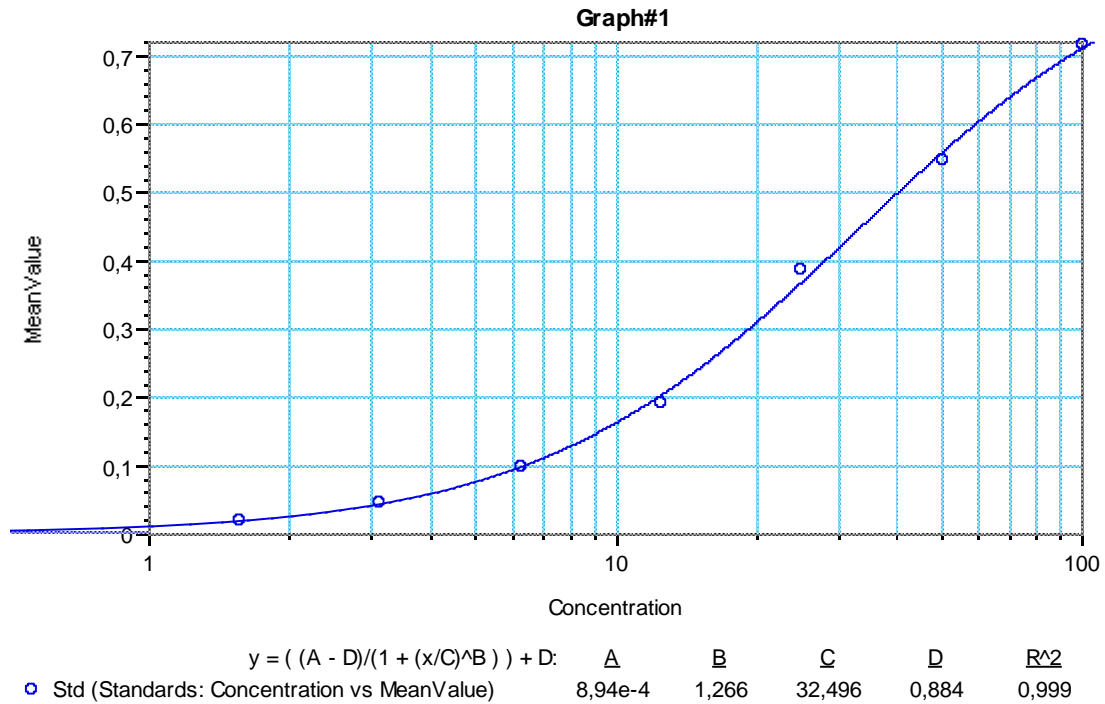
Correct with each control group (UDSCC2)

48 hours (%)			24 hours (%)			12 hours (%)		
100.00	106.99	75.86	100.00	102.68	69.80	100.00	106.43	102.33
100.00	102.69	76.16	100.00	103.69	67.12	100.00	113.08	100.14
100.00	105.39	76.07	100.00	103.50	77.92	100.00	105.86	96.67
100.00	104.58	68.84	100.00	103.83	75.47	100.00	100.33	95.62
100.00	105.96	0.47	100.00	103.00	12.07	100.00	101.16	31.77
100.00	102.92	0.86	100.00	101.91	12.51	100.00	108.16	35.03
100.00	100.86	0.58	100.00	103.89	10.18	100.00	107.42	31.38
100.00	99.69	0.36	100.00	100.18	9.41	100.00	92.43	27.64

Viability of UDSCC2 after cisplatin treatment (UDSCC2)

Treatment time	48 hours		24 hours		12 hours	
Cisplatin concentration	average	std	average	std	average	std
0.1	104.91	1.79	103.43	0.51	106.42	5.22
1	102.36	2.75	102.25	1.59	102.29	7.28
10	74.23	3.60	80.49	4.98	98.69	3.10
100	0.57	0.21	11.04	1.49	31.46	3.03

Standard Curve: (SCC9)



Schematic of 96-wells plate (SCC9)

◇	1	2	3	4	5	6	7	8	9	10	11	12
	Standard (%)		48 hours				24 hours			12 hours		
A	100	100	control	control	0.1	10	control	0.1	10	control	0.1	10
B	50	50	control	control	0.1	10	control	0.1	10	control	0.1	10
C	25	25	control	control	0.1	10	control	0.1	10	control	0.1	10
D	12.5	12.5	control	control	0.1	10	control	0.1	10	control	0.1	10
E	6.25	6.25	control	control	1	100	control	1	100	control	1	100
F	3.12	3.12	control	control	1	100	control	1	100	control	1	100
G	1.56	1.56	control	control	1	100	control	1	100	control	1	100
H	0	0	control	control	1	100	control	1	100	control	1	100

Original data of absorbance value (SCC9)

◇	1	2	3	4	5	6	7	8	9	10	11	12
	Standard		48 hours				24 hours			12 hours		
A	0.706	0.726	0.762	0.749	0.728	0.748	0.682	0.719	0.724	0.683	0.724	0.769
B	0.524	0.571	0.727	0.722	0.667	0.700	0.707	0.667	0.699	0.689	0.676	0.703
C	0.394	0.379	0.695	0.695	0.722	0.714	0.664	0.678	0.692	0.651	0.682	0.730
D	0.204	0.180	0.692	0.684	0.648	0.714	0.674	0.659	0.635	0.655	0.638	0.658
E	0.106	0.090	0.701	0.653	0.697	0.103	0.660	0.658	0.439	0.652	0.682	0.695
F	0.048	0.047	0.682	0.692	0.706	0.107	0.635	0.673	0.479	0.667	0.675	0.635
G	0.024	0.014	0.691	0.686	0.733	0.101	0.655	0.690	0.381	0.651	0.705	0.550
H	0.001	-0.001	0.699	0.752	0.645	0.119	0.670	0.693	0.402	0.623	0.553	0.410

Cells viability after cisplatin treatment (calculate by standard curve) (SCC9)

◇	1	2	3	4	5	6	7	8	9	10	11	12
	Standard (%)		48 hours (%)				24 hours (%)			12 hours (%)		
A	96.636	108.112	137.838	125.535	109.374	125.103	84.897	103.986	107.069	85.200	106.812	145.349
B	43.645	52.111	108.773	105.413	78.865	93.347	97.123	78.675	92.843	87.776	82.420	94.785
C	27.350	25.870	90.584	91.018	105.476	100.768	77.514	82.997	89.348	72.967	84.725	110.939
D	12.515	11.044	89.489	85.897	72.070	100.826	81.728	75.877	67.923	74.330	69.047	75.521
E	6.683	5.800	94.010	73.609	91.948	6.540	76.272	75.450	32.069	73.440	85.070	90.873
F	3.348	3.300	84.897	89.208	96.475	6.751	68.103	81.166	37.094	78.942	82.052	67.953
G	1.850	1.200	88.695	86.560	112.970	6.381	74.434	88.279	26.069	73.068	95.676	48.061
H	0.052	0.000	92.593	128.276	71.254	7.449	79.944	90.058	28.101	64.604	48.651	28.881

Correct with each control group (SCC9)

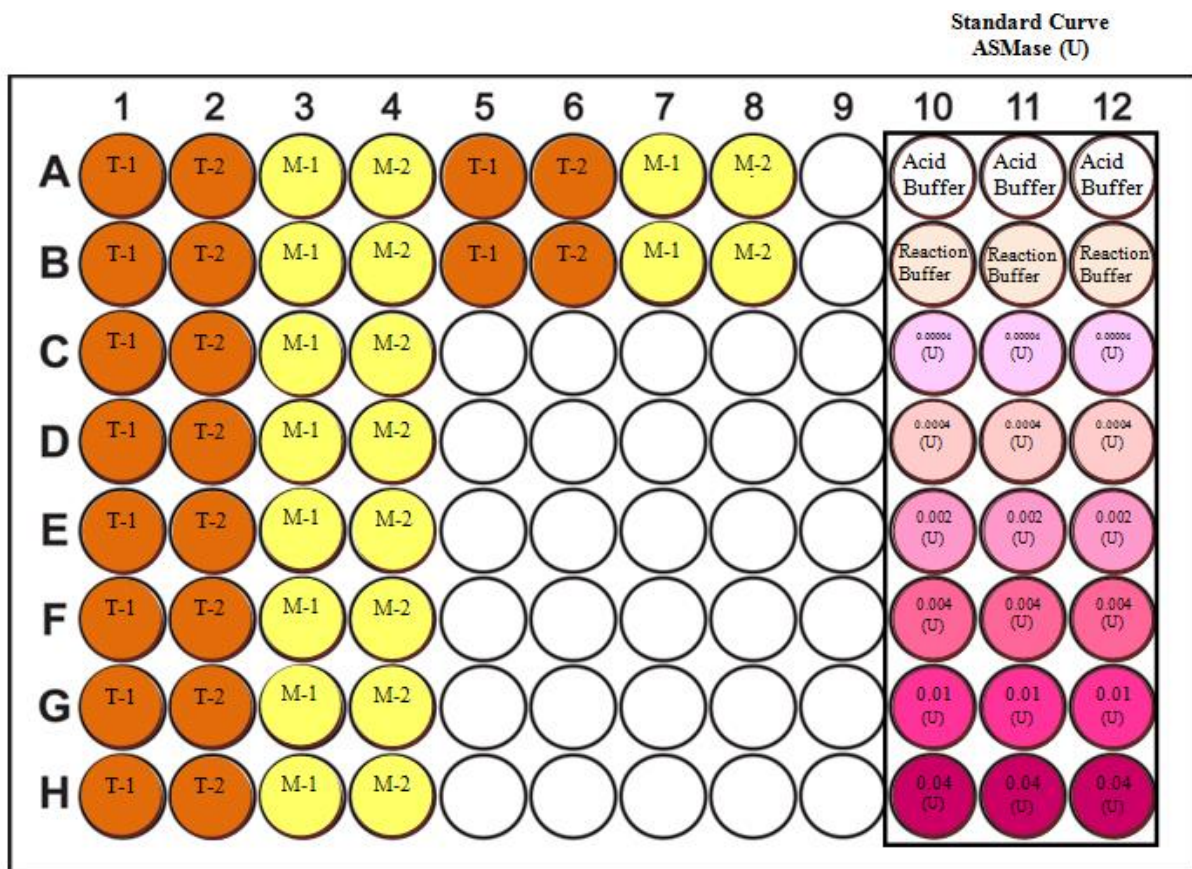
48 hours (%)			24 hours (%)			12 hours (%)		
100.00	111.29	127.30	100.00	129.98	133.83	100.00	140.01	190.52
100.00	80.25	94.99	100.00	98.34	116.05	100.00	108.03	124.24
100.00	107.33	102.54	100.00	103.74	111.68	100.00	111.06	145.42
100.00	73.33	102.60	100.00	94.84	84.90	100.00	90.50	98.99
100.00	93.56	6.65	100.00	94.31	40.09	100.00	111.51	119.11
100.00	98.17	6.87	100.00	101.45	46.37	100.00	107.55	89.07
100.00	114.95	6.49	100.00	110.35	32.59	100.00	125.41	63.00
100.00	72.50	7.58	100.00	112.57	35.13	100.00	63.77	37.86

Viability of SCC9 after cisplatin treatment (SCC9)

Treatment time	48 hours		24 hours		12 hours	
Cisplatin concentration	average	std	average	std	average	std
0.1	93.05	19.05	106.73	15.93	112.40	20.51
1	94.80	17.47	104.67	8.41	102.06	26.65
10	106.85	14.09	111.62	20.22	139.79	38.78
100	6.90	0.48	38.54	6.08	77.26	34.87

7.9 aSMase activity of HNSCC and muscle in mice

Schematic of 96-wells plate

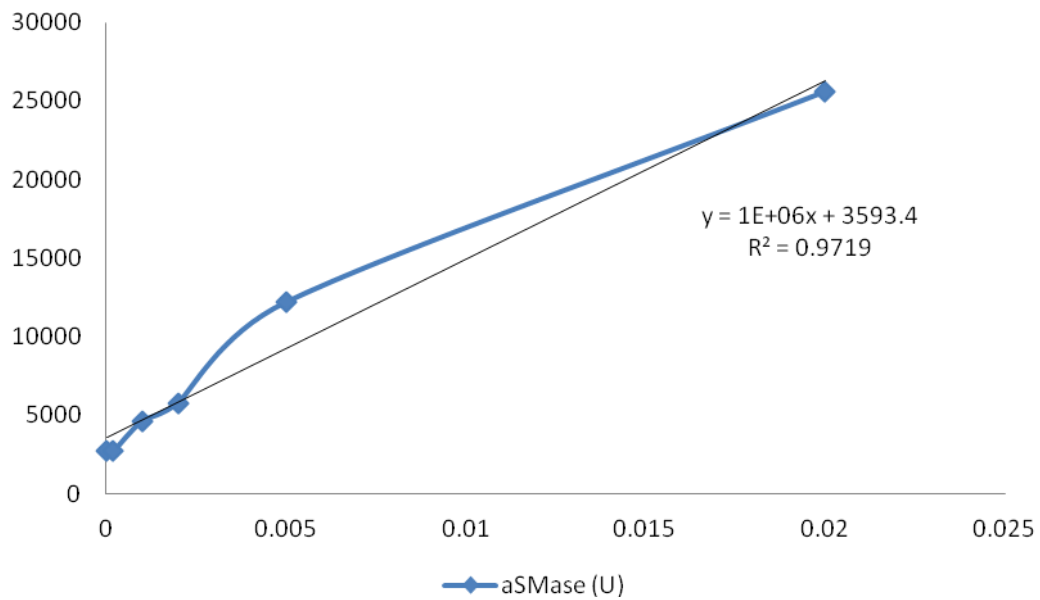


<>	1	2	3	4	5	6	7	8	9	10	11	12
A	T1	T2	M1	M2	T1	T2	M1	M2		Acid buffer		
B	T1	T2	M1	M2	T1	T2	M1	M2		Reaction buffer		
C	T1	T2	M1	M2						aSMase 0.00002 U		
D	T1	T2	M1	M2						aSMase 0.0002 U		
E	T1	T2	M1	M2						aSMase 0.001 U		
F	T1	T2	M1	M2						aSMase 0.002 U		
G	T1	T2	M1	M2						aSMase 0.005 U		
H	T1	T2	M1	M2						aSMase 0.02 U		

Original data of absorbance value

<>	1	2	3	4	5	6	7	8	9	10	11	12
A	19558	21458	10716	12752	31079	26735	8974	8560	19	2935	2665	2265
B	45587	44718	10526	11776	24025	20193	10793	12469	21	2314	2251	2432
C	30934	24206	13737	10681	29	28	31	34	26	2823	2788	2581
D	33370	49749	9865	15877	24	38	32	31	19	2707	2638	2751
E	25628	39701	11553	10089	25	32	38	32	16	4610	4606	4585
F	33058	31817	22521	17678	29	24	36	46	30	5841	5834	5681
G	29953	31348	8021	6915	41	27	24	23	34	12624	12177	11752
H	21683	29886	9521	11620	35	26	39	35	11	25591	45	36

Standard curve



aSMase release of mice tissue (U)

No.	Tumor-1	Tumor-2	Muscle-1	Muscle-2
1	0.01596	0.01786	0.00712	0.00916
2	0.04199	0.04112	0.00693	0.00818
3	0.02734	0.02061	0.01014	0.00709
4	0.02978	0.04616	0.00627	0.01228
5	0.02203	0.03611	0.00796	0.00650
6	0.02946	0.02822	0.01893	0.01408
7	0.02636	0.02775	0.00443	0.00332
8	0.01809	0.02629	0.00593	0.00803
9	0.02749	0.02314	0.00538	0.00497
10	0.02043	0.01660	0.00720	0.00888

Weight of mice tissue (mg)

No.	Tumor-1	Tumor-2	Muscle-1	Muscle-2
1	0.088	0.060	0.078	0.047
2	0.131	0.094	0.063	0.062
3	0.147	0.156	0.085	0.062
4	0.065	0.113	0.052	0.091
5	0.048	0.077	0.057	0.042
6	0.062	0.147	0.111	0.070
7	0.067	0.064	0.042	0.048
8	0.037	0.054	0.038	0.060
9	0.067	0.072	0.050	0.065
10	0.054	0.069	0.047	0.055

aSMase release of mice tissue per gram (aSMase U/mg)

No.	Tumor-1	Tumor-2	Muscle-1	Muscle-2	Tumor average	Muscle average
1	0.181	0.298	0.091	0.195	0.240	0.143
2	0.321	0.437	0.110	0.132	0.379	0.121
3	0.186	0.132	0.119	0.114	0.159	0.117
4	0.458	0.408	0.121	0.135	0.433	0.128
5	0.459	0.469	0.140	0.155	0.464	0.147
6	0.475	0.192	0.171	0.201	0.334	0.186
7	0.393	0.434	0.105	0.069	0.414	0.087
8	0.489	0.487	0.156	0.134	0.488	0.145
9	0.410	0.321	0.108	0.076	0.366	0.092
10	0.378	0.241	0.153	0.161	0.309	0.157

Tumor		Muscle		p value
MEAN	SD	MEAN	SD	
0.359	0.102	0.132	0.030	9.23×10^{-5}

8. Acknowledgement

The writing of this dissertation has been one of the most significant academic challenges I have ever had to face. Without the support, patience and guidance of the following people, this study would not have been completed. It is to them that I owe my deepest gratitude.

Foremost, I would like to express my sincere gratitude to Prof. Dr. med. Dr. med. dent. Jörg Wiltfang, director of the department of Oral and Maxillofacial Surgery, for his invitation and great supports of my visit and training at Kiel University.

Besides, I sincerely thank my advisor Prof. Dr. rer. nat. Yahya Ail, director of the laboratory, for his scientific instruction of this research program, for the continuous support of my M.D. study and research, and for his motivation, enthusiasm, immense knowledge, insightful comments and encouragement.

Special thanks should be given to Dr. Tuula Peñate Medina, Dr. Oula Peñate Medina and Dr. Mirko Gerle, for their excellent direction and enthusiastic supports throughout the project. I enjoyed their insightful supervision and wonderful help with my training. Their guidance helped me in all the time of research and writing of this thesis. They are also carefully and patiently correction of this dissertation. I could not have imagined having a better mentor for my M.D. study.

Thanks also give to Ms. Frau Refrath and lab mates in the Molecular Imaging North Competence Center (MOIN CC), for their excellent expert technical assistance as well as their great help with my training. I enjoyed working with them. I sincerely thank Mr. Ritter and other fellows of International Department of Christian–Albrecht-University. They always gave me timing help needed from an international scholar.

Finally, I should sincerely thank my dear parents and beloved wife Yun Chu, for their supporting me spiritually throughout staying in Germany and their unbelievable love.

9. Publication

Acid sphingomyelinase activity as an indicator of the cell stress in HPV-positive and HPV-negative head and neck squamous cell carcinoma.

Med Oncol. 2018 Mar 21;35(4):58. doi: 10.1007/s12032-018-1117-4.

Gerle M, Medina TP, Gülses A, **Chu H**, Naujokat H, Wiltfang J, Açil Y.

Medical Oncology (2018) 35:58
<https://doi.org/10.1007/s12032-018-1117-4>

ORIGINAL PAPER



Acid sphingomyelinase activity as an Indicator of the cell stress In HPV-positive and HPV-negative head and neck squamous cell carcinoma

Mirko Gerle¹ · Tuula Peñate Medina² · Aydin Gülses¹ · Hanwen Chu² · Hendrik Naujokat¹ · Jörg Wiltfang¹ · Yahya Açil¹

Received: 2 March 2018 / Accepted: 18 March 2018 / Published online: 21 March 2018
 © Springer Science+Business Media, LLC, part of Springer Nature 2018

Abstract

Human papillomavirus (HPV) infection, especially HPV-16 and HPV-18, has been increasingly associated with head and neck squamous cell carcinoma. The treatment of HPV-positive squamous cell carcinoma has a better response to both radiotherapy and chemotherapy and presents a better prognosis for the patient. Defining the underlying mechanism of the difference might help in developing future treatment options and could be an important factor in personal therapy planning. Endogenously secreted acid sphingomyelinase (ASMase) levels in the cellular stress caused by irradiation and cisplatin were investigated. MTT assay was performed to evaluate the viability of the treated cells. Keratinocytes were used to evaluate the effects of radiation on normal tissues. Irradiation caused a dose-dependent increase in ASMase activity in both SCC9 HPV-negative, and UDSCC2 HPV-positive cells. ASMase activity in UDSCC2 cells was significantly higher than that in SCC9 cells. UDSCC cells were more sensitive to cisplatin treatment than SCC cells, and the dose-response in the activity was observed in long-time treatments when high doses of cisplatin were used. The results of the current study have clearly showed that HPV positivity should be considered as one of the determinative factors which should be considered when tumor treatments are planned. However, further studies are needed to determine the differences in cellular responses and pathways among HPV-negative and HPV-positive cells.

Keywords Acid sphingomyelinase · HPV · Squamous cell carcinoma · Cell stress

Introduction

Head and neck squamous cell carcinoma (HNSCC) constitute approximately 4% of all cancers worldwide. Its incidence increases with age and carries a mortality rate of over 50% [1–3]. Each year, more than a half-million new cases were diagnosed [1–3]. Whereas surgery and radiotherapy remain as primary modalities for management of early and

loco-regionally advanced HNSCC, non-selective chemotherapy (e.g., cisplatin, axitinib) is another option, which could be usually associated with severe adverse effects. Considering the limitation of the above mentioned therapeutic options in the management of recurrent and metastatic HNSCC cases, the estimated 5-year survival rate could not be significantly improved [3–5].

Although HNSCC is thought to be mainly caused by molecular effects of environmental carcinogens, human papillomavirus (HPV), especially HPV-16 and HPV-18, has been widely reported to be associated with the condition [5, 6]. HPV-associated HNSCC comprise a distinct molecular, clinical and pathologic entity that has a better prognosis than HPV-negative cancers. It has been suggested that future therapeutic concepts for HNSCC may be personalized in relation to HPV status to avoid drug-induced side effects, which makes understanding of the relationship between HPV and HNSCC more important than ever [7].

Mirko Gerle and Tuula Peñate Medina have contributed equally and should be considered as co-first authors.

✉ Aydin Gülses
agulses@mkg.uni-kiel.de

¹ Department of Oral and Maxillofacial Surgery, Christian Albrechts University, Campus Kiel, Arnold-Heller-Strasse 3, 24105 Kiel, Germany

² Department of Radiology and Neuroradiology, Christian Albrechts University, Kiel, Germany

M. Gerle, **H. Chu**, C.-C. Glüer, J. Wiltfang, Y. Açil, M. Hoffmann, T. Grörögh, T. Peñate Medina, O. Peñate Medina. Acid sphingomyelinase activity as a cell stress indicator in HPV positive and negative head and neck carcinoma cell lines. *66. Jahrestagung der Arbeitsgemeinschaft für Kieferchirurgie & 37. Jahrestagung des Arbeitskreises für Oralpathologie und Oralmedizin . Poster presentation*



Saure Sphingomyelinase-Aktivität als Indikator für Zellstress HPV-positiver und -negativer Kopf-Halskarzinome



M. Gerle¹, H. Chu², C.-C. Glüer³, J. Wiltfang¹, Y. Açil¹, M. Hoffmann¹, T. Grörögh¹, T. Peñate Medina³, O. Peñate Medina³

¹Klinik für Mund-, Kiefer- und Gesichtschirurgie, Christian-Albrechts-Universität, Kiel

²Dept. of Oral and Maxillofacial Surgery, Second Affiliated Hospital, Zhejiang University School of Medicine, Hangzhou, China

³Molecular Imaging North Competence Center, Sektion für biomedizinische Bildgebung, Christian-Albrechts-Universität, Kiel

⁴Klinik für Hals-Nasen-Ohrenheilkunde - Kopf- und Halschirurgie, Christian-Albrechts-Universität, Kiel

Einführung

Die Inzidenz von Karzinomen des Kopf-Halsbereichs, die in ihrer Entstehung mit "high risk" humanen Papillomaviren (HPV Typ16, 18) in Zusammenhang gebracht werden, nimmt stetig zu. Die Therapie von HPV-positiven Plattenepithelkarzinomen in diesem Bereich ist insbesondere durch ein besseres Ansprechen auf die Strahlentherapie und somit günstigere Prognose für den Patienten gekennzeichnet. Die Mechanismen zu verstehen, wie der HPV-Status das unterschiedliche Therapieansprechen von Kopf-Halskarzinomen beeinflusst, könnte helfen in Zukunft die Diagnostik und Therapie dieser Tumoren zu verbessern.

Es wird angenommen, dass Zellstress, ausgelöst zum Beispiel durch Bestrahlung, Hypoxie oder Chemotherapie, eine Degradation von Sphingomyelin-Lipiden in der Zellmembran triggert. Die hydrolytische Spaltung dieser Lipide durch das Enzym saure Sphingomyelinase (sSMase) führt zur Entstehung von Ceramid, welches als Second-Messenger die Apoptose bzw. lysosomale Nekrose einleiten kann. Ziel dieser Untersuchung ist die Bestimmung der sauren Sphingomyelinase-Aktivität HPV-positiver und -negativer Tumorzellen nach Bestrahlung bzw. Cisplatinbehandlung.

Material und Methode

In dieser Studie wurden die beiden Plattenepithelkarzinomzelllinien UDSCC2 (HPV-positiv) und SCC9 (HPV-negativ) hinsichtlich ihrer unterschiedlichen Sphingomyelinase-Aktivität nach Bestrahlung (120y, 240y, 360y) und Cisplatinbehandlung (0,1µM, 1µM, 10µM für 24h und 36h) untersucht. Die Enzymaktivität wurde mit Hilfe eines Amplex-Red Assay Kits bestimmt.

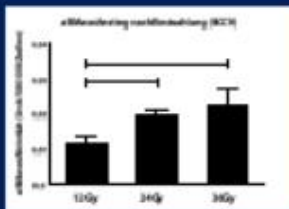


Abb. 1 Die Bestrahlung führte bei SCC9 (HPV-negativ) Tumorzellen dosisabhängig zum Anstieg der Sphingomyelinase-Aktivität.

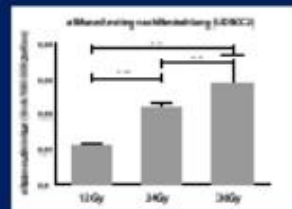


Abb. 2 Auch bei den UDSCC2 (HPV-positiv) Tumorzellen kam es nach Bestrahlung dosisabhängig zum Anstieg der Sphingomyelinase-Aktivität.

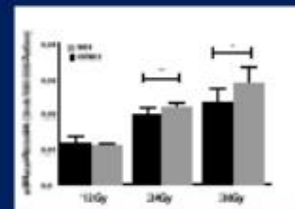


Abb. 3 Im Vergleich beider Tumorzelllinien zeigen die HPV-positiven UDSCC2 Tumorzellen nach 240y und 360y Bestrahlung eine signifikant höhere Sphingomyelinase-Aktivität.

Ergebnisse

In beiden Zelllinien konnte ein signifikanter, dosisabhängiger Anstieg der sSMase-Aktivität eine Stunde nach Bestrahlung gezeigt werden (Abb. 1, 2). Die HPV-positive UDSCC2 Tumorzelllinie hatte gegenüber der HPV-negativen SCC9 Tumorzelllinie nach 240y und 360y Bestrahlung eine signifikant höhere sSMase-Aktivität (Abb. 3). Nach Cisplatinbehandlung zeigte nur die HPV-positive UDSCC2 Tumorzelllinie einen signifikanten dosis- und zeitabhängigen Anstieg der sSMase-Aktivität (Abb. 4, 5).

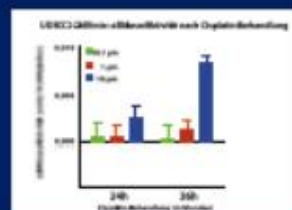


Abb. 4 Nach Behandlung der UDSCC2 (HPV-positiv) Tumorzellen kam es zu einem dosis- und zeitabhängigen Anstieg der Sphingomyelinase-Aktivität.

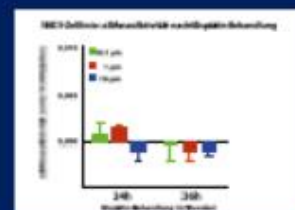



Abb. 5 Nach Behandlung der SCC9 (HPV-negativ) Tumorzellen kam es weder zu einem dosis- noch zeitabhängigen Anstieg der Sphingomyelinase-Aktivität.

Zusammenfassung

Aus der Literatur ist bekannt, dass HPV-positive Kopf-Halskarzinome ein besseres Therapieansprechen auf Bestrahlung zeigen als HPV-negative. Dennoch sind die genauen biologischen und molekularen Mechanismen, die hierfür verantwortlich sind, nicht bekannt. Das Enzym saure Sphingomyelinase, das auch durch Zellstress (u.a. Bestrahlung, Chemotherapie) induziert wird, könnte einen Erklärungsansatz aufzeigen. In dieser Untersuchung konnte gezeigt werden, dass HPV-positive UDSCC2 Plattenepithelkarzinomzellen eine signifikant höhere, dosisabhängige sSMase-Aktivität nach Bestrahlung bzw. Cisplatinbehandlung entwickelten, als HPV-negative SCC9 Tumorzellen.


Die exzellenten Überlebensdaten HPV-positiver Patienten führt dazu, dass der HPV-Status in der Therapieentscheidung zunehmend berücksichtigt wird. In Zukunft könnte ergänzend die sSMase-Aktivität im Rahmen des Stagings evaluiert und als prognostischer Marker für den Behandlungserfolg herangezogen werden und somit zu einer höheren Individualisierung der Patientenbehandlung führen. Das unterschiedliche Ansprechen HPV-positiver und -negativer Kopf-Halskarzinomen zu verstehen könnte darüber hinaus für eine zielgerichtete Therapie mit Reduktion der Nebenwirkungen genutzt werden.

M. Gerle, **H. Chu**, O. Will, C.-C. Glüer, J. Wiltfang, Y. Açil, T. Peñate Medina, O. Peñate Medina. Optical imaging and local drug release of oral squamous cell carcinoma in vivo using magneto-enzymatic sensitive liposome. 66. Kongress der Deutschen Gesellschaft für Mund-, Kiefer- und Gesichtschirurgie und Praxisführungsseminar, Poster



Christian-Albrechts-Universität zu Kiel
Molekulare Bildgebung

Molekulare Bildgebung und lokale Wirkstofffreisetzung in der Therapie des oralen Plattenepithelkarzinoms unter Verwendung von „Magneto-Enzymatic-Sensitive Liposomes“ (MESL)



UKSH

M. Gerle¹, **H. Chu**², O. Will¹, C.-C. Glüer¹, J. Wiltfang¹, Y. Açil¹, T. Peñate Medina¹, O. Peñate Medina¹

¹ Klinik für Mund-, Kiefer- und Gesichtschirurgie, Christian-Albrechts-Universität, Kiel
² Dept. of Oral and Maxillofacial Surgery, Second Affiliated Hospital, Zhejiang University School of Medicine, Hangzhou, China
³ Molekulare Imaging North Competence Center, Sektion für biomedizinische Bildgebung, Christian-Albrechts-Universität, Kiel

Einleitung

Das Mundhöhlenkarzinom (OSCC) gehört zu den häufigsten Malignomenkrankungen von Männern und Frauen mit weiterhin steigender Inzidenz. Die Krebserkrankung ist aufgrund ihres oft fortgeschrittenen Tumorstadiums bei Diagnosestellung durch eine schlechte Prognose und 5-Jahres-Überlebensrate gekennzeichnet (44-55%)¹. Eine intraoperative molekulare Bildgebung des Tumors mit Darstellung seiner Grenzen sowie

eine gezielte, lokale Wirkstofffreisetzung von Chemotherapeutika im Tumorgewebe könnten in Zukunft zu einer individualisierteren Therapie mit geringerer Mortalität und Morbidität der betroffenen Patienten führen. In dieser Untersuchung wurden Nanopartikel (Liposomen) als sog. drug delivery system zur molekularen in vivo Bildgebung des OSCC und gezielter, lokaler Wirkstofffreisetzung im Tumorgewebe in einem Xenograft Maus Modell verwendet.

Material und Methode

SCC-9 Plattenepithelkarzinomzellen wurden in den Mundboden von athymischen Nacktmäusen (Rj:NMRI-Foxnu/Foxnu) inkuliert und führten innerhalb von 2 Wochen zur lokalen Tumorausbildung. Die Liposomen wurden anschließend wöchentlich intravenös (Schwanzvene) appliziert und erhielten den Fluoreszenzfarbstoff Indocyaningrün (ICG) zur visuellen Markierung bzw. das Chemotherapeutikum Cisplatin zur Behandlung der Mundbodentumore. Nach Injektion kommt es vor allem aufgrund der erhöhten Permeabilität der Kapillaren im Tumorgewebe (EPR-Effekt, enhanced permeability and retention effect) zu einer lokalen Akkumulation der Liposomen². Die Wirkstofffreisetzung aus den Liposomen wurde zum einen durch ein alternierendes Magnetfeld (AMF; Abb. 1) getriggert, das lokal auf die

Kopf-Halsregion für 20min appliziert wurde und mit Eisenpartikeln in der Lipidschicht der Liposomen interagiert. Zum anderen führte der Einfluss des Enzyms saure Sphingomyelinase, welches vermehrt in Tumorzellen gebildet wird, zu einer enzymatisch getriggerten Freisetzung (daher MESL: Magneto-Enzymatic-Sensitive-Liposomes). Zur visuellen Darstellung der Tumore wurde eine in vivo Fluoreszenzbildgebung durchgeführt (Abb. 2 OP-Mikroskop, Abb. 3 NightOwl Fluoreszenzlampe). Das Tumorwachstum wurde mittels Kleinflutraschall verfolgt (Abb. 4). Insgesamt gab es zwei Versuchsgruppen mit jeweils 10 Mäusen. Die Liposomen, die der Gruppe 1 injiziert wurden, erhielten nur ICG, die der Gruppe 2 ICG und Cisplatin.




Abb. 1 Nach Injektion der Liposomen über die Schwanzvene akkumulieren diese aufgrund des EPR-Effektes im Mundbodentumor. Ein alternierendes Magnetfeld (2mT, 100kHz) triggert die lokale Wirkstofffreisetzung aus den Liposomen.




Abb. 2a OP-Mikroskop Aufnahme einer Nacktm Maus mit Mundbodentumor. Zur besseren Darstellung der Tumorgrenzen wurde die Haut im Halsbereich entfernt. **Abb. 2b** Nach Injektion der Fluoreszenzfarbstoff-enthaltenden Liposomen akkumulieren diese im Tumor. Unter Verwendung eines Fluoreszenzfilters ist eine visuelle Markierung des Tumors möglich.




Abb. 3 Aufnahme in der Fluoreszenzlampe (NightOwl, Fa. Berthold) nach Injektion der Fluoreszenzfarbstoff-enthaltenden Liposomen. Auch hier ist nach Akkumulation der Liposomen eine visuelle Markierung des Mundbodentumors möglich. Aufgrund der bilätralen Ausscheidung ist in der Leber ebenfalls ein Signal zu sehen.

Ergebnisse

Nach Anreicherung der Liposomen im Tumorgewebe und Applikation eines alternierenden Magnetfeldes, konnten die Mundbodentumore mit Hilfe der Fluoreszenzbildgebung visuell markiert und dargestellt werden (Gruppe 1). Die lokale Cisplatinfreisetzung aus den Liposomen führte zu einem signifikant ($p=0,007$) verlangsamten Tumorwachstum (Gruppe 2) im Vergleich zur Kontrollgruppe (Gruppe 1).

Abb. 4 Die Nacktmäuse, denen wöchentlich Cisplatin-enthaltende Liposomen Injektion wurde (Gruppe 2), zeigten unter sonographischer Kontrolle eine geringere Zunahme der Tumorgöße, als die Kontrollgruppe (Gruppe 1).

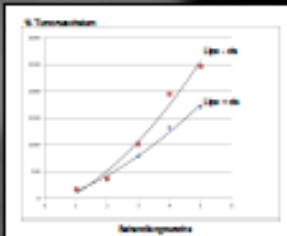


Abb. 4 Tumorwachstum

Beobachtungstage	Gruppe 1 (Control)	Gruppe 2 (Liposomes)
0	~100	~100
3	~150	~120
6	~250	~150
9	~400	~180
12	~600	~220
14	~800	~250

Zusammenfassung

Liposomale Nanopartikel können in Zukunft helfen intraoperativ Kopf-Halskarzinome visuell zu markieren und darzustellen. Dies würde die Sicherheit bei der chirurgischen Tumoresektion erhöhen und gleichzeitig

helfen wichtige anatomische Strukturen zu schonen. Darüber hinaus können Liposomen verwendet werden, um lokal Chemotherapeutika (Cisplatin) im Tumorgewebe freizusetzen und somit die systemischen Nebenwirkungen einer solchen Therapie zu mindern.

Literatur

1 RKI Krebs in Deutschland, 9. Ausgabe
 2 Drug delivery systems: entering the mainstream, Allen TM et al., Science. 2004 Mar 19;303(5665):1818-22

10. Academic Resume

Personal information

<i>Name</i>	Hanwen Chu	<i>Gender</i>	Male
<i>Date of Birth</i>	18.Nov.1986	<i>Place of Birth</i>	Ningbo, Zhejiang
<i>Marriage status</i>	Married	<i>Nationality</i>	P. R. China.
<i>Address</i>	Department of oral and maxillofacial surgery, the second affiliated hospital of Zhejiang University, 88# Jiefang Road, Hangzhou, 310009, P. R. China.		
<i>Email</i>	chuhanwen@zju.edu.cn chuhanwen@hotmail.com		
<i>Cell phone</i>	+86 13486184728 (China)		

Career Experience and Academic Degrees

<i>09.2005-07.2010</i>	Zhejiang University, College of Stomatology, P. R. China Bachelor Degree of Medicine GPA: 3.45 / 4 Zhejiang University, Honors College of Chu Kochen, P. R. China Minor: Public Administration
<i>07.2007-09.2007</i>	Hong Kong University, College of Medicine, Hong Kong Exchange Student
<i>09.2010-11.2010</i>	Georgia's Health Sciences University, College of Dentistry, USA Exchange Student
<i>09.2010-07.2012</i>	Zhejiang University, College of Stomatology, P. R. China Master Degree of Medicine GPA:3.95 / 4
<i>08.2012-03.2015</i>	Second Affiliated Hospital, College of Medicine, Zhejiang University Department of Oral and Maxillofacial Surgery, Resident Doctor
<i>04.2015-07.2016</i>	University of Schleswig-Holstein, Campus Kiel, Department of Oral and Maxillofacial Surgery, Visiting Scholar
<i>04.2015-Present</i>	University of Schleswig-Holstein, Campus Kiel, Department of Oral and Maxillofacial Surgery, Doctoral Candidate
<i>12.2016-Present</i>	Second Affiliated Hospital, College of Medicine, Zhejiang University Department of Oral and Maxillofacial Surgery, Attending Doctor

Research Fund

<i>2017.1- Present</i>	The research about the mechanism of differentiation from periodontal ligament stem cells to Schwann cells. Natural Science Foundation of Zhejiang Province, China
------------------------	---

Publication

- 03.2018 Acid sphingomyelinase activity as an indicator of the cell stress in HPV-positive and HPV-negative head and neck squamous cell carcinoma.
Med Oncol. 2018 Mar 21;35(4):58. doi: 10.1007/s12032-018-1117-4.
 Gerle M, Medina TP, Gülses A, **Chu H**, Naujokat H, Wiltfang J, Açil Y.
- 06.2016 Magnetoenzymatic carrier system for imaging and targeted release of multifunctional nanotheranostic particles
Nano Letters **Article Revision**
 T. Peñate Medina., M. Gerle*, J. Humbert*, **H. Chu***, R. Barkmann., V. Haramus., B. Sanz., N. Purcz., O. Will., L. Appold., R. Willumeit., J. Wiltfang, G. Goya., H. Kalthoff., C.C. Glüer., O. Peñate Medina *researchers contributed equally
- 06.2016 Optical imaging and local drug release of oral squamous cell carcinoma in vivo using magneto-enzymatic sensitive liposome
 66. *Kongress der Deutschen Gesellschaft für Mund-, Kiefer- und Gesichtschirurgie und Praxisführungsseminar*, **Poster**
 M. Gerle, **H. Chu**, O. Will, C.-C. Glüer, J. Wiltfang, Y. Açil, T. Peñate Medina, O. Peñate Medina
- 05.2016 Acid sphingomyelinase activity as a cell stress indicator in HPV positive and negative head and neck carcinoma cell lines
 66. *Jahrestagung der Arbeitsgemeinschaft für Kieferchirurgie & 37. Jahrestagung des Arbeitskreises für Oralpathologie und Oralmedizin*. **Poster presentation**
Win the excellent prize of presentation in Conference
 M. Gerle, **H. Chu**, C.-C. Glüer, J. Wiltfang, Y. Açil, M. Hoffmann, T. Grörögh, T. Peñate Medina, O. Peñate Medina
- 08.2012 Application of CAD / CAM techniques in three-dimensional reconstruction of zygomatic complex defect
11th Asian Congress on oral and maxillofacial surgery, Poster
Journal of Zhejiang University. 2012 May;41(3):245-9.
Hanwen Chu, Fangpin Shi, Guanfu Chen
- 12.2014 Oral malignant acanthosis nigricans associated with endometrial adenocarcinoma
International Journal of Oral Science 2014 Dec;6(4):247-9
Hanwen Chu, Jingmin Li, Guanfu Chen, Jingyuan Ma